NASA TM-77006

SA TECHNICAL MEMORANDUM

NASA TM-77006

NASA-TM-77006 19830022168

CONVERGENCE BEHAVIOR THAT CONTROLS ADAPTIVE WIND TUNNEL WALLS NEAR THE TEST SECTION IN THE HIGH ANGLE OF ATTACK RANGE

Jonny Ziemann

Translation of "Das Konvergenzverhalten der Regelung Adaptiver Windkanalwande bei Profiluntersuchungen im Hochanstellwinkel-Bereich", Technischr Universitat, Berlin, Institut fur Luft- und Raumfahrt (W. Ger.), Rept. no. ILR-Mitt-66, Jan. 1980, 76 p.

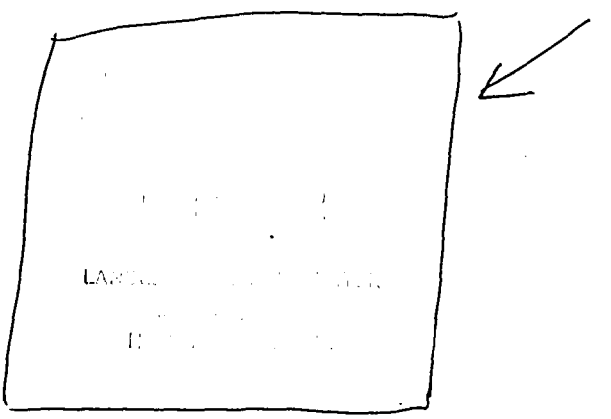

NATIONAL AERONAUTICS AND SPACE ADMINISTRATION
WASHINGTON, D.C. 20546 NOVEMBER 1982

STANDARD TITLE PAGE

1. Report No.	2. Government Accession No.	3. Recipient's Catalog No.
NASA TM-77006		

4. Title and Subtitle	5. Report Date
CONVERGENCE BEHAVIOR THAT CONTROLS ADAPTIVE WIND TUNNEL WALLS NEAR THE TEST SECTION IN THE HIGH ANGLE OF ATTACK RANGE	November 1982
	6. Performing Organization Code
7. Author(s) Jonny Ziemann	8. Performing Organization Report No.
	10. Work Unit No.
9. Performing Organization Name and Address SCITRAN Box 5456 Santa Barbara, CA 93108	11. Contract or Grant No. NASw 3542
	13. Type of Report and Period Covered Translation
12. Sponsoring Agency Name and Address National Aeronautics and Space Administration Washington, D.C. 20546	14. Sponsoring Agency Code

15. Supplementary Notes

Translation of "Das Konvergenzverhalten der Regelung Adaptiver Windkanalwande bei Profiluntersuchungen im Hochanstellwinkel-Bereich", Technischr Universitat, Berlin, Institut fur Luft- und Raumfahrt (W. Ger.), Rept. no. ILR-Mitt-66, Jan. 1980, 76 p.

16. Abstract

The NACA 0012 profile at Mach 0.5 is investigated in a wind tunnel with adaptive walls. It is found that adaptation of the flexible walls is possible in the high angle of attack range on both sides of maximum lift. Oil film photographs of the flow at the profile surface show three-dimensional effects in the region of the corners between the profile and the sidewall. It is concluded that pure two-dimensional separated flow is not possible.

17. Key Words (Selected by Author(s))	18. Distribution Statement
	Unclassified - Unlimited

19. Security Classif. (of this report)	20. Security Classif. (of this page)	21. No. of Pages	22. Price
Unclassified	Unclassified	80	

TABLE OF CONTENTS

/1*

* Numbers in margin indicate pagination of foreign text

NOTATIONS

/2

c_p	pressure coefficient
h	dimension of the separating pieces
i	iteration step
l	profile chord
m	inclination of calibration line
p_∞	static pressure
x,y	coordinates
K	control factor
M_∞	Mach number
P_{Bar}	barometric pressure
P_∞	stagnation pressure
R_e	Reynolds number
T_∞	stagnation temperature
α	angle of attack
β	inclination angle of calibration line
κ	isentropic exponent

Abbreviations:

DFVLR	German Research and Test Facility for Aerodynamic and Space Flight
ARA	Aircraft Research Association Limited

1. Introduction

/3 *

The finite dimensions of a wind tunnel test section as a rule lead to a disturbance in the flow around the model being measured. The measurement results have interference and, therefore, have to be corrected for a flow field which is unlimited in space.

Using adaptive flexible test section walls, it becomes possible to avoid the wall interferences for the most part and to prevent blocking of the test section for transonic flow. In this method, the walls are deformed in such a manner that they take on the shape of those streamlines which would be present at that location if the flow were unlimited to the side.

In the practical application of the method, there are a number of problems to be solved. The first basic investigations on the method for adaptive walls have resulted especially in problems at high angles of attack and for transonic flow. At high angles of attack especially, one has to clarify whether it is possible that measured values without interference can be obtained above the stall condition.

2. Test installation

For the experimental investigations, we use the high speed tunnel of the Institute for Aerodynamics and Space Flight which was propelled with a hot water jet ejector. The air is sucked in from the free atmosphere.

The test section with the flexible adjustable walls has an area of 150 x 150 mm^2 and a length of 690 mm (Figure 1). The flexible walls are made of glass fiber reinforced plastic and can be deformed using eight double jointed adjustable members on bearings. For the adjustment, the pressure distribution along the flexible walls can be measured using 23 static pressure taps.

---

*Numbers in the margin indicate pagination of foreign text.

As a model, we had available the measured profile NACA 0012 (lent from the DFVLR) with a profile chord of l = 100 mm (Figure 2). The profile results in a geometric blocking of 8%. To the side of the central section of the model, there are 21 pressure taps of 0.3 mm diameter along the topside and bottomside. There is an additional tap in the symmetry plane at the profile leading edge. The span of the model of 340 mm required that a cavity be introduced into the side walls in order to accept the model (Figure 3). Using eccentric support of the profile by means of circular disks, when there is an angle of attack change, at the same time there is a vertical displacement of the profile from the central plane of the test section. This means that the stagnation point streamline always has a central position between the flexible walls for any angle of attack. /4

For the pressure measurements, there was a 0 to 15 psia pressure transducer and a ±15 psid pressure transducer as well as two Scanivalves of type DS 48. The measured values were displaced using two digital volt meters. For collecting and evaluating the measurement data, a computer Wang System 2200 was used.

3. Experimental work

3.1 Test execution

All of the tests were carried out with boundary layer transition over the profile, that is, without roughness strips. The Mach number was $M_\infty = 0.50$ and the Re number was $Re = 1.0 \times 10^{+6}$. The angle of attack of the profile was varied in the range $\alpha = 0°$ to $\alpha = 12.647°$. The selection of the angle of attack was done considering the test results of ARA which were used as comparison values. The adaptation of the flexible walls was done as follows:

Starting with the flap wall (iteration step 0) after each measurement the new wall contour was calculated and adjusted. A computer program was available. The iteration was cut off when the

difference between two wall shapes was within the adjustment tolerance or when it became obvious that the change in the profile pressure distribution would no longer show convergence. For an angle of attack of the profile up to 10 control steps were carried out.

3.2 Calibration of pressure transducers

For the profile measurement, the pressure transducer 1 (10 V difference pressure transducers serial no. 53924), for the wall measurements the pressure transducer 2 (5 V absolute pressure transducer serial no. 50128) were used.

During the investigations, calibration measurements were carried out repeatedly for the pressure transducers. For this purpose, various pressures were applied to the pressure transducer and compared with the corresponding voltage reading on the digital volt meter. The calibration curves determined in this way are straight lines with the inclination /5

$$m = \tan \varphi = (x_2 - x_1)/(y_2 - y_1)$$

$x_{1,2}$ = voltage in mV
$y_{1,2}$ = pressure in mmHg

During the first calibration for pressure transducer 1, we found an inclination of $m_1 = -22.6$ mV/mmHg and for the pressure transducer 2 an inclination of $m_2 = -10.2$ mV/mmHg. Repeated measurements for the two pressure transducers showed deviations from the calibration line of up to $|\Delta m| = 0.1$ mV/mmHg, (Figures A1 and A2). This means that for a static pressure of $p_\infty = 640$ mmHg ($M_\infty = 0.500$) measurement inaccuracies of less than 0.08% occur for pressure transducer 1 and less than 0.18% for pressure transducer 2.

These erroneous readings include the error which is produced by the fluctuating display in the digital volt meter: The digital volt meters connected to the pressure transducers fluctuated in their readings by up to 2 mV, which at a pressure of $p_\infty = 640$ mmHg corresponds to a reading inaccuracy of 0.01 to 0.03%.

3.3 Determination of Mach number

The Mach number is determined in the usual way using a measurement of static pressure and stagnation pressure with the formula

$$M_\infty^2 = \frac{2}{\varkappa - 1}\left[\left(\frac{P_\infty}{p_\infty}\right)^{\frac{\varkappa-1}{\varkappa}} - 1\right]$$

The stagnation pressure in the test section was determined with a calibration measurement as $p_\infty = 0.996\ P_{Bar}$. The static pressure of the incident flow was measured through the first pressure tap in the lower wall which was located 2.45 profile chords upstream from the leading edge of the profile.

The Mach number varied between $M_\infty = 0.499$ and $M_\infty = 0.503$ for the measurement performed.

3.4 Determination of the Re number

The Reynolds number depends on stagnation pressure P_∞ and stagnation temperature T_∞ in the test section, (Figures 4 and A3, A4). The stagnation temperature of the air sucked in from the free atmosphere was approximately determined with a temperature measurement of air in the test room. We can assume that in this way the maximum air was $\Delta T_\infty = 3°C$, which corresponds to a Reynolds number inaccuracy /6 of $\Delta Re = 0.015 \times 10^6$.

With consideration of the pressure fluctuations as well, the Re number in all tests was between $Re = 0.99 \times 10^6$ and $Re = 1.02 \times 10^6$.

3.5 Adjustment of angle of attack

The angle of attack adjustment was done by rotating the two acrylic glass side disks which support the profile. Starting with 0°, any desired angle of attack can be adjusted using separators

between two stops on a circular disc and the housing on each side. This is shown in Figure A5. The zero line adjustment is done by comparing the two pressure distributions on the top side and the bottom side of the profile for a nondeflected wall. Symmetric pressure distributions were achieved for a separator piece with dimensions h = 1.20 mm. This corresponds to a manufacturing tolerance in the alignment of the stop lever of 0.3619°.

The adjustment tolerance of the angle of attack consists of two factors:

- since the 0° adjustment was done by simple comparison of the pressure distribution curves for the topside and the bottom side, we then find an estimated error of $\Delta\alpha = \pm 0{,}05^{\circ}$.

- due to the play between the two side disks and the housing, we find $|\Delta h| = 0{,}5\,mm$. From this we find an error in the angle of attack of $|\Delta\alpha_{max}| = 0{,}15^{\circ}$.

The pressure difference which results in this is $\overline{\Delta c_{p_{max}}} = \pm 0{,}01$ for nonseparated flow.

3.6 Measurement value fluctuations

In order to estimate the order of magnitude of the measured value fluctuations, tests were made for an angle of attack and unchanged wall shape several times.

We found average deviations of $|\overline{\Delta c_p}| = 0{,}0025$ if the flow was not separated at the profile. The fluctuations can be explained by the play in the wall adjustment installation, the wall deformation due to aerodynamic forces and the wall manufacturing tolerances as well as the measurement inaccuracies. The testing of the wall installation after a test showed deviations of 1 - 3/100 mm and in exceptional cases of 1/10 mm.

For separated profile flow, there were substantially greater /7
fluctuations in the measured c_p values. This can be explained by the fact that the flow was not steady. The fluctuations were between $|\overline{\Delta c_p}| = 0{,}0160$ (for $\alpha = 9.664°$) and $|\overline{\Delta c_p}| = 0.0220$ (for 12.647°).

4. Experimental results

4.1 The extent of wall interferences

In order to first give an idea about the extent of wall interferences for the NACA 0012 profile with 8% geometric blocking, we show a number of pressure distributions in Figures 5 to 11. This shows the profile pressure distributions for all investigated angles of attack for plane walls and adaptive walls and these are compared with one another. With increasing angle of attack, the discrepancies on the topside of the profile become larger. This can be explained from the fact that the angle of attack increase is related to a vertical displacement of the profile towards the upper wall.

The demonstration that the pressure distributions measured for adaptive walls can be looked upon as measured values without interference, can only be done to a limited extent here. For comparison, we have measured values of the ARA for an NACA 0012 profile [1]. The ARA tunnel has a test section of 8" x 18", so that for a 5" chord profile, a geometric blocking of 3.33% results. This means that these values can be looked upon as having almost no interference. For comparison, however, one has to consider that there were different Reynolds numbers (5×10^6 for ARA compared with 1×10^6 at the TU Berlin). In addition, differences in the model accuracy could play a role. In Figures 12 to 18, we show the comparison of measured values. At $\alpha = 0°$ there is completely satisfactory agreement, but at $\alpha = 3.829°$ and $\alpha = 7.686°$, there are differences in the pressure distribution along the bottom side of the profile which first cannot be explained. It is possible that empirical curvature and downwind angle corrections play a role here which were used for the ARA

measured values. Basic differences in the pressure distributions occur when the flow separates over the profile. Because of the different Reynolds numbers, there is a different separation behavior so that the pressure distribution deviates strongly.

/8

4.2 Convergence behavior of the control for high angles of attack

In the following we will analyze the convergence behavior of the adaptive walls for an angle of attack just below the stall condition ($\alpha = 7.7°$) as well as for four angles of attack with separated profile flow ($\alpha = 9.7$, 10.7, 11.7 and 12.7°). The basis for the evaluation of convergence are the pressure distributions measured along the topside of the profile and the deflections of the upper channel wall.

In the following Figures 19 to 23, we show changes of the measured pressure values for various profile stations x/l as a function of the iteration step. The purpose of this plot was to make visible the local different effects of wall control on the profile flow. In general, one can see convergence of the adaptation method for all investigated flow cases. Depending on the control factor*, two to four iteration steps are required. For the flow cases mentioned here, a factor of K = 0.25 seems to lead to the fastest convergence. Residual fluctuations in the pressure coefficients are especially large in general in the region of the profile nose, that is, in the region of large pressure gradients.

*For adaptation of the walls, the pressure distribution measured along the channel wall is compared with a calculated pressure distribution. The calculation is done for each wall shape under the assumption of a fictitious outer flow which is unlimited to the side. The difference between the calculated and the measured pressure distribution is used for correcting the wall shape. Using the control factor K, this difference is weighted. A small factor K means smaller weight of the measured pressure distribution (see [2]).

In order to obtain summarizing information about the convergence and residual fluctuations, it is imaginable that one could determine the lift coefficients from the integration of the pressure distributions and then represent these values as a function of the iteration steps. However, one obtains similar information in a simpler manner by forming the average over all of the measured pressure coefficients. This means that this is a very accurate possibility of convergence control which also saves time. This is especially important because control is to be on line (during the wind tunnel tests).

The average values of the pressures measured along the profile topside are shown in Figures 24 to 28 for all individual flow cases. The changes in these average pressure coefficients during the iteration steps give an indication of the convergence of the control method.

The convergence is influenced by the control factor. Different control factors were selected for the individual flow cases. Figure 29 gives a comparison of the convergence curves with different control factors. The adapted wall shape is reached faster, the smaller the factor K. This, however, can only occur up to a certain limit and it seems that K = 0.25 is already the optimum control factor for the flow cases discussed here. It is also remarkable that the convergence behavior was independent of angle of attack for the cases investigated.

At this point we have to explain the selection of the control factors used during the test. The evaluation of the first test with adaptive walls showed that the most favorable control factor was K = 0.35. However, this was for smaller angles of attack and other Mach numbers. This means that we started with this control factor for the other tests as well. The control factor K = 0.35, however, led to a relatively large upper harmonic of the wall deflection which led to especially large wall deformations during the first iteration step at the high angles of attack. For the angle of attack

α = 10.7° for example, with K = 0.35 a maximum wall deflection of 28 mm would have been required, whereas with K = 0.25, the deflection for the first iteration step remained limited to a maximum of 13 mm. It was only to avoid large wall deformations that the control factor was then varied. Based on the evaluation performed now, we can now establish that in this way a control factor was used which was more favorable for convergence.

In Figures 30 to 34, we again show the control behavior on a larger scale starting with the second iteration. In this way, the residual fluctuations can be seen especially clearly.

For an angle of attack α = 7.7° (Figure 30), the average pressure deviation between the two last control steps is still $|\overline{\Delta c_p}| = 0{,}0017$ and, therefore, is still within the measurement accuracy of $|\overline{\Delta c_p}| = 0{,}0025$. For the angle of attack cases with separated flow, we clearly had larger residual fluctuations. The fluctuations just above the stall condition α = 10.7° (Figure 32) were especially large. During the first iteration step the average pressure coefficients first fluctuated around the average value and then varied in a nonsystematic way within a scatter range as the iteration was continued. The fluctuation width is $|\overline{\Delta c_p}| = 0{,}0201$ and is therefore one order larger than for nonseparated flow. This /10 fluctuation width therefore is of the same order as the measurement fluctuations for separated flow so that when reaching this value, the wall can be looked upon as having been adapted. Here we should point out that in the representation of the pressure distribution for the profile surface (for example, Figure 15), the point blackness corresponds to the average measured fluctuations (ϕ about Δc_p = 0.02). When the measured value fluctuations went beyond this value, then this was especially noted.

Another possibility to obtain information about convergence is to represent the average wall deflection $\bar{y}$ as a function of the iteration step (Figures 35 to 39). We proceeded in the same way as for the measured pressure values. Here one can see convergence of

the control as well. For specifying the required iteration steps, it would be possible to use the gradient between two iterations: if the change in the wall shape is inside a specified value, then the control can be broken off. However, there is one danger in the possibility that control will end prematurely when the gradient does not decrease monotonically.

Basically, it makes more sense to evaluate the convergence behavior of control using the average pressure coefficient. This is especially clear for the case $\alpha = 10.7°$. Starting with the third and up to the eighth iteration, the wall was only deflected by more than 0.8 mm (Figure 37). The pressure over the profile hardly changed. This is remarkable because therefore we have shown that for the separated flow case the wall adjustment apparently only has a small influence on the measured results.

Figure 40 shows the residual fluctuations of pressure compared with the wall deflection for the different angles of attack cases. This summarizing representation shows that with both parameters, one can obtain similar information about the convergence behavior. For attached flow the residual fluctuations are minimum; a maximum value is reached when the flow has just completely separated.

4.5 Influence of sidewalls

Finally, we indicate by means of oil film photographs the extent to which deviations from a two-dimensional flow can be found for the wind tunnel tests and the influence that the sidewalls have.

/11

For the case of attached flow, $\alpha = 7.7$ (Figure 41), the wall streamlines in the central region of the profile are for the most part parallel. In the corners between the profile and the wall, however, there are extensive zones with 3D flow effects which certainly influence the flow conditions in the central profile section. In addition, the figure also shows that at this angle of attack, the flow just starts separating. The oil accumulation at the profile

nose indicates a separation bubble, whereas the material accumulation in the rear part of the model allows one to conclude that there are only small wall shear stresses.

For the cases with separated flow for example, at $\alpha = 9.7°$ (Figure 42), and also for the higher angles of attack (Figures 43 to 45), we no longer can speak of a 2D flow. We have to realize that apparently there is no two-dimensional and completely separated flow. This is one realization which was also made in the investigation elsewhere of profiles with extremely large span. It is not clear what the influence of the sidewall boundary layer is on the development of this 3D flow. For the same angle of attack, the oil film photograph from one test to the next was different within certain limits but remained the same for the most part during the test. This indicates that the structure of the flow field is specified by the start-up process. Under these conditions, it does not make a great deal of sense to carry out flow investigations in the post stall range with profiles. In practice, such purely two-dimensional flows are hardly of any importance anyway because they would only be expected with unswept wings with extremely large aspect ratio.

5. Summary /12

The investigations of a NACA 0012 profile at Mach 0.5 in the wind tunnel with adaptive walls have shown that adaptation of the flexible walls is possible also in the high angle of attack range both on this side and the other side of maximum lift. For determining the iteration steps required for adaptation, one can use an average pressure coefficient which is the result of the sum of all of the pressure values measured along the topside of the profile. If one suitably selects the control factor(for the cases investigated here, we use $k = 0.25$) adaptation already is reached after two iteration steps. The residual fluctuations of the average pressure coefficient for nonseparated flow are extremely low ($\Delta c_p = 0.0017$) and for separated flow they are higher by one order of magnitude. These residual fluctuations are caused by measurements on the one hand, and

also for separated flow, they are a consequence of unsteady flow effects. The changes in the average pressure coefficient for continued iteration of the wall adjustment are always smaller than the residual fluctuations. This means the control process can be terminated when the change in the average pressure coefficient is smaller than the residual fluctuation established for each flow case. It is remarkable that for separated flow a wall deformation has only a very small influence on the pressure distribution over the profile.

Oil film photographs of the flow at the profile surface show three-dimensional effects in the region of the corners between the profile and the sidewall. The extent to which the profile flow is deteriorated by these effects could not be clarified. It would be desirable to investigate this.

For separated profile flow, the oil film photographs show complete three-dimensional flow. A pure two-dimensional separated flow apparently is not possible.

/13

6. REFERENCES

[1] Sawyer, J.: Results of tests on aerofoil M.102/9 (NACA 0012) in the ARA 2D tunnel.
ARA model test note M.102/9, Oct. 1978

[2] Ganzer, U.: Wind tunnels with adaptive walls to remove wall interferences.
Z. Flugwiss. Weltraumforsch. Vol. 3, no. 2, March/April 1979

/14

FIGURES

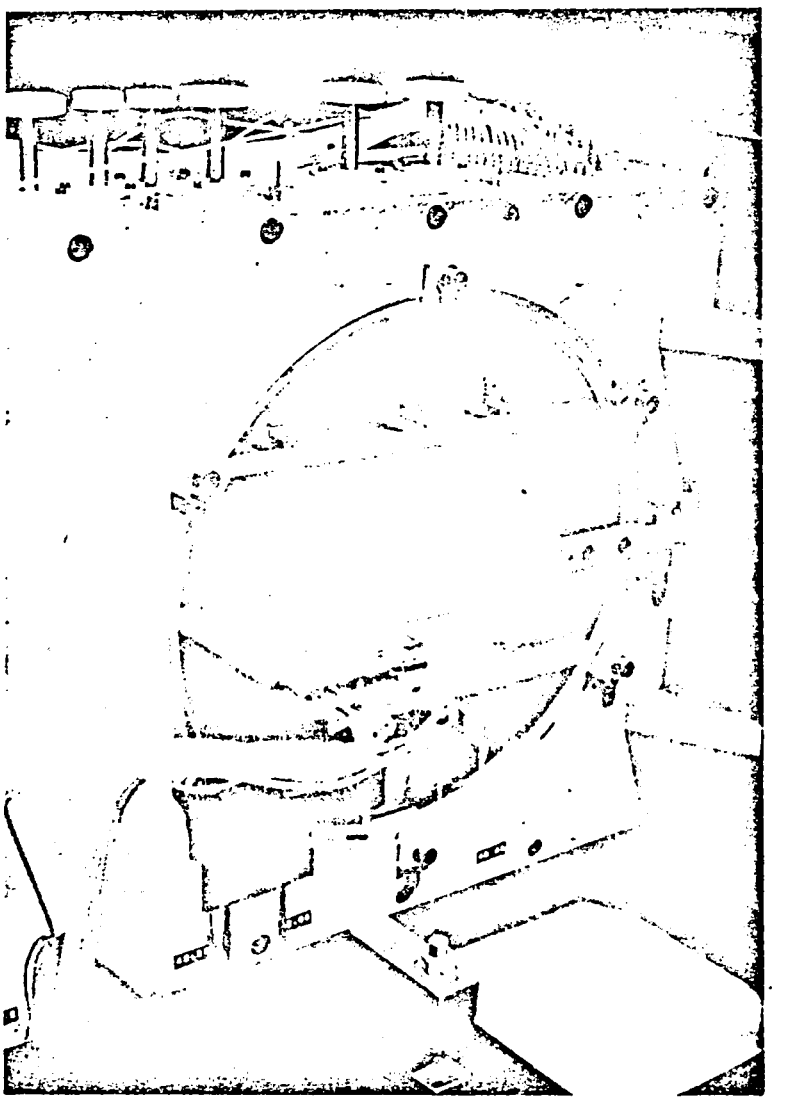

Figure 1. TEST SECTION WITH PROFILE MODEL

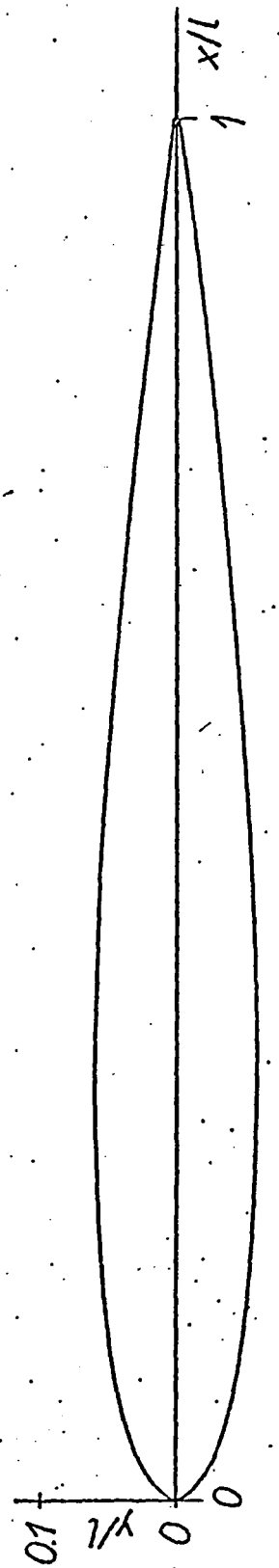

Figure 2a. NACA 0012 PROFILE

/17

	topside		
	theory	Model	deviations
x/l.	y/l.	y/l.	Δy/l.
0.000	0.00000	0.00000	0.00000
0.007	0.01436	0.01373	-0.00063
0.015	0.02064	0.01988	-0.00076
0.023	0.02517	0.02440	-0.00077
0.030	0.02840	0.02763	-0.00077
0.037	0.03119	0.03042	-0.00077
0.051	0.03585	0.03507	-0.00078
0.070	0.04086	0.04015	-0.00071
0.092	0.04542	0.04479	-0.00063
0.110	0.04843	0.04784	-0.00059
0.130	0.05119	0.05066	-0.00053
0.150	0.05345	0.05303	-0.00042
0.170	0.05529	0.05500	-0.00029
0.195	0.05708	0.05690	-0.00018
0.220	0.05839	0.05830	-0.00009
0.240	0.05913	0.05906	-0.00007
0.270	0.05981	0.05976	-0.00005
0.295	0.06001	0.06000	0.00001
0.320	0.05993	0.05997	0.00004
0.350	0.05949	0.05961	0.00012
0.375	0.05886	0.05905	0.00019
0.395	0.05821	0.05846	0.00025
0.420	0.05723	0.05757	0.00034
0.445	0.05606	0.05652	0.00046
0.465	0.05501	0.05554	0.00053
0.490	0.05356	0.05418	0.00062
0.520	0.05164	0.05236	0.00072
0.555	0.04916	0.05003	0.00087
0.580	0.04724	0.04821	0.00097
0.605	0.04522	0.04628	0.00106
0.625	0.04353	0.04465	0.00112
0.655	0.04087	0.04209	0.00122
0.685	0.03808	0.03941	0.00133
0.715	0.03516	0.03662	0.00146
0.745	0.03212	0.03373	0.00161
0.775	0.02896	0.03069	0.00173
0.800	0.02623	0.02803	0.00180
0.825	0.02342	0.02526	0.00184
0.855	0.01994	0.02180	0.00186
0.885	0.01633	0.01826	0.00193
0.910	0.01322	0.01523	0.00201
0.935	0.01003	0.01217	0.00214
0.960	0.00677	0.00902	0.00225
0.985	0.00335	0.00645	0.00310
1,000	0,00126	-	-

Figure 2b. PROFILE COORDINATES FOR NACA 0012

bottomside

	theory	Model	deviations
x/l.	y/l.	y/l.	Δy/l.
0.000	0.00000	0.00000	0.00000
0.002	-0.00781	-0.00835	0.00054
0.010	-0.01704	-0.01774	0.00070
0.023	-0.02517	-0.02554	0.00037
0.037	-0.03119	-0.03154	0.00035
0.055	-0.03701	-0.03738	0.00037
0.074	-0.04178	-0.04215	0.00037
0.094	-0.04578	-0.04614	0.00036
0.115	-0.04918	-0.04958	0.00040
0.140	-0.05238	-0.05279	0.00041
0.160	-0.05442	-0.05483	0.00041
0.190	-0.05676	-0.05720	0.00044
0.220	-0.05839	-0.05894	0.00055
0.250	-0.05941	-0.06012	0.00071
0.275	-0.0r987	-0.06074	0.00087
0.305	-0.06001	-0.06108	0.00107
0.330	-0.05982	-0.06105	0.00123
0.360	-0.05926	-0.06063	0.00137
0.390	-0.05839	-0.05983	0.00144
0.410	-0.05764	-0.05910	0.00146
0.440	-0.05631	-0.05779	0.00148
0.470	-0.05473	-0.05624	0.00151
0.495	-0.05325	-0.05482	0.00157
0.520	-0.05164	-0.05329	0.00165
0.545	-0.04989	-0.05161	0.00172
0.575	-0.04763	-0.04940	0.00177
0.600	-0.04563	-0.04744	0.00181
0.630	-0.04310	-0.04497	0.00187
0.665	-0.03996	-0.04190	0.00194
0.695	-0.03712	-0.03915	0.00203
0.725	-0.03416	-0.03628	0.00212
0.755	-0.03108	-0.03333	0.00225
0.775	-0.02896	-0.03131	0.00235
0.800	-0.02623	-0.02870	0.00247
0.820	-0.02398	-0.02657	0.00261
0.845	-0.02111	-0.02383	0.00272
0.875	-0.01755	-0.02039	0.00284
0.895	-0.01510	-0.01801	0.00295
0.915	-0.01259	-0.01552	0.00293
0.930	-0.01068	-0.01362	0.00294
0.945	-0.00872	-0.01165	0.00293
0.960	-0.00674	-0.00966	0.00292
0.975	-0.00471	-0.00766	0.00295
0.980	-0.00403	-0.00703	0.00300
0.985	-0.00335	-0.00645	0.00310
1.000	-0.00126	-	-

Figure 2c. PROFILE COORDINATES FOR NACA 0012

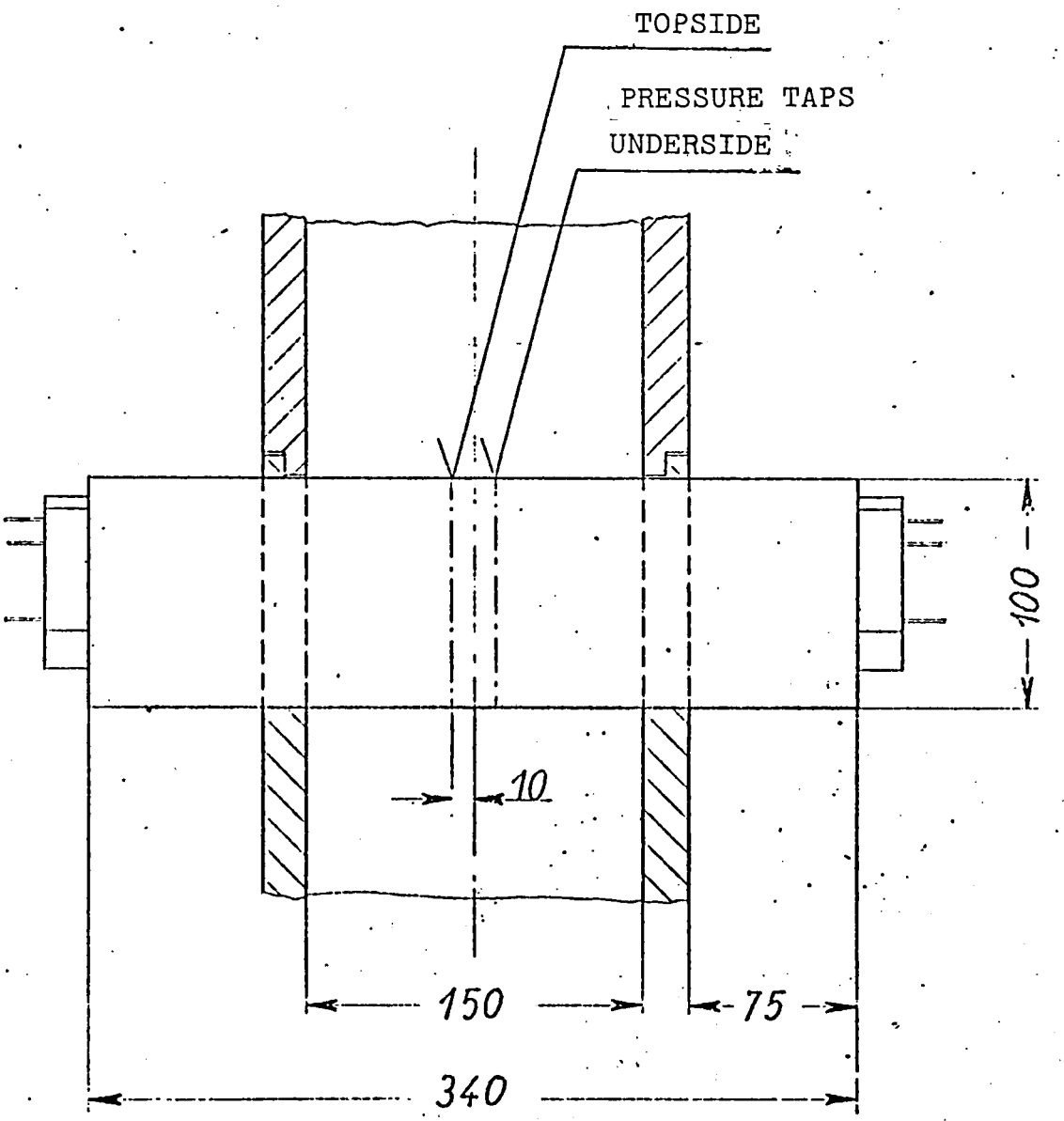

Figure 3. MODEL SUPPORT IN THE TEST SECTION

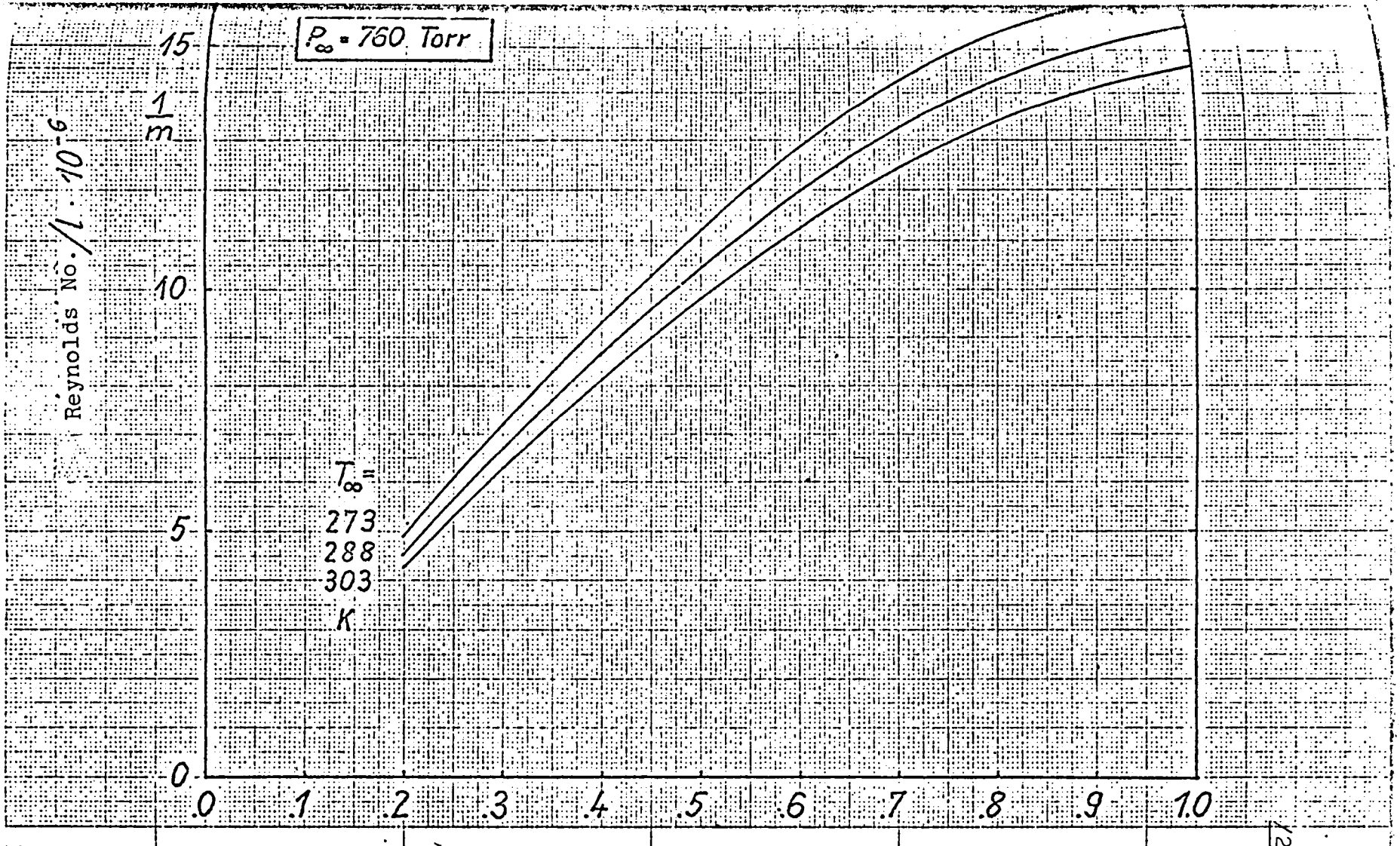
P_∞ = 760 Torr
Reynolds No. $/l \cdot 10^{-6}$
$\frac{1}{m}$
15
10
5
0
T_∞ =
273
288
303
K
.0
.1
.2
.3
.4
.5
.6
.7
.8
.9
1.0
Mach no. M_∞

FIGURE 4

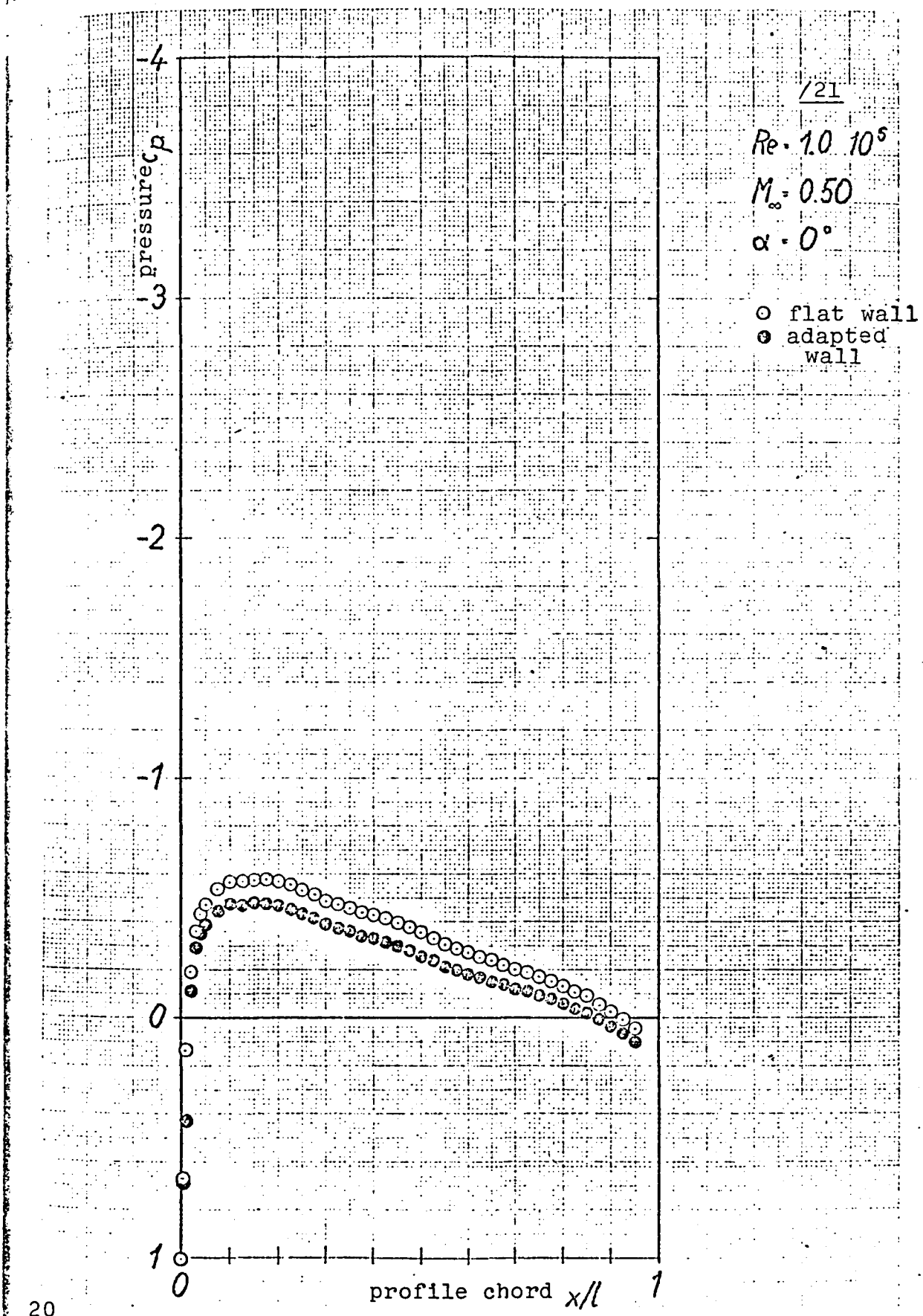

Figure 5. PRESSURE DISTRIBUTION FOR NACA 0012

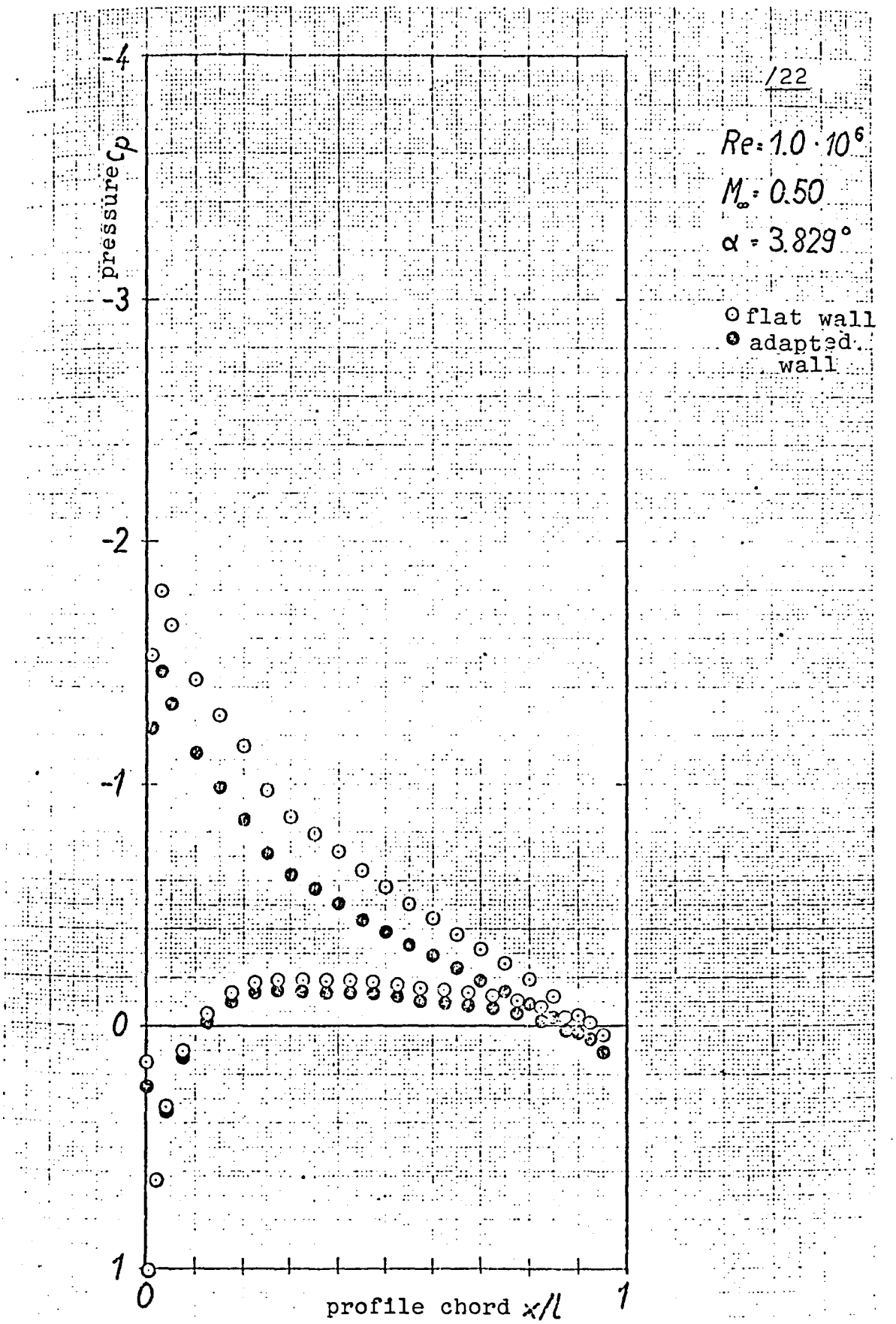

FIGURE 6. PRESSURE DISTRIBUTION FOR NACA 0012

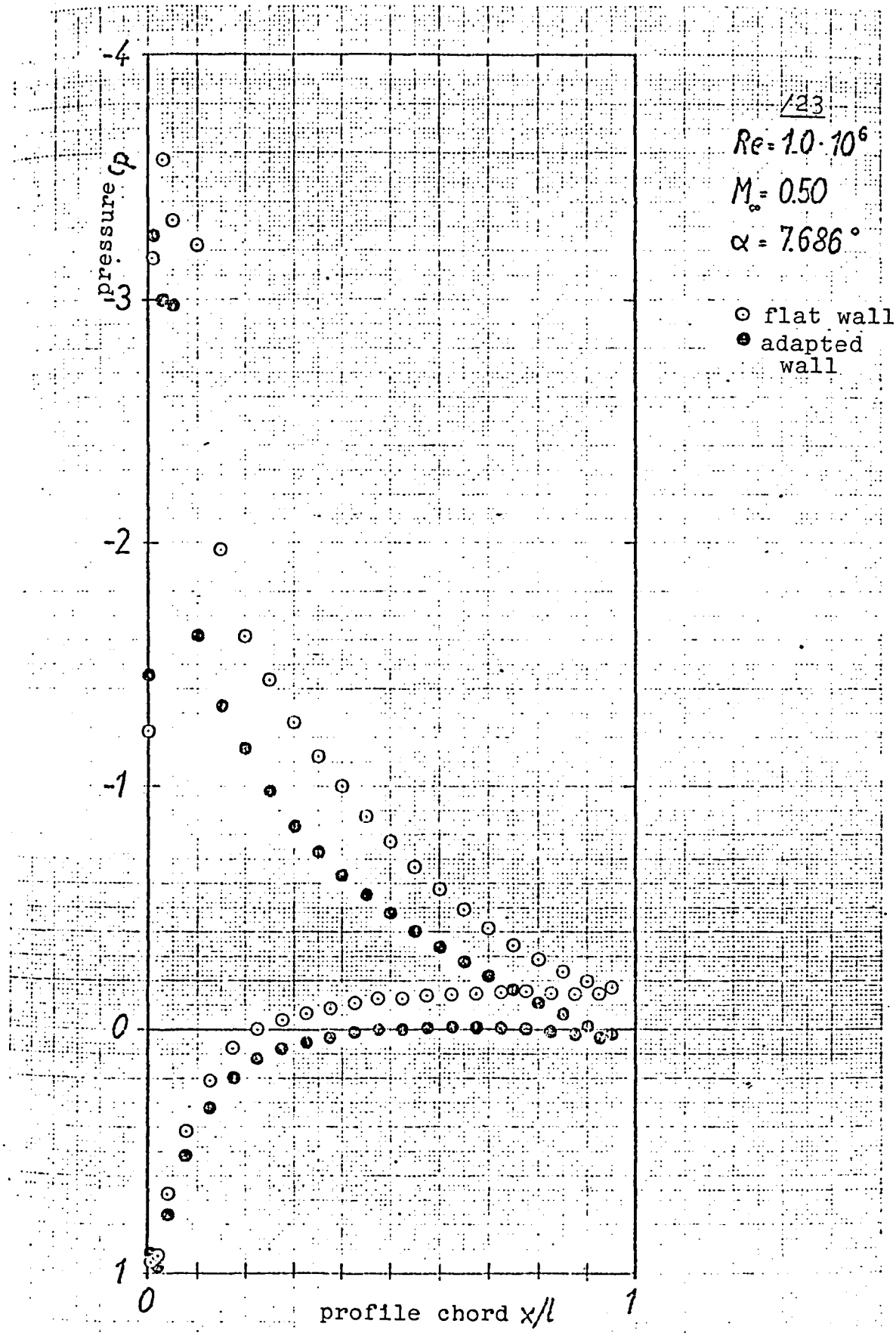

22 FIGURE 7. PRESSURE DISTRIBUTION FOR NACA 0012

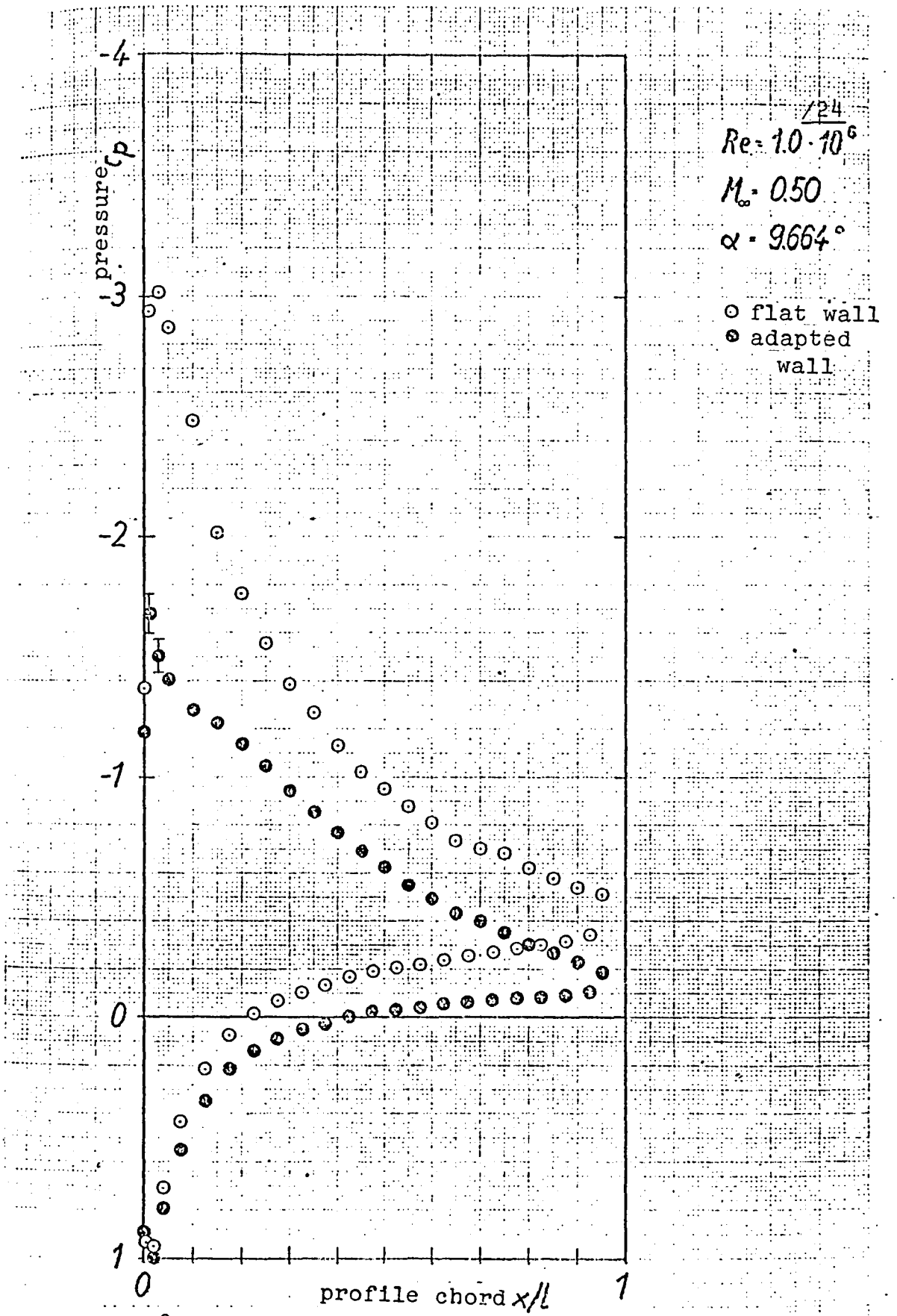

FIGURE 8. PRESSURE DISTRIBUTION FOR NACA 0012

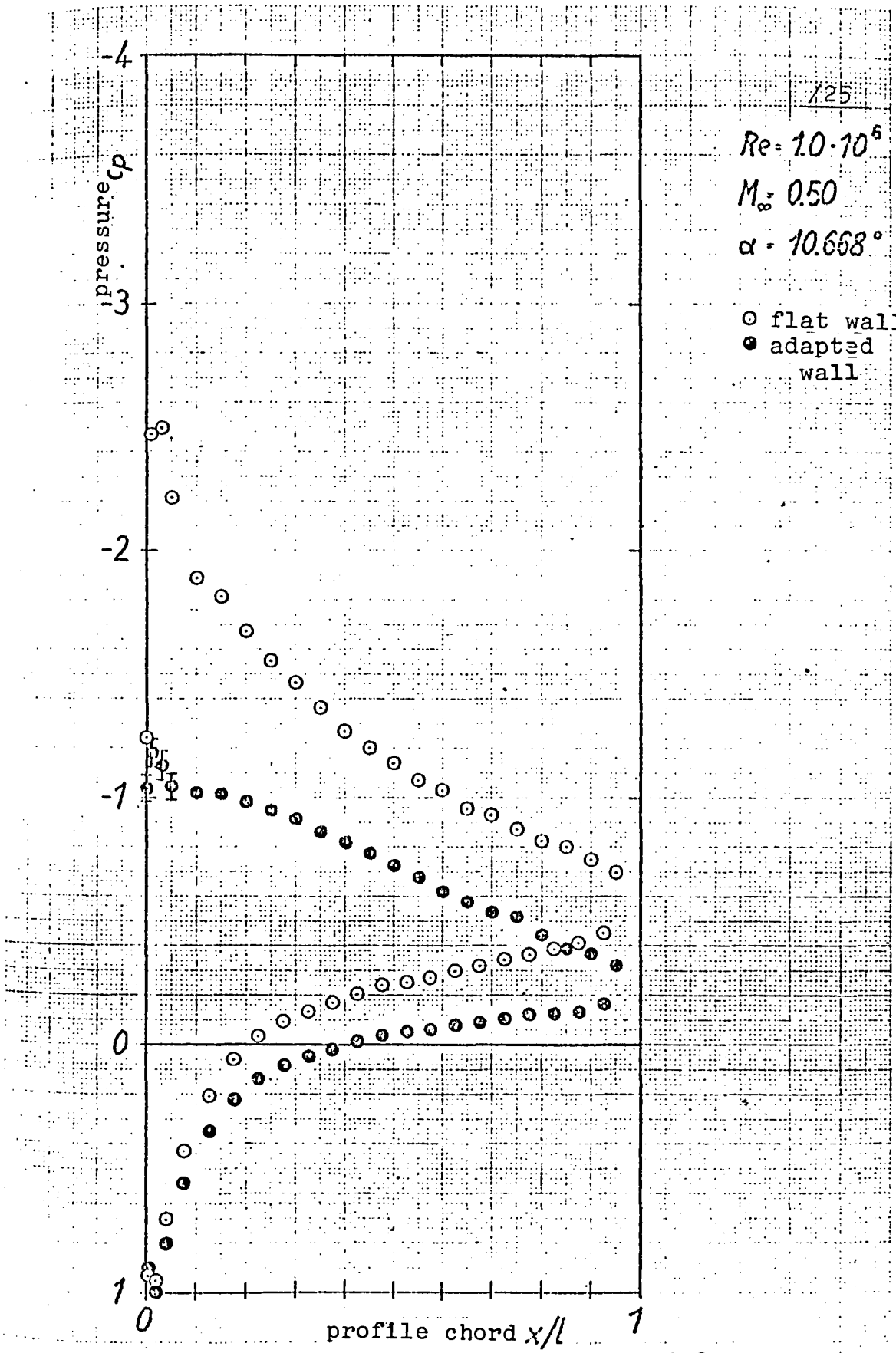

24 FIGURE 9. PRESSURE DISTRIBUTION FOR NACA 0012

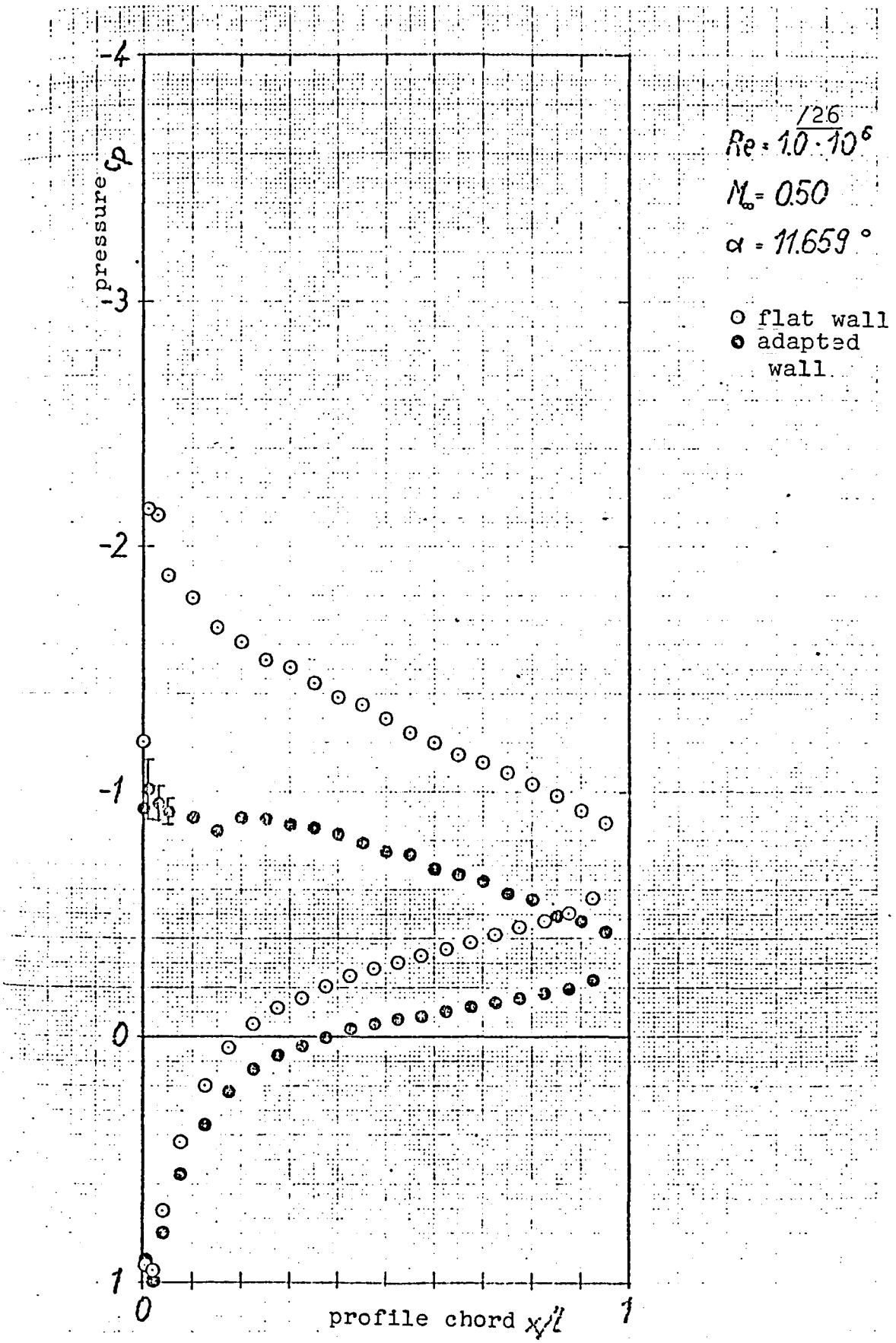

FIGURE 10. PRESSURE DISTRIBUTION FOR NACA 0012

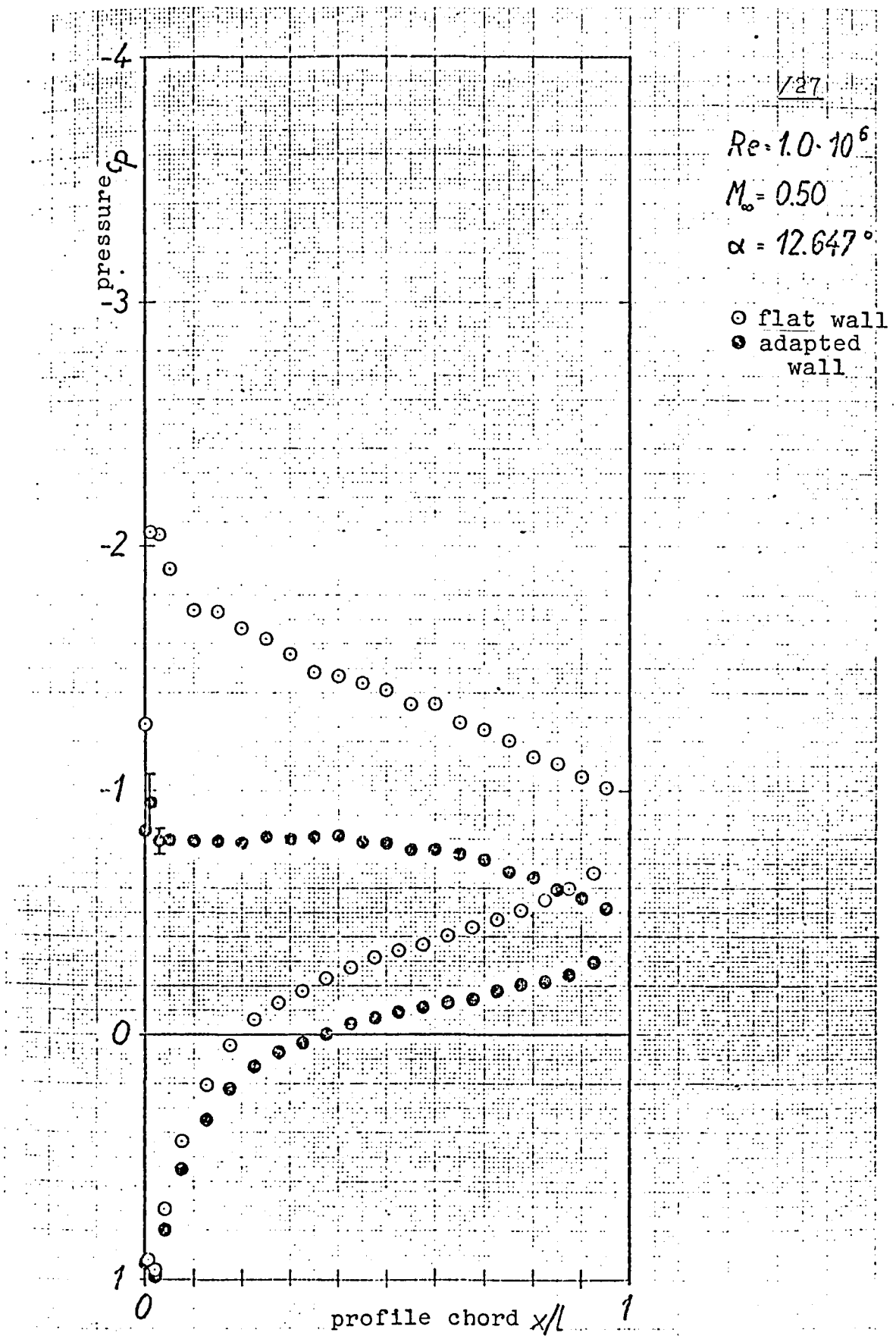

FIGURE 11. PRESSURE DISTRIBUTION FOR NACA 0012

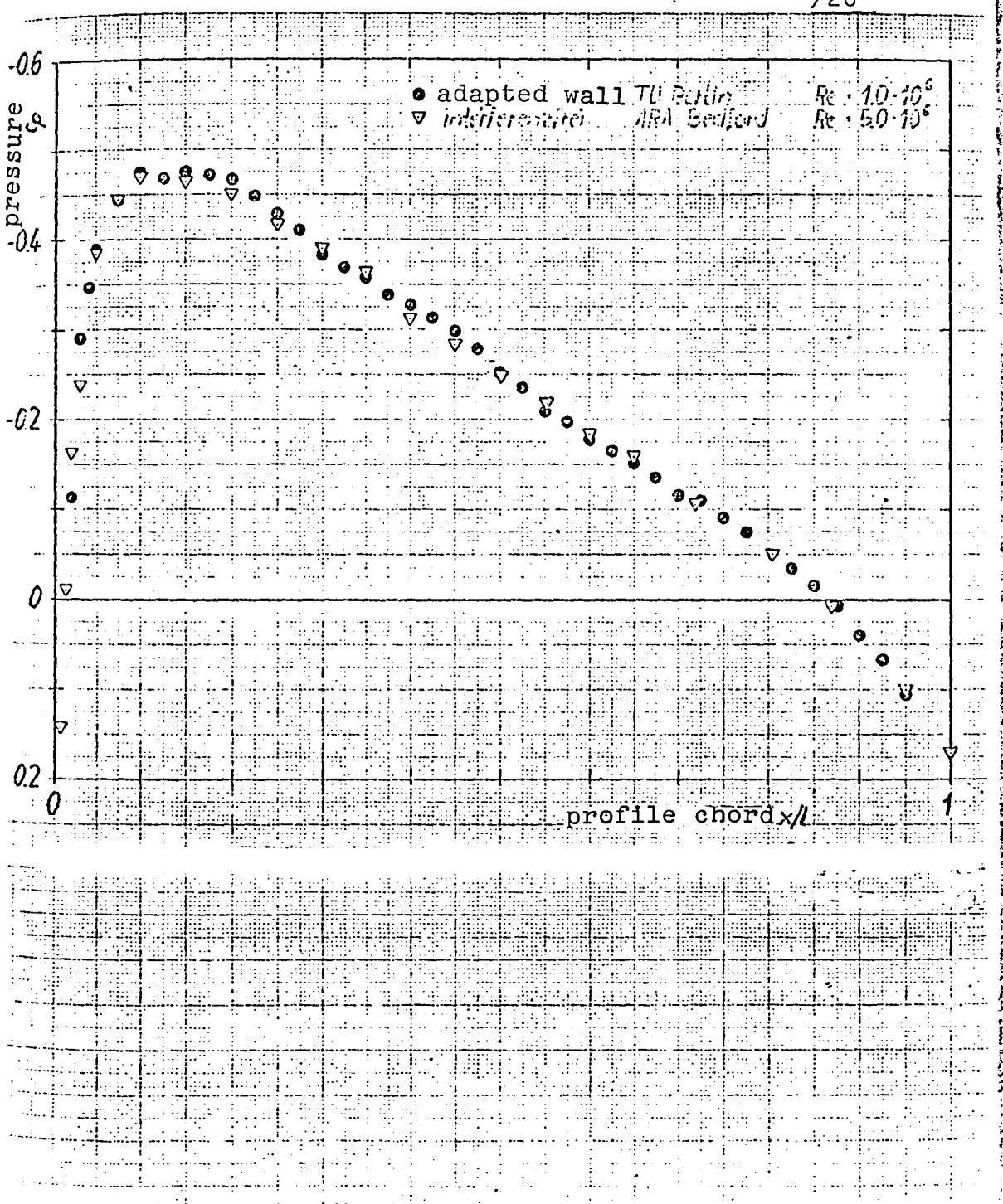

FIGURE 12. PRESSURE DISTRIBUTION FOR NACA 0012/
FREE BOUNDARY LAYER TRANSITION M_∞=0.50 α=0°

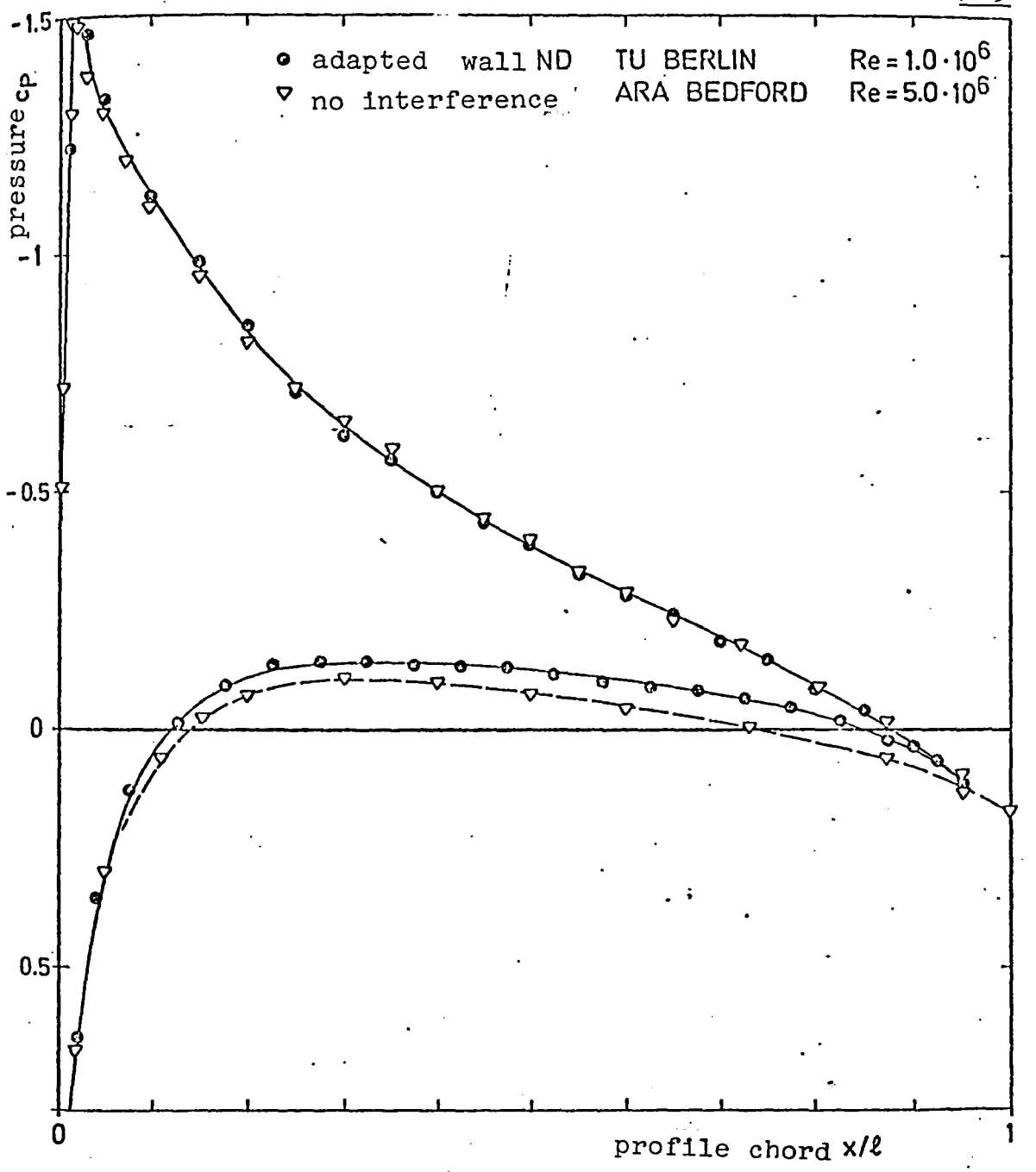

FIGURE 13a. PRESSURE DISTRIBUTION FOR NACA 0012/ FREE BOUNDARY LAYER TRANSITION

$M_\infty = 0.50$ $\alpha = 3.829°$

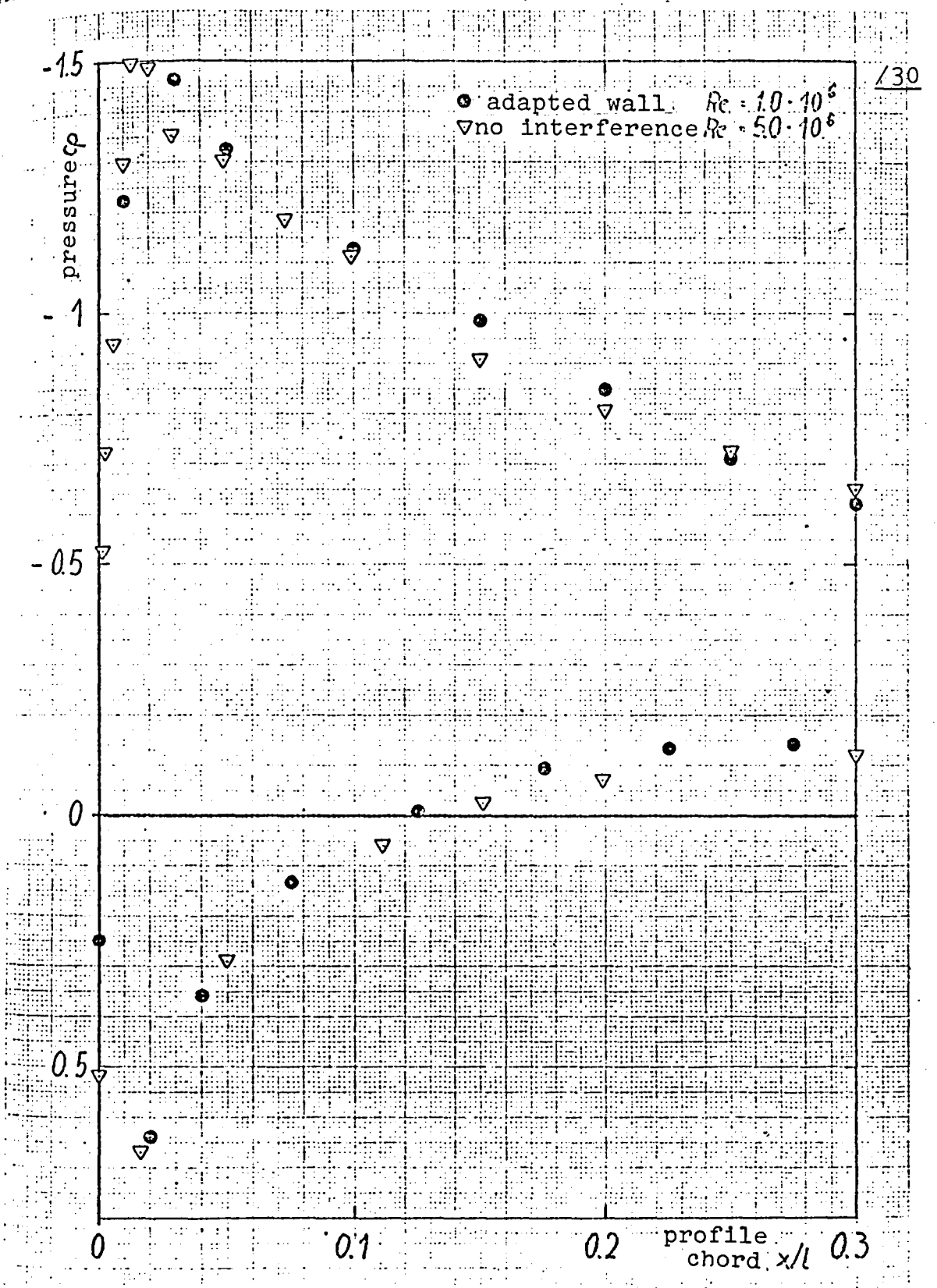

FIGURE 13b. PRESSURE DISTRIBUTION FOR NACA 0012/
FREE BOUNDARY LAYER TRANSITION

M = 0.50 α = 3.879°

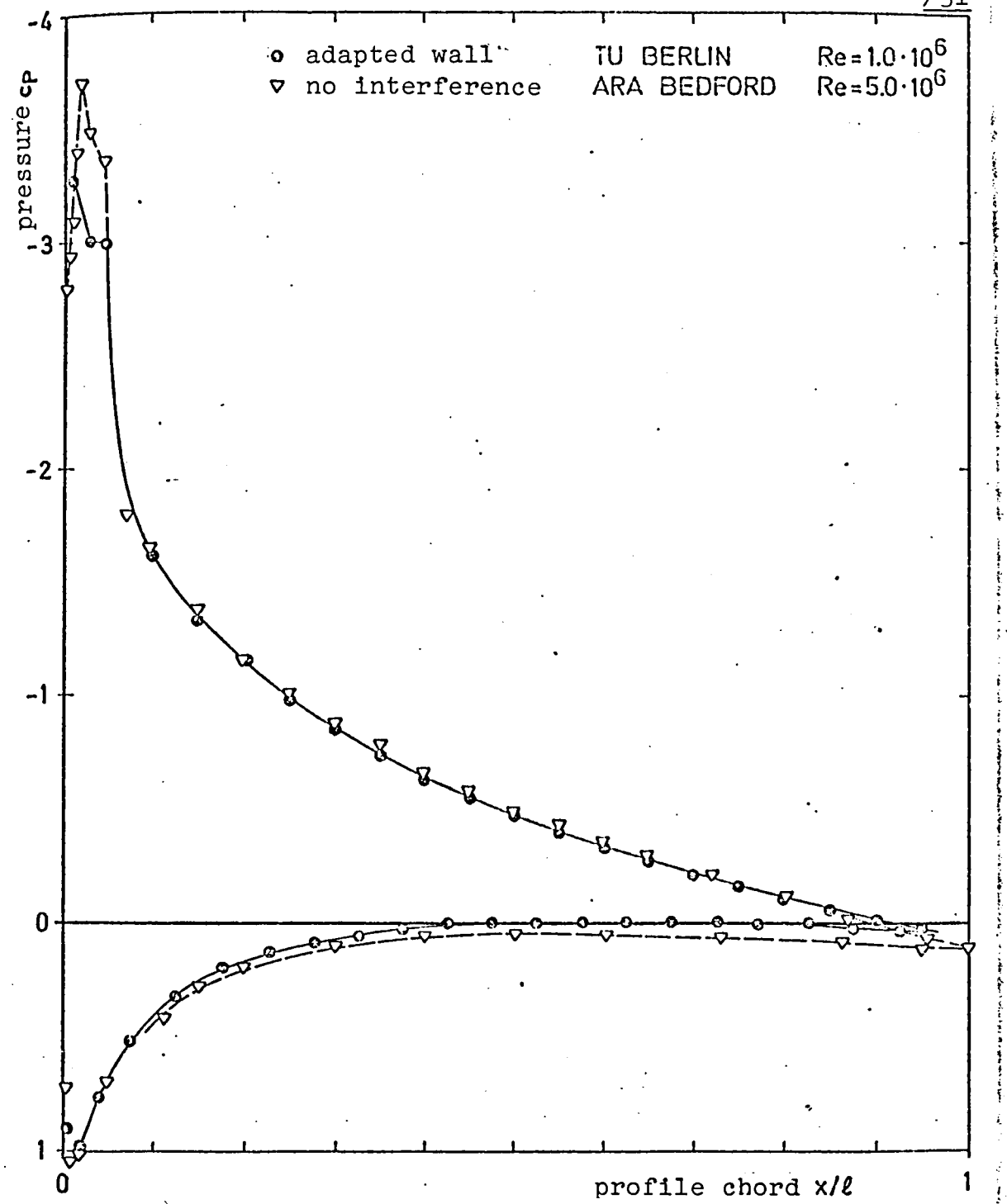

FIGURE 14a. PRESSURE DISTRIBUTION FOR NACA 0012/
FREE BOUNDARY LAYER TRANSITION

$M_\infty = 0.50$ $\alpha = 7.686°$

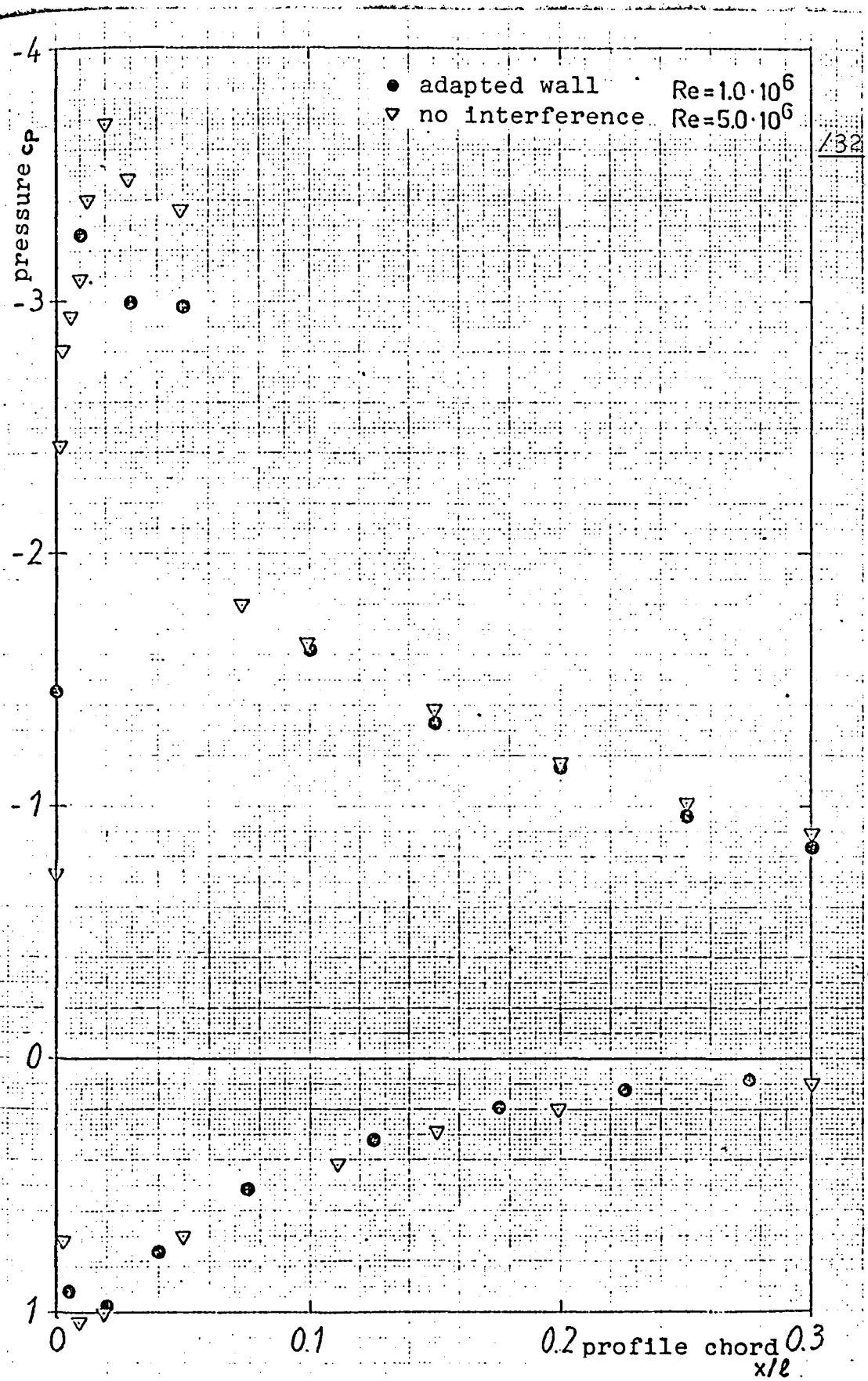

FIQURE 14b. PRESSURE DISTRIBUTION FOR NACA 0012/FREE BOUNDARY LAYER TRANSITION

$M_\infty = 0{,}50$ $\alpha = 7{,}686°$

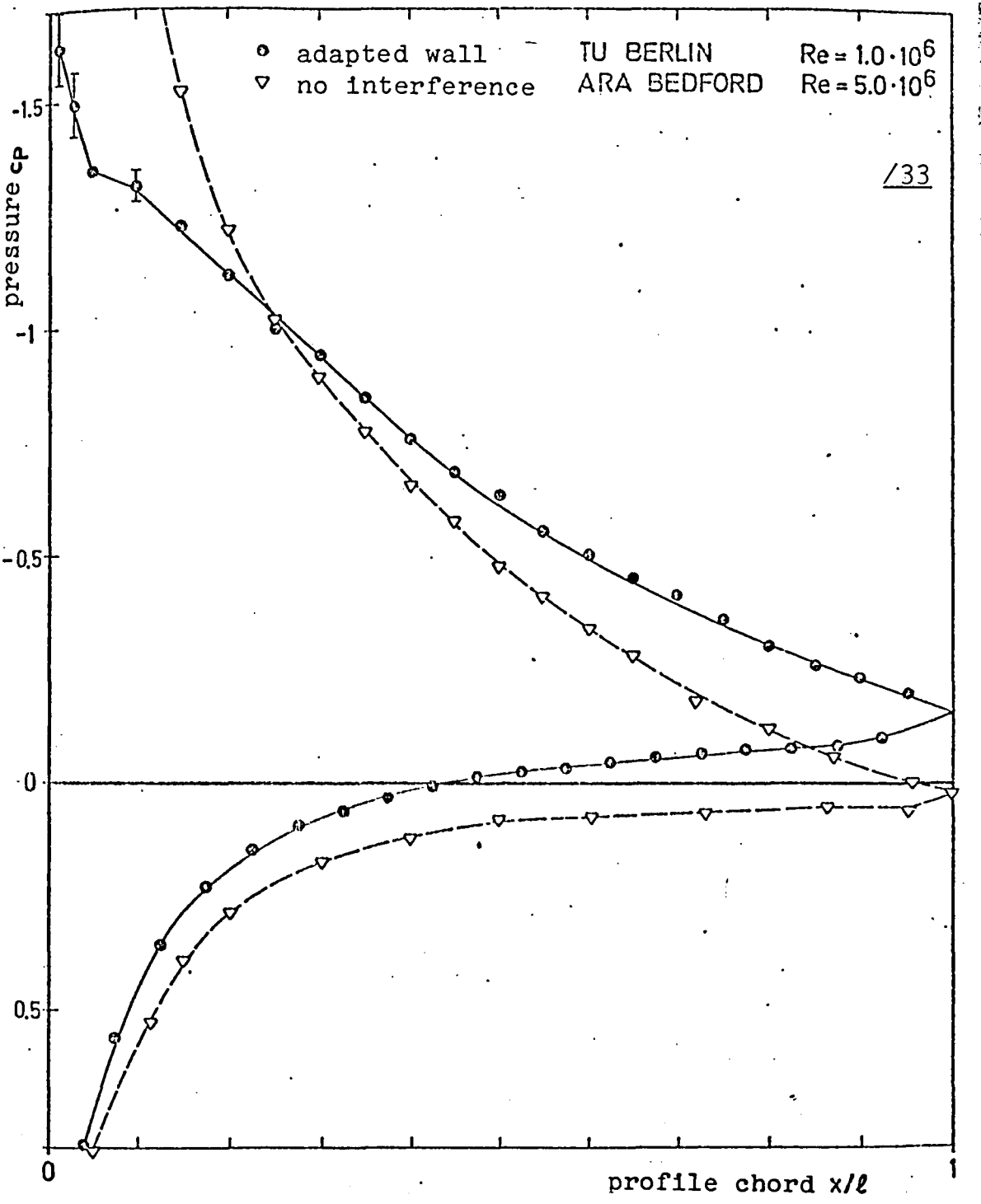

FIGURE 15. PRESSURE DISTRIBUTION FOR NACA 0012

FREE BOUNDARY LAYER TRANSITION

$M_\infty = 0.50$ $\alpha = 9.664°$

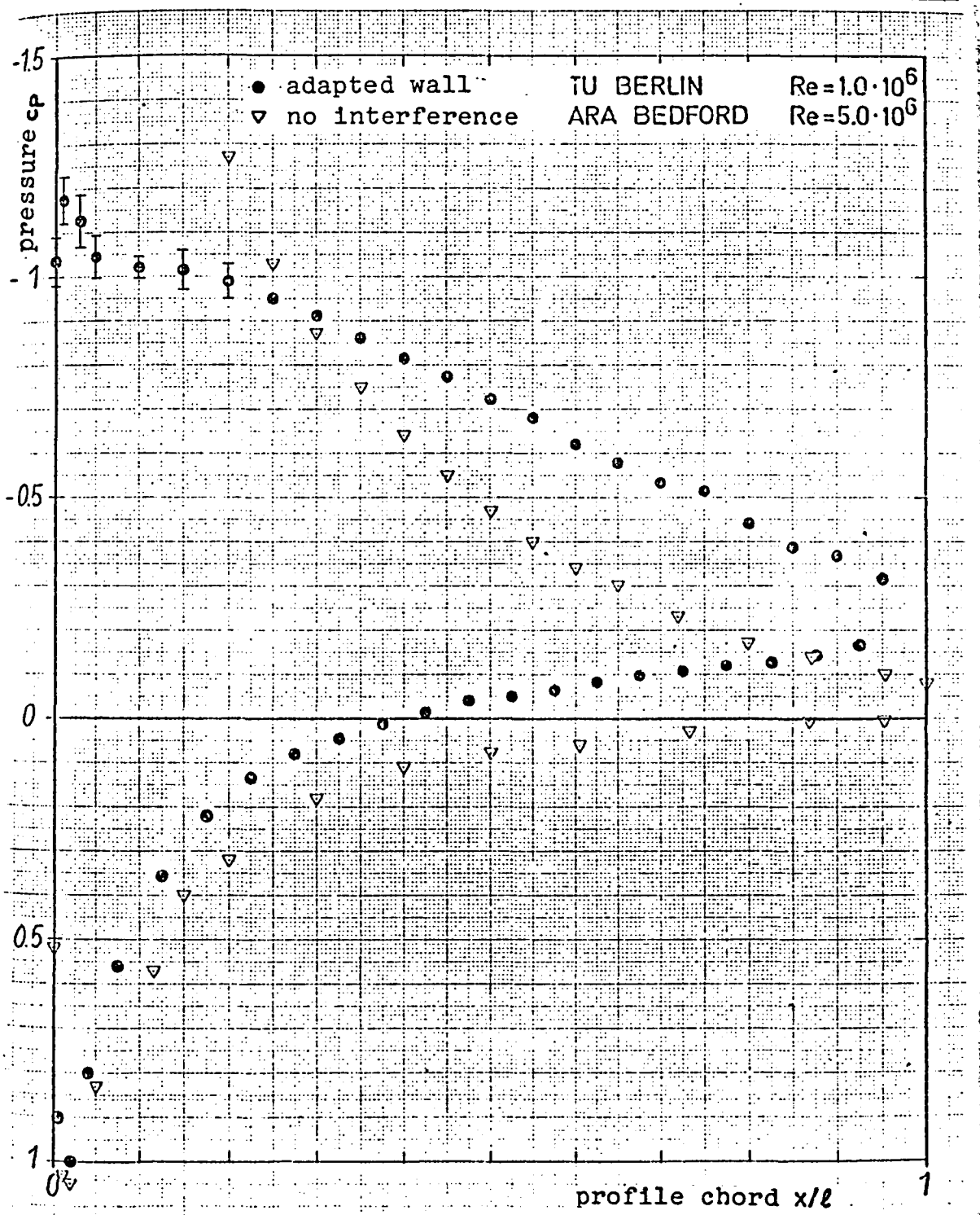

FIGURE 16. PRESSURE DISTRIBUTION FOR NACA 0012 /M=0.50 α=10.668°
FREE BOUNDARY LAYER TRANSITION

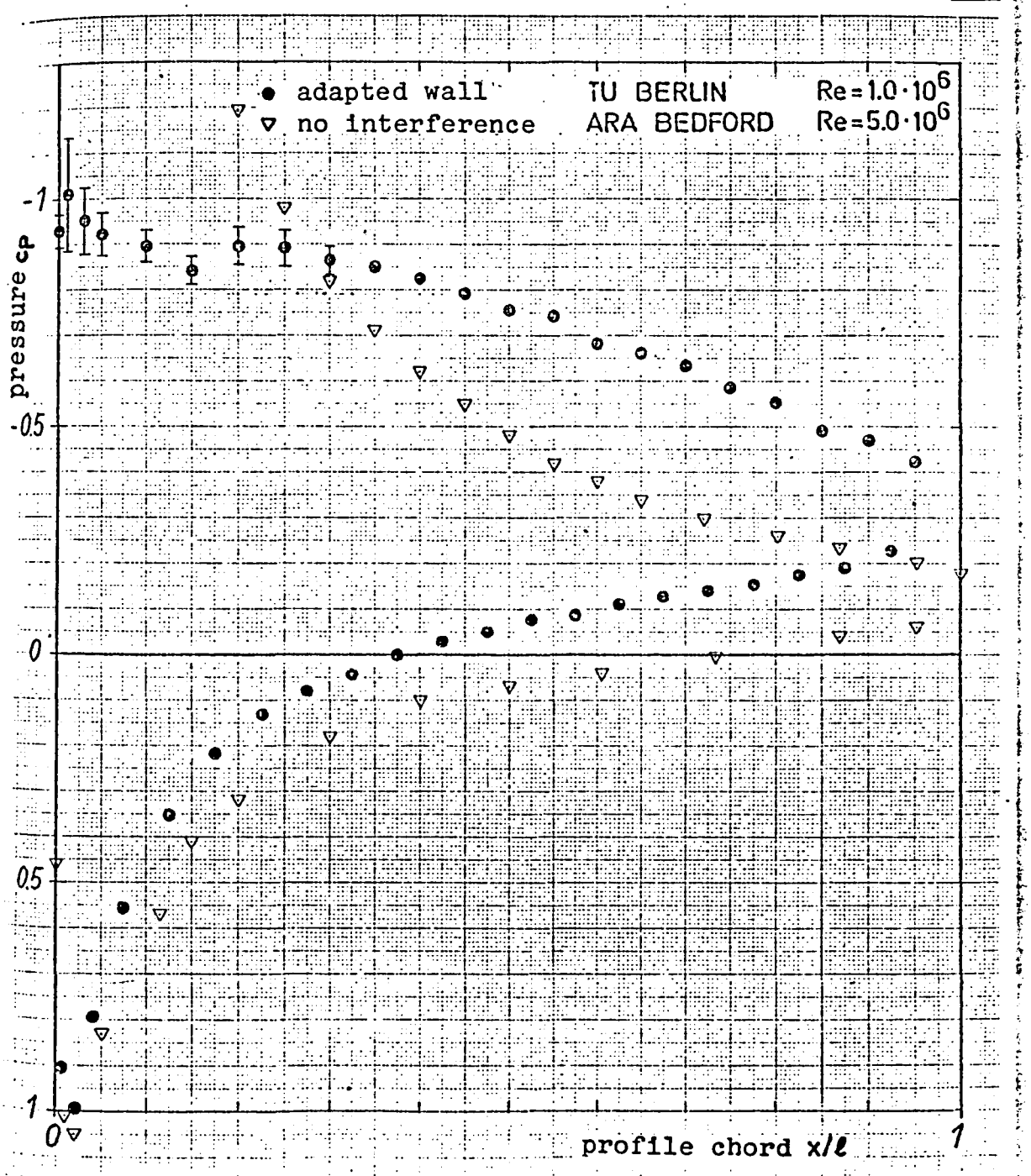

FIGURE 17. PRESSURE DISTRIBUTION FOR NACA 0012 M=0,50 α=11,659°
FREE BOUNDARY LAYER TRANSITION

/36

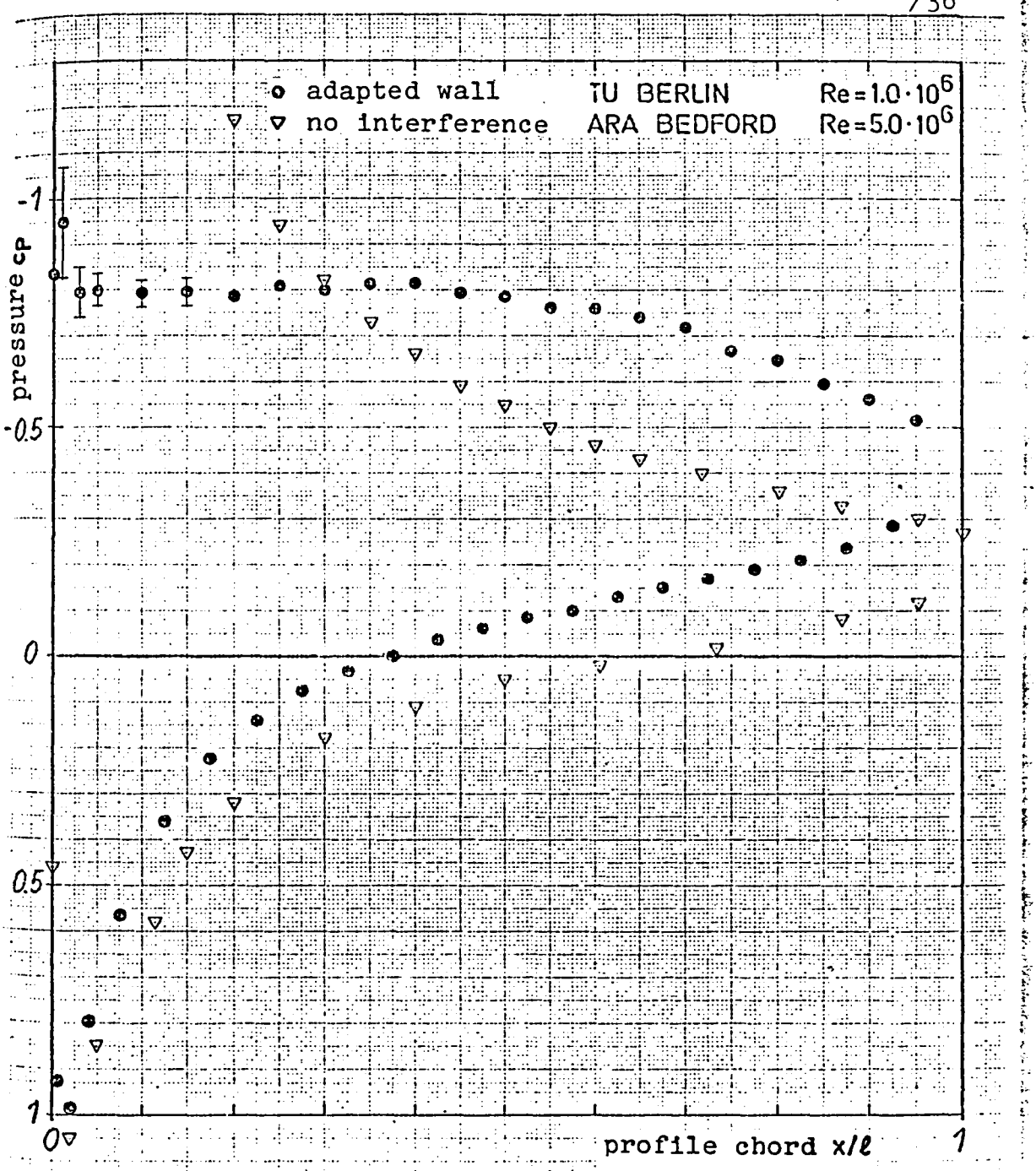

FIGURE 18. PRESSURE DISTRIBUTION FOR NACA 0012 $M_\infty = 0.50$ $\alpha = 12.647°$
FREE BOUNDARY LAYER TRANSITION

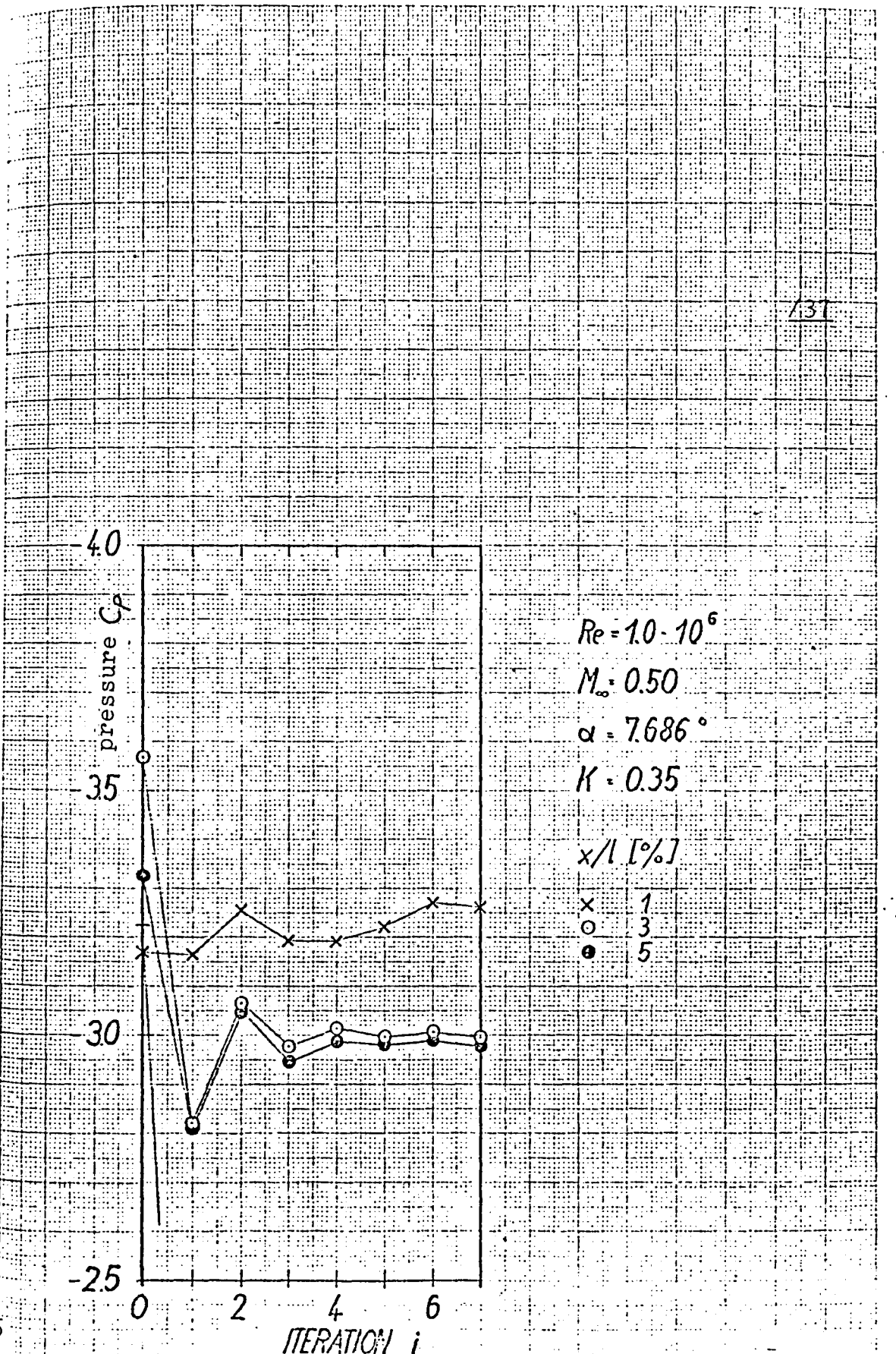

FIGURE 19a. CHANGES IN THE MEASURED PRESSURE COEFFICIENT

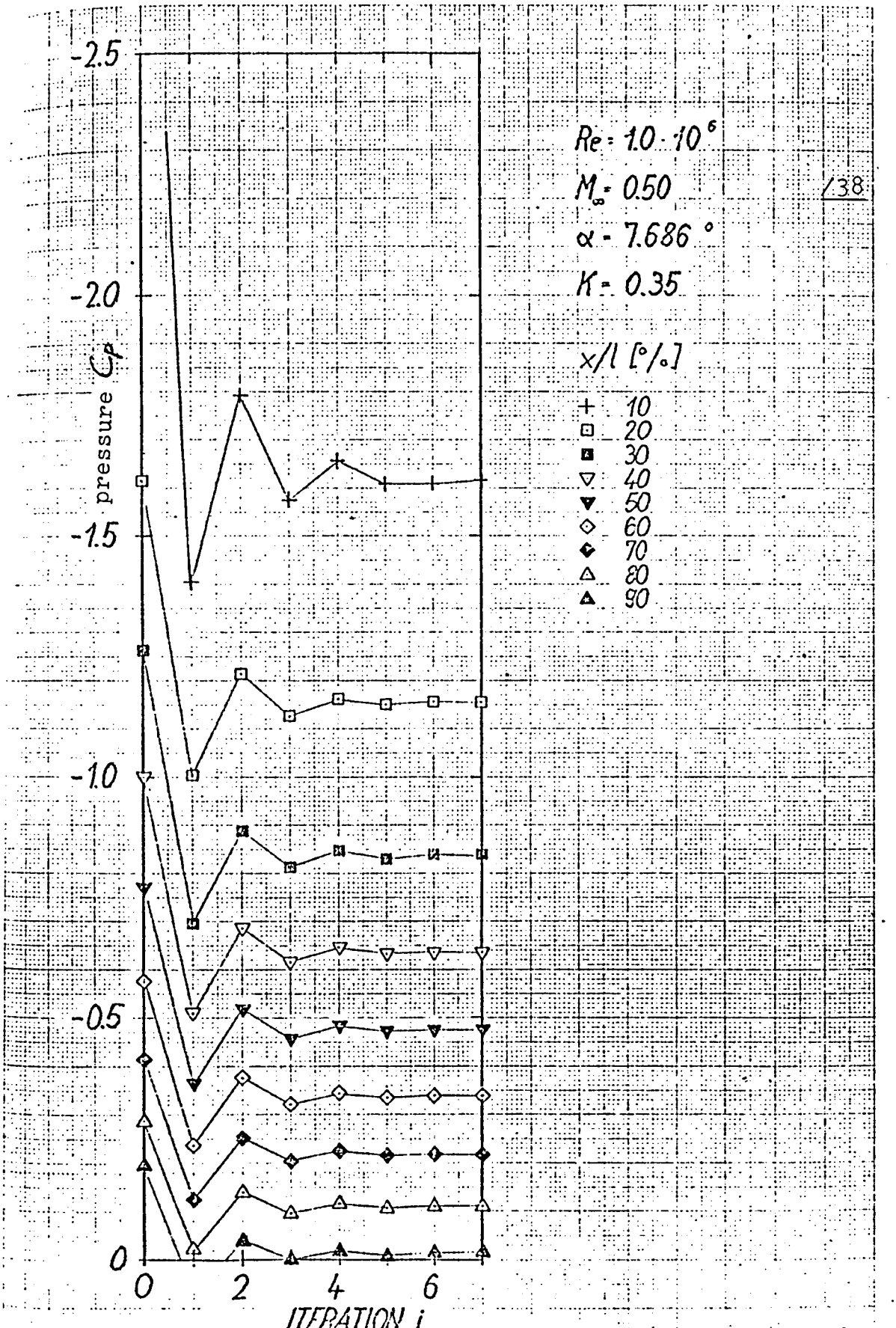

/38

FIGURE 19b. CHANGES IN THE MEASURED PRESSURE COEFFICIENT

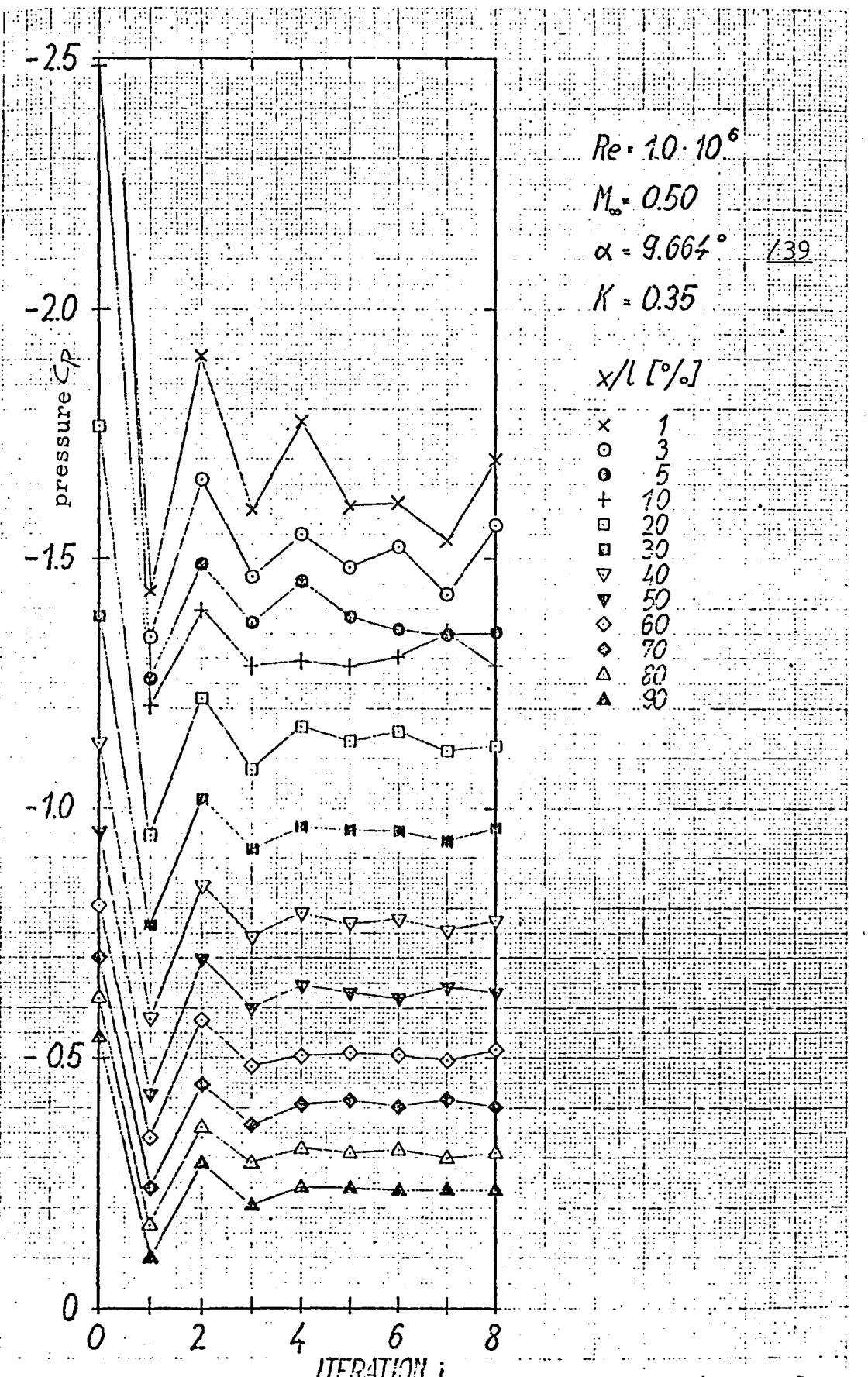

FIGURE 20. CHANGES IN THE MEASURED PRESSURE COEFFICIENT

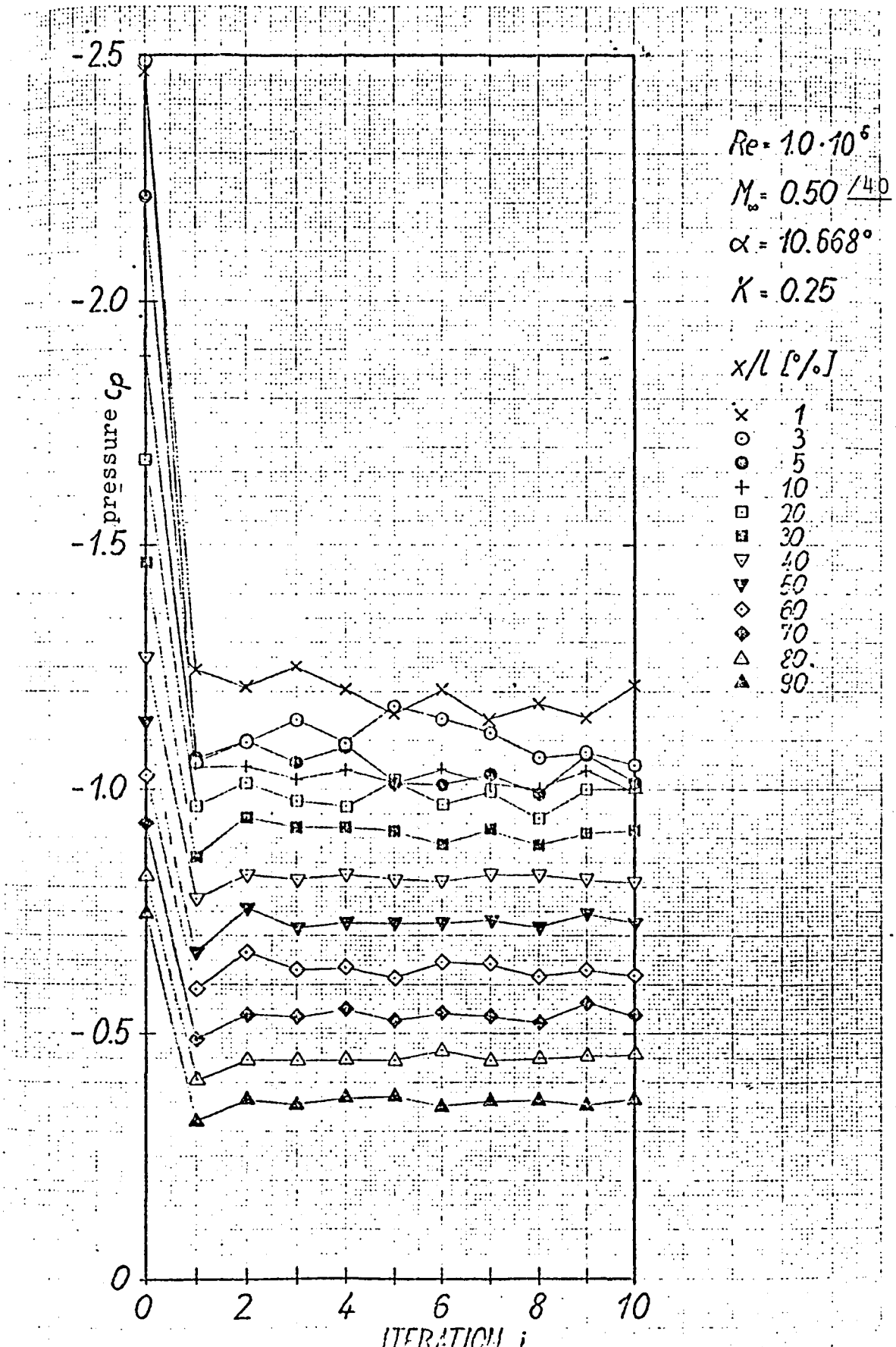

FIGURE 21. CHANGES IN THE MEASURED PRESSURE COEFFICIENT

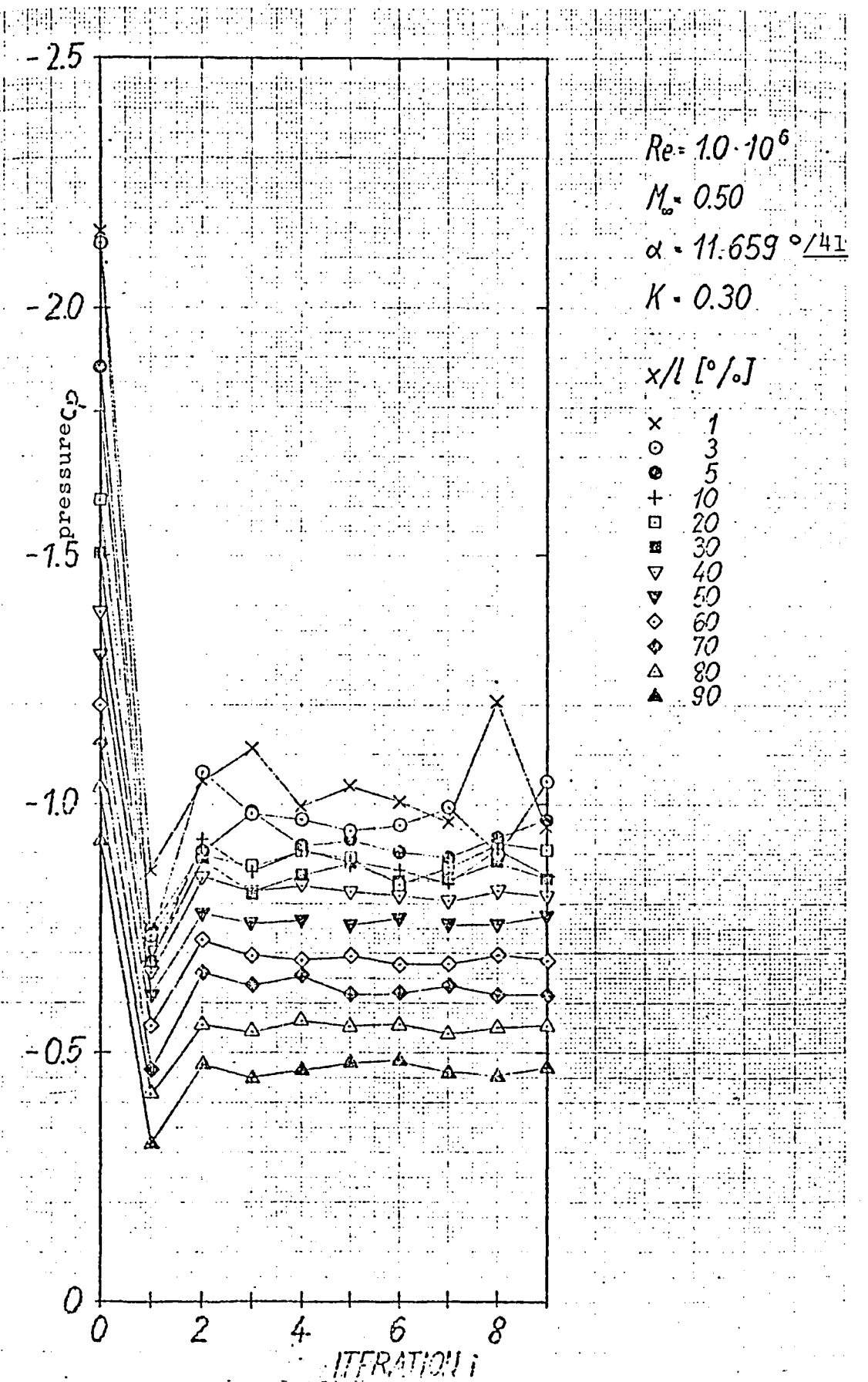

FIGURE 22. CHANGES IN THE MEASURED PRESSURE COEFFICIENT

40

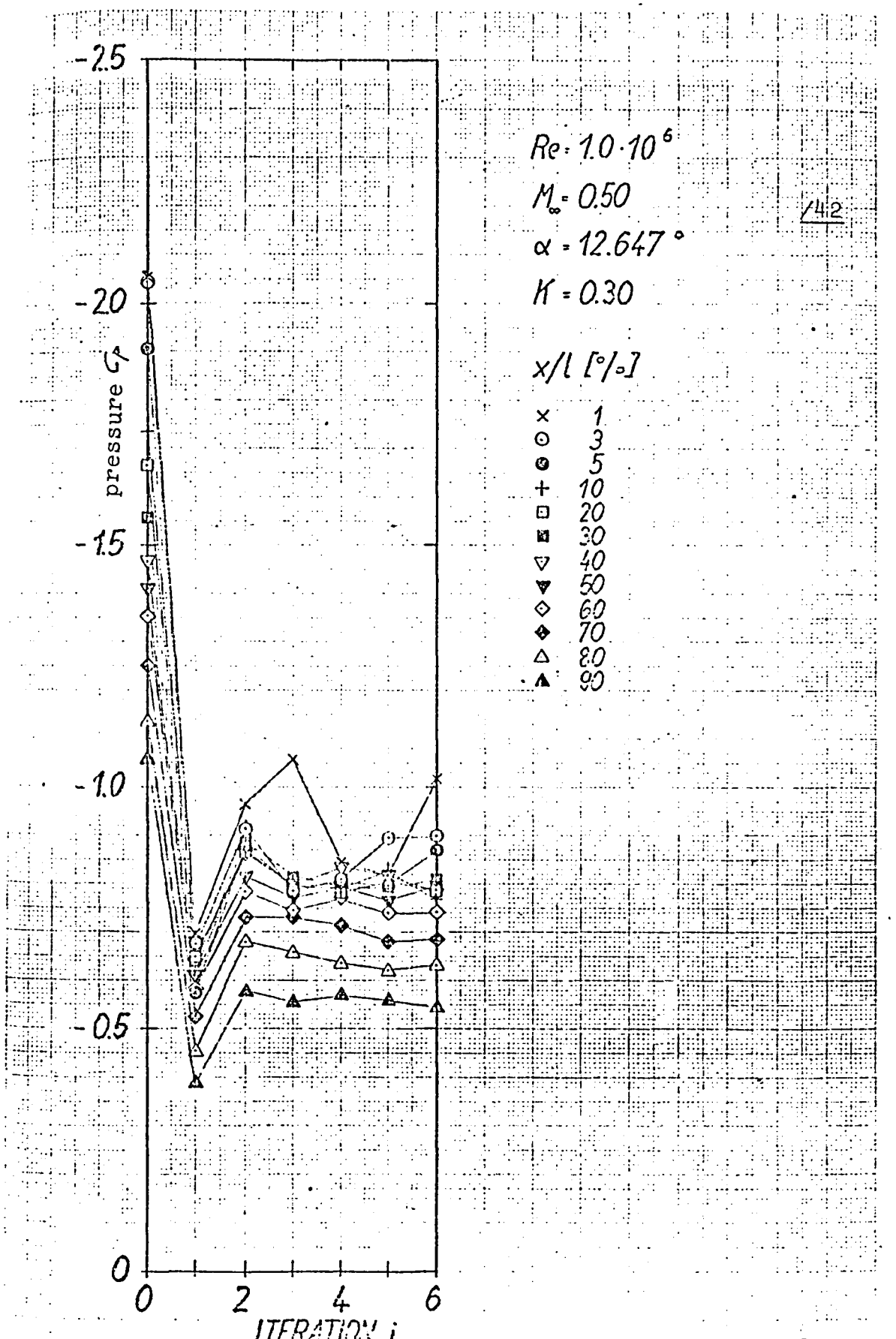

FIGURE 23. CHANGES IN THE MEASURED PRESSURE COEFFICIENT

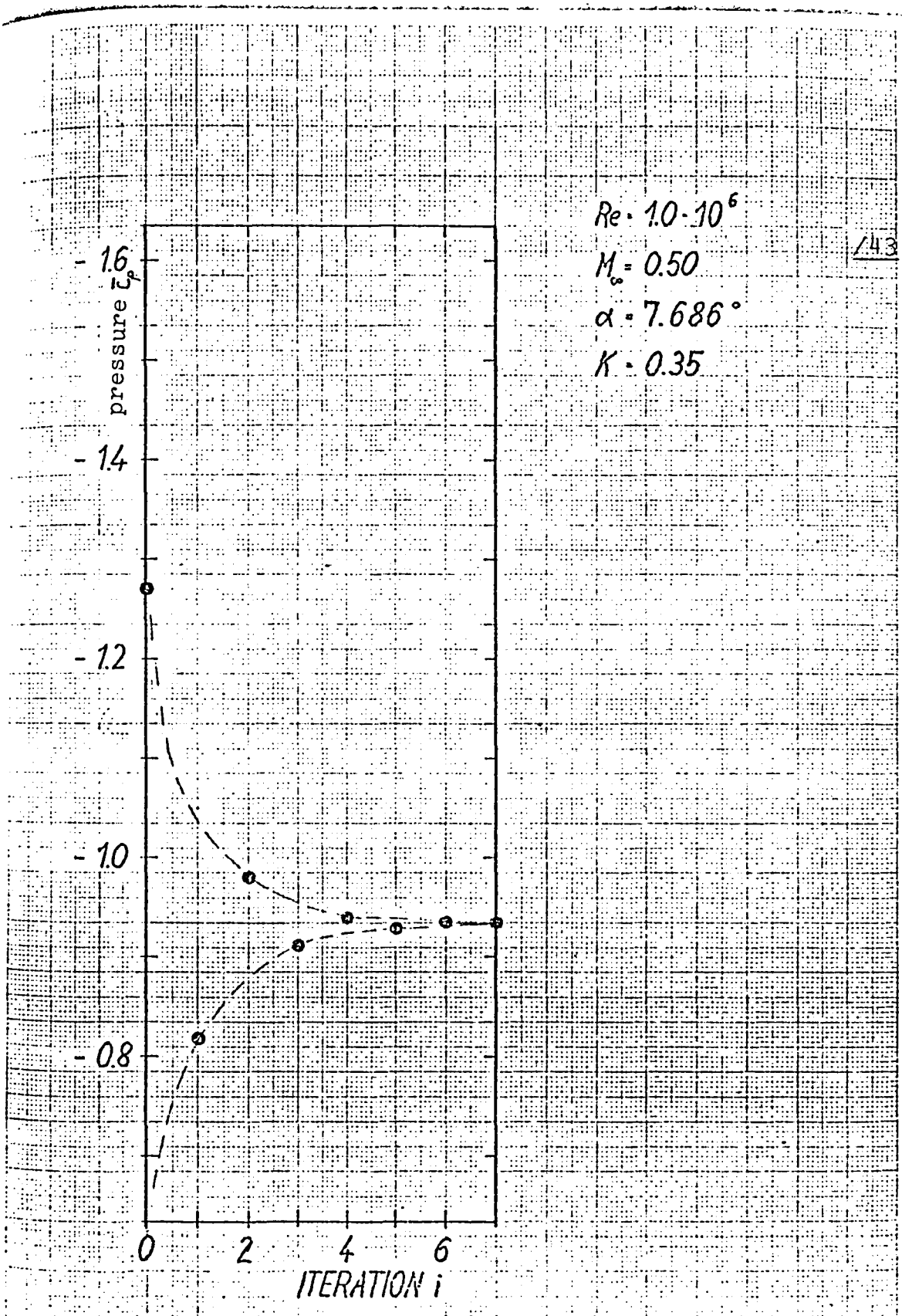

FIGURE 24. CHANGE IN THE AVERAGE PRESSURE COEFFICIENT

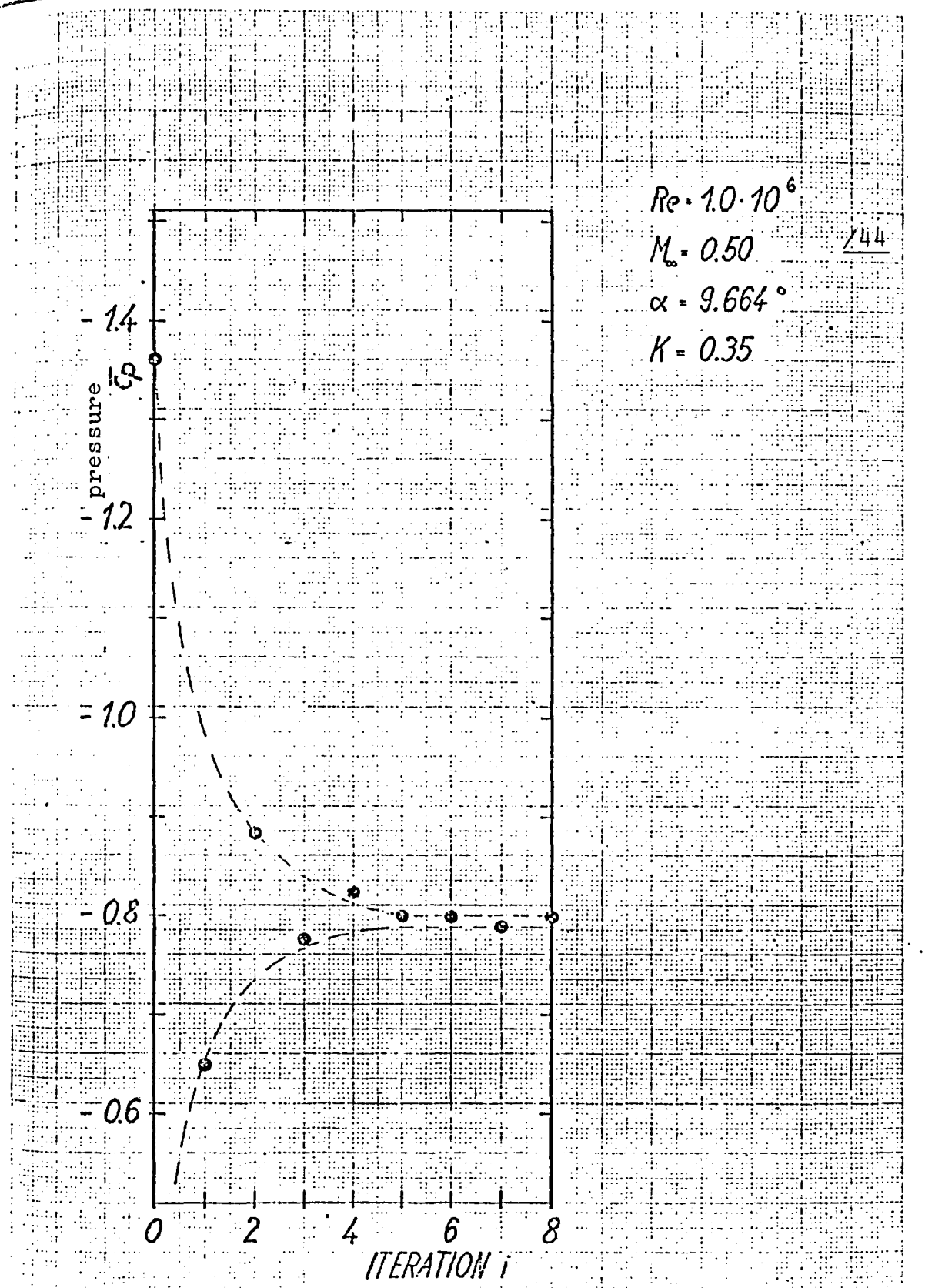

FIGURE 25. CHANGE IN THE AVERAGE PRESSURE COEFFICIENT

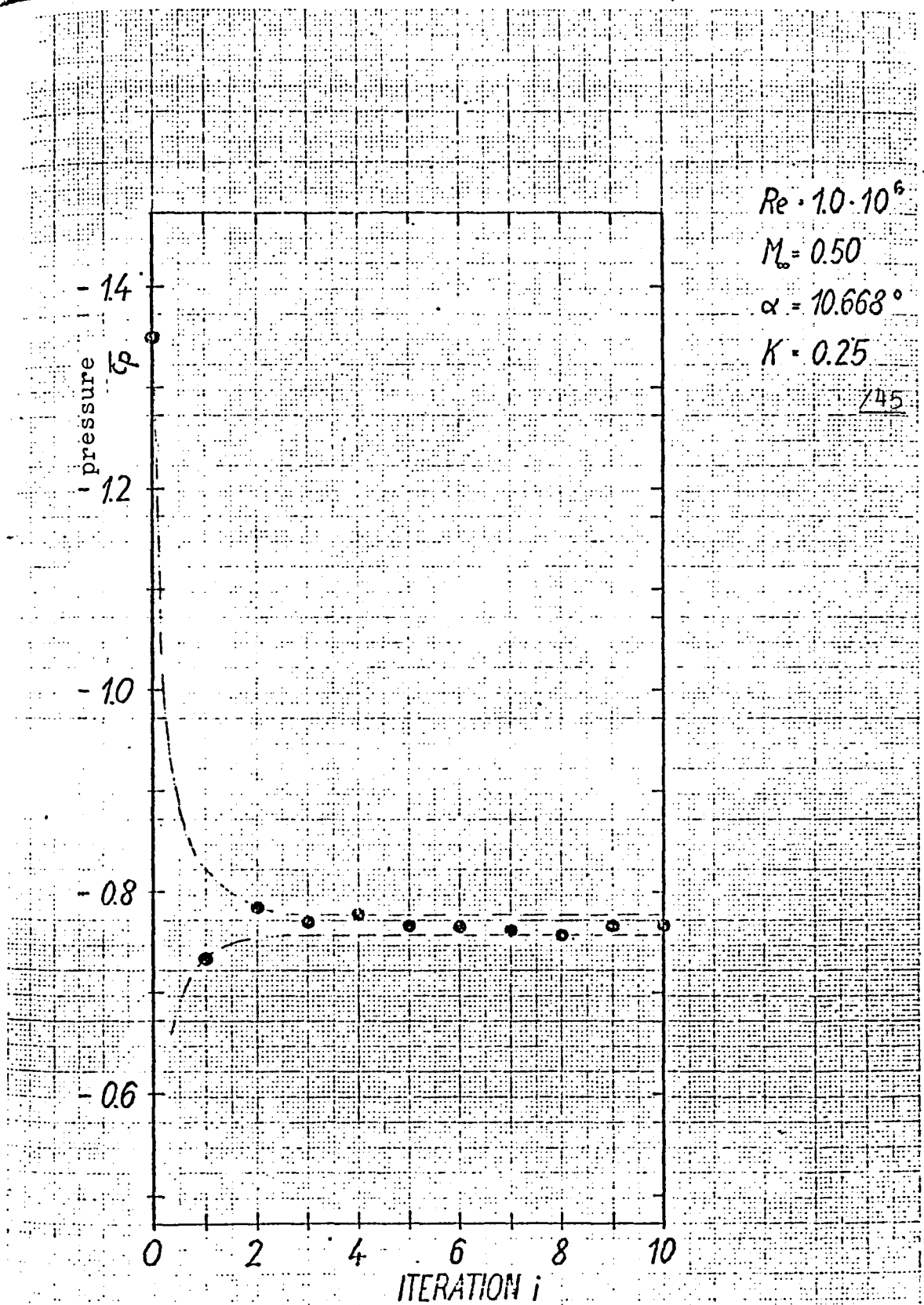

FIGURE 26. CHANGE IN THE AVERAGE PRESSURE COEFFICIENT

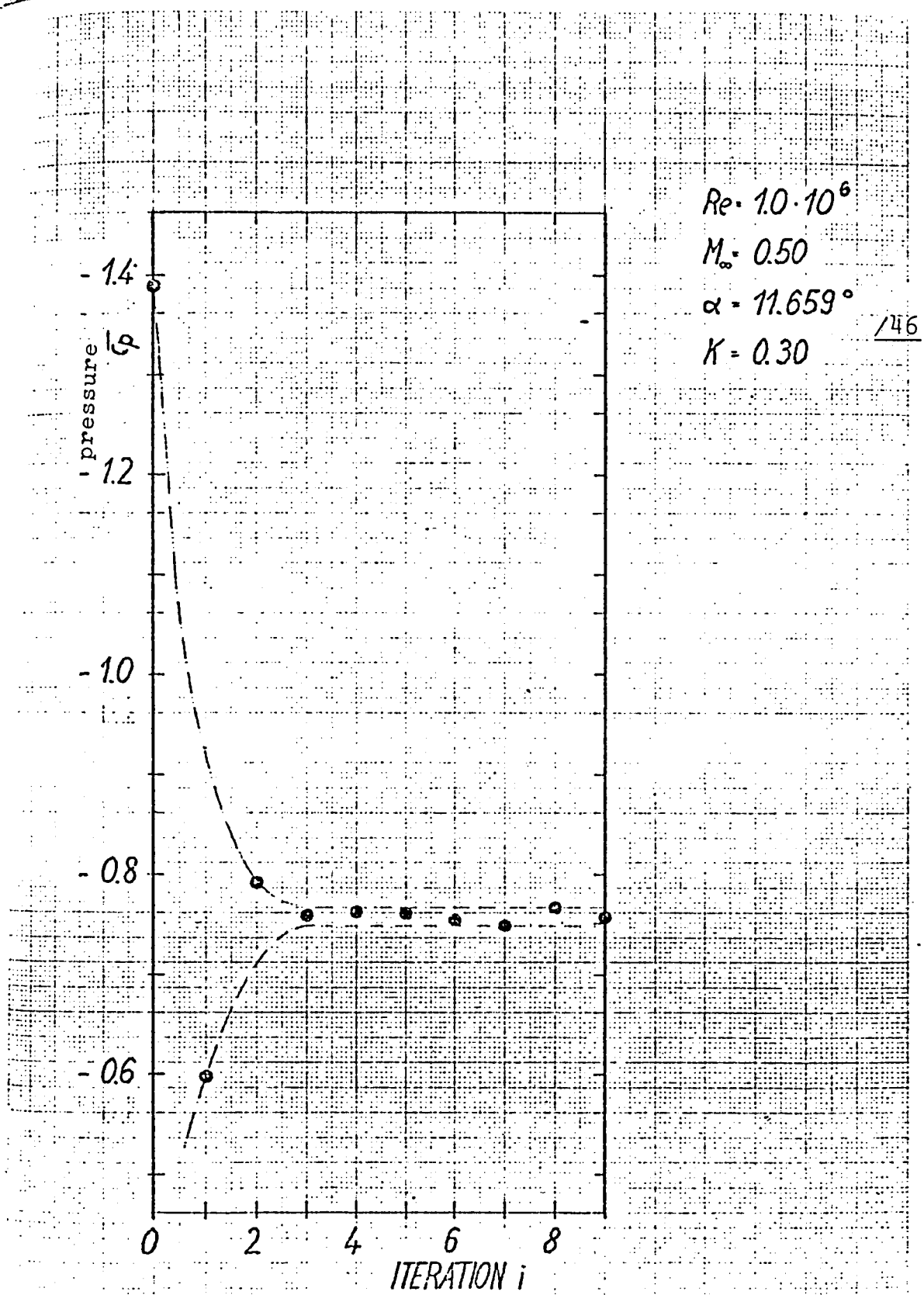

FIGURE 27. CHANGE IN THE AVERAGE PRESSURE COEFFICIENT

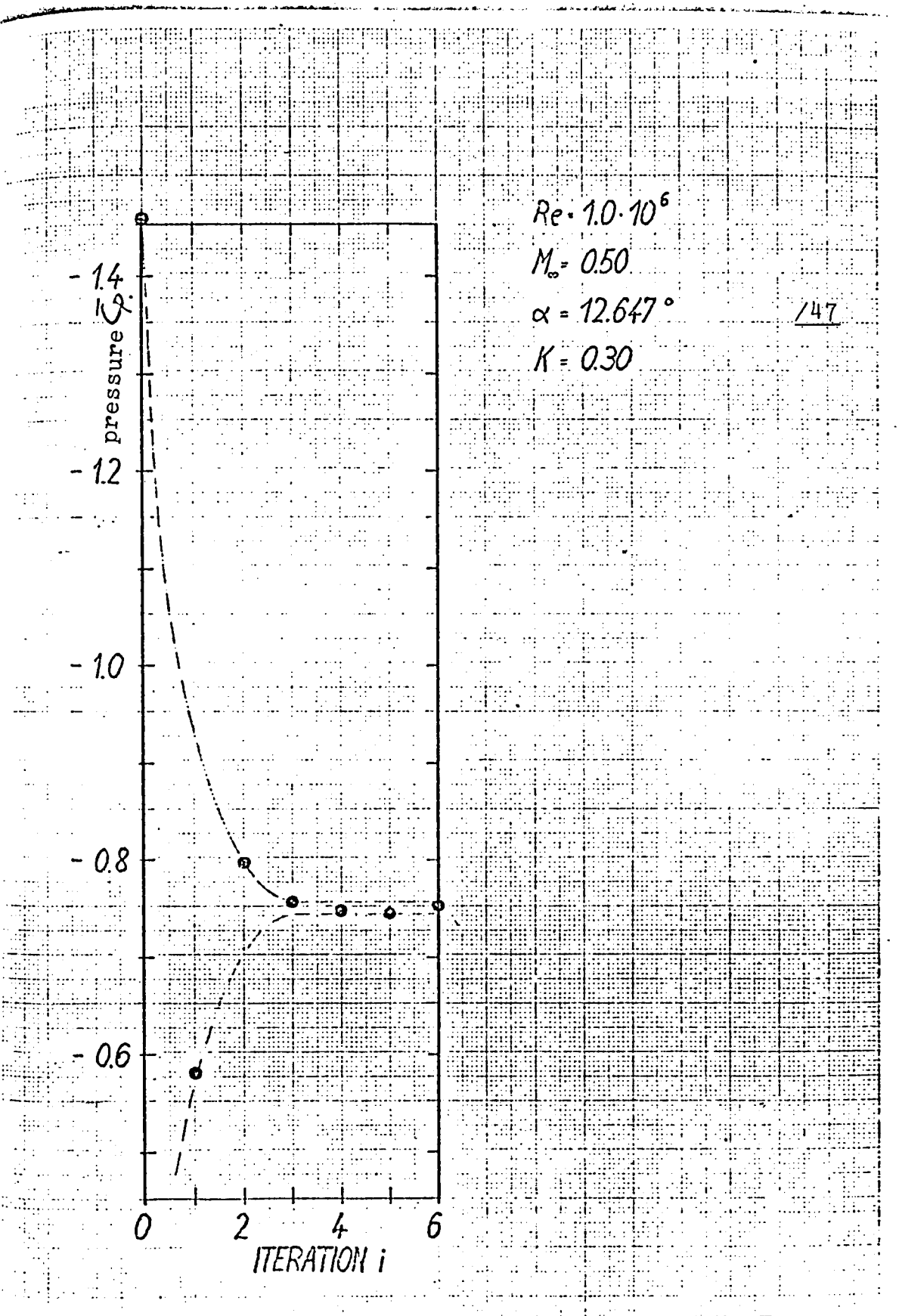

FIGURE 28. CHANGE IN THE AVERAGE PRESSURE COEFFICIENT

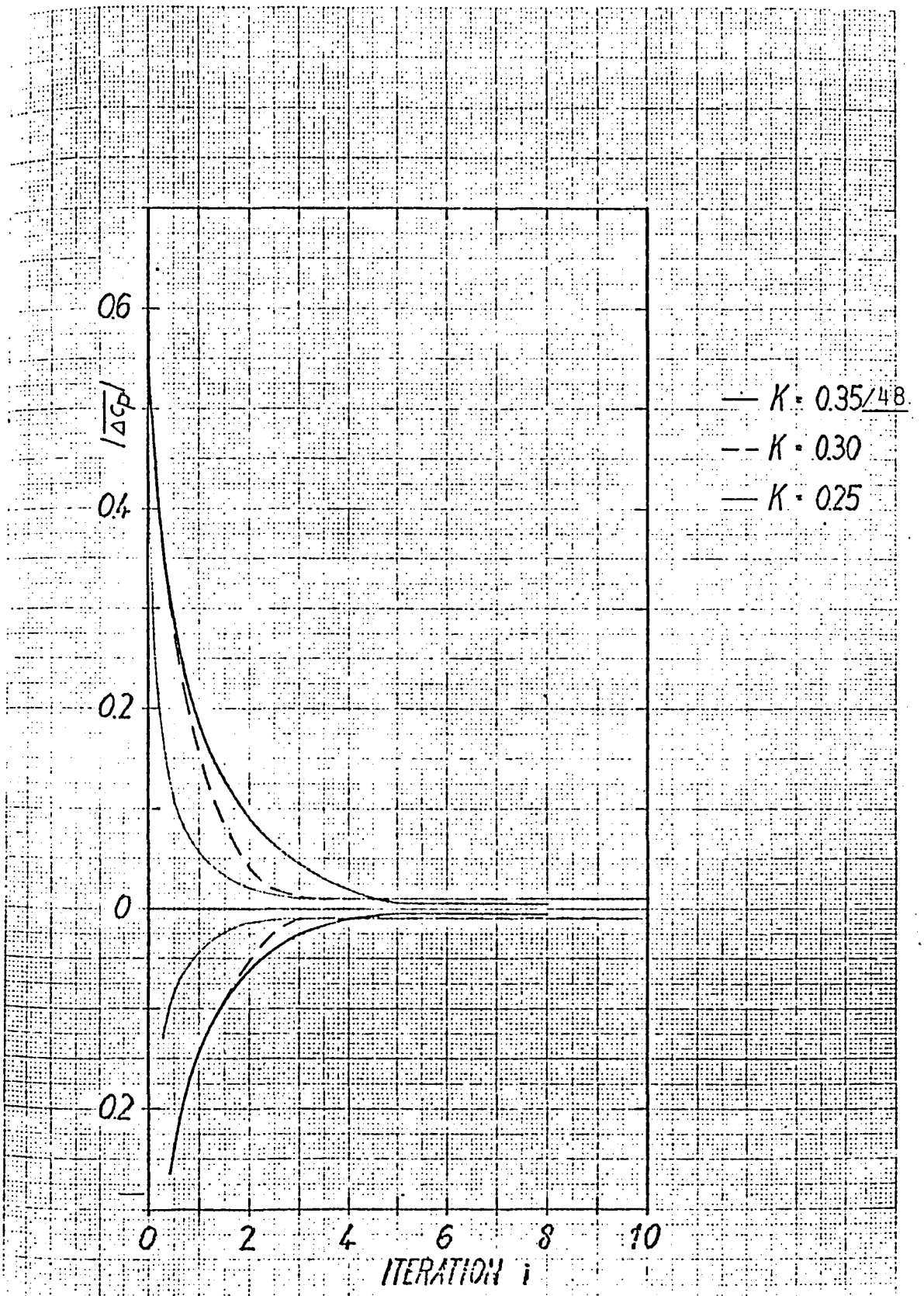

FIGURE 29. CONVERGENCE CURVE.

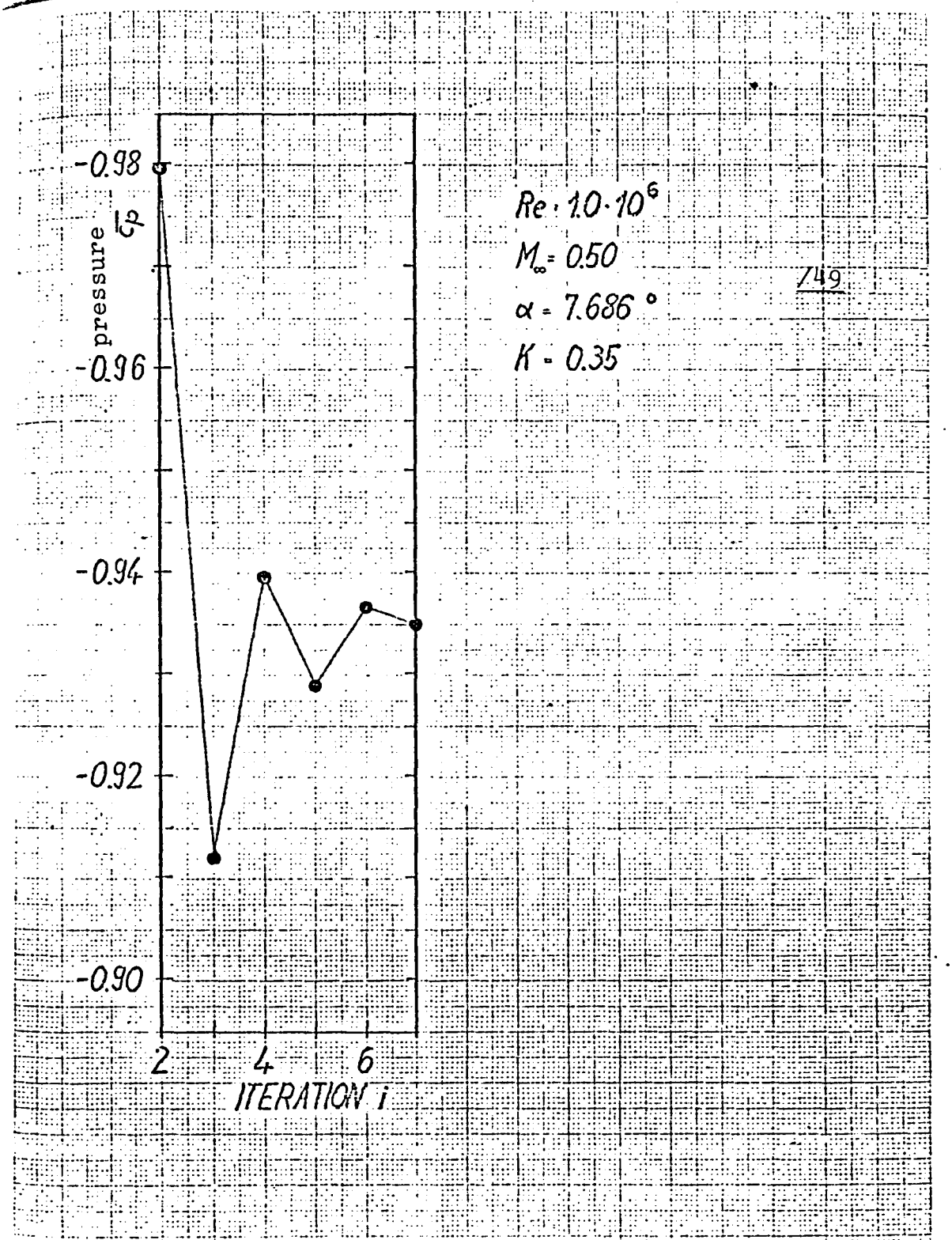

FIGURE 30. CHANGE IN THE AVERAGE PRESSURE COEFFICIENT

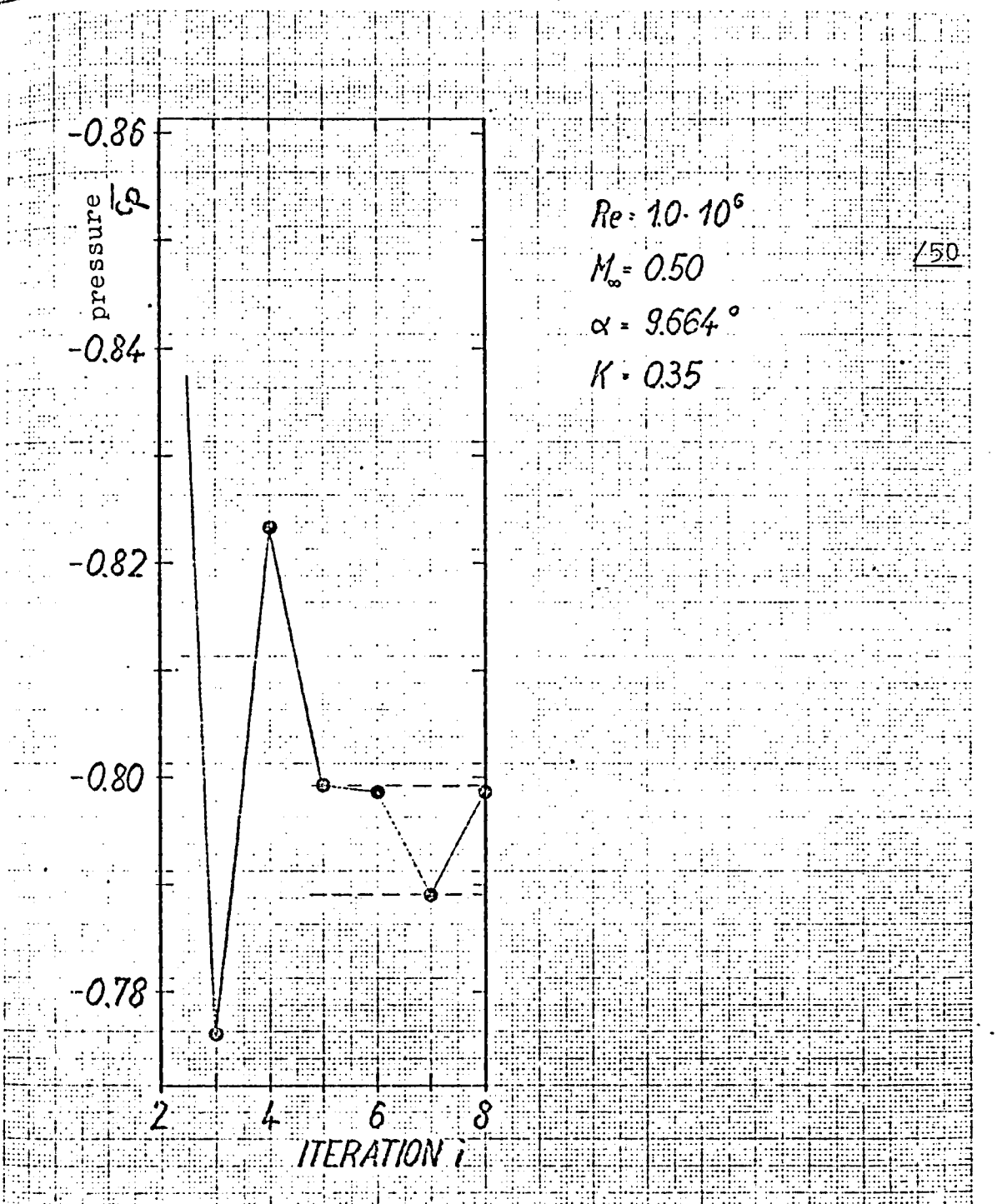

FIGURE 31. CHANGE IN THE AVERAGE PRESSURE COEFFICIENT

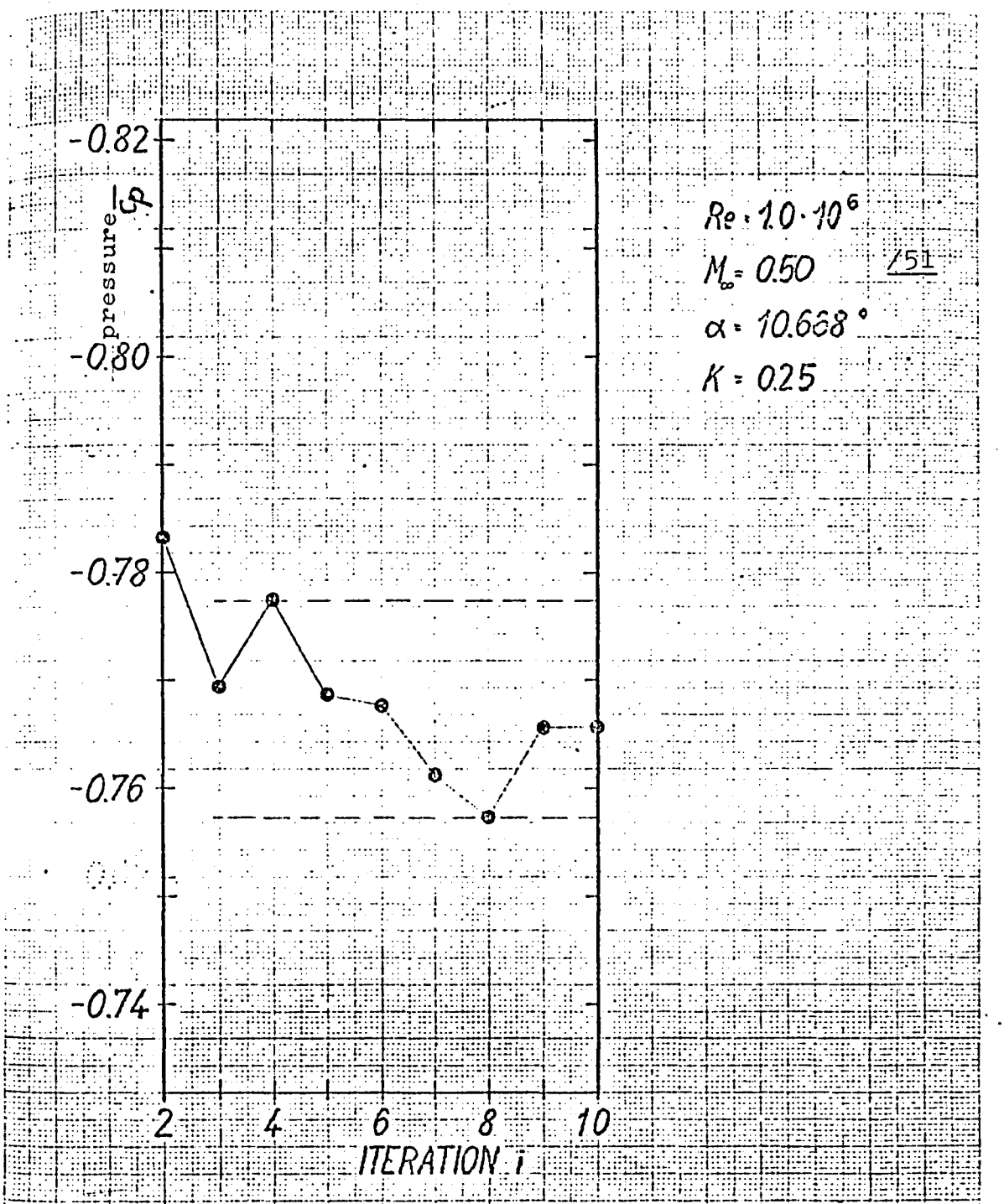

FIGURE 32. CHANGE IN THE AVERAGE PRESSURE COEFFICIENT

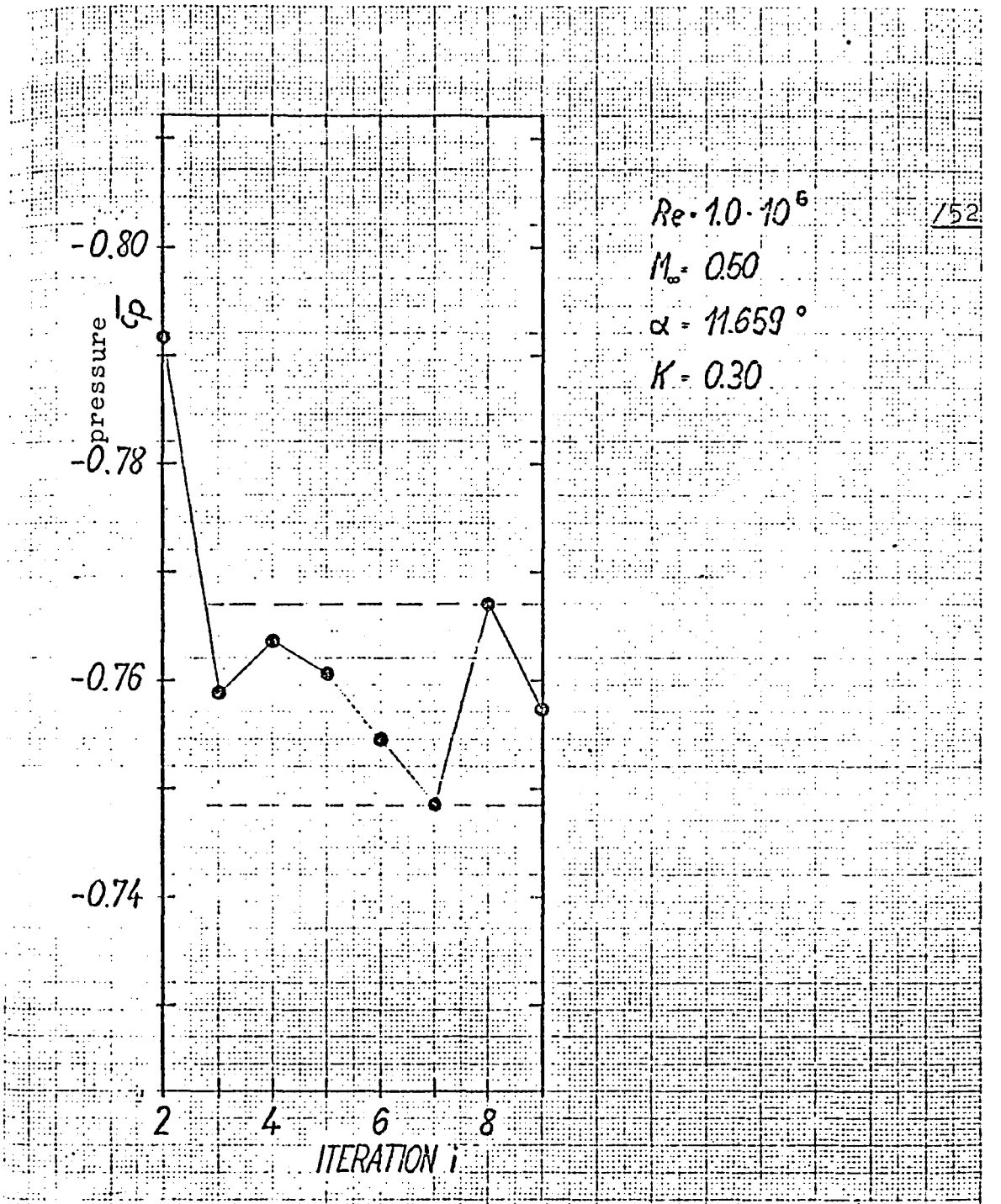

FIGURE 33. CHANGE IN THE AVERAGE PRESSURE COEFFICIENT

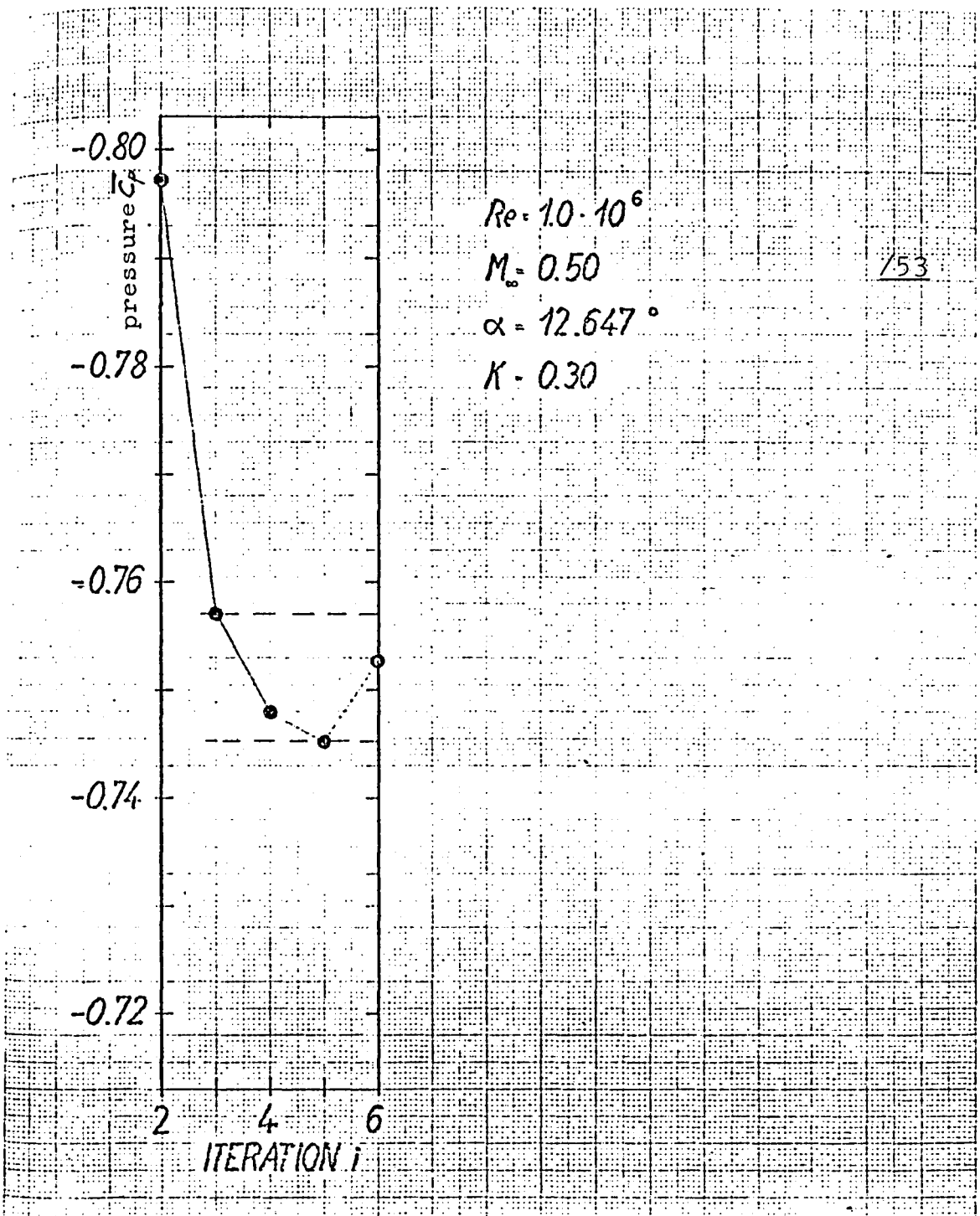

FIGURE 34. CHANGE IN THE AVERAGE PRESSURE COEFFICIENT

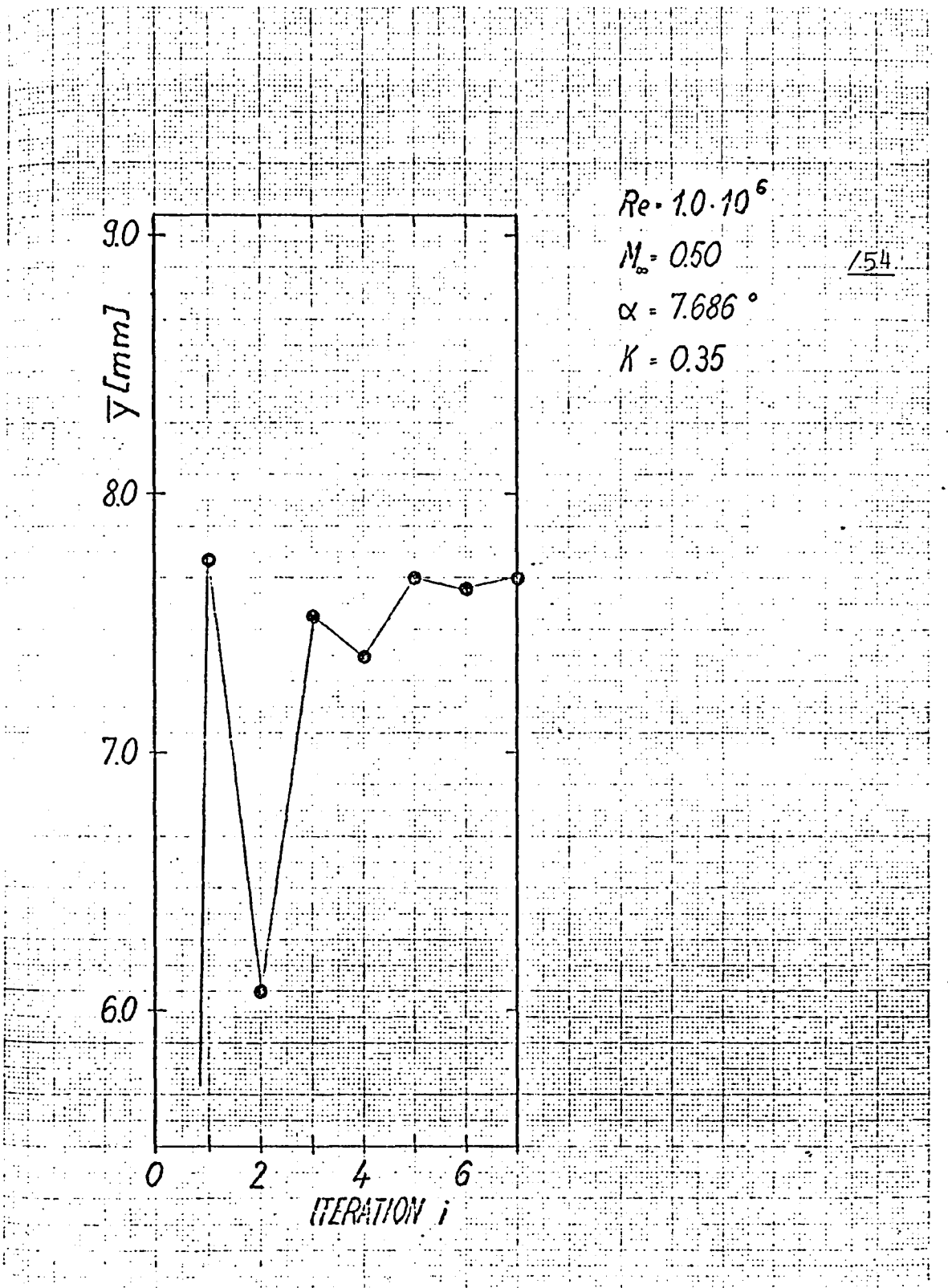

FIGURE 35. CHANGE IN THE AVERAGE WALL DEFLECTION

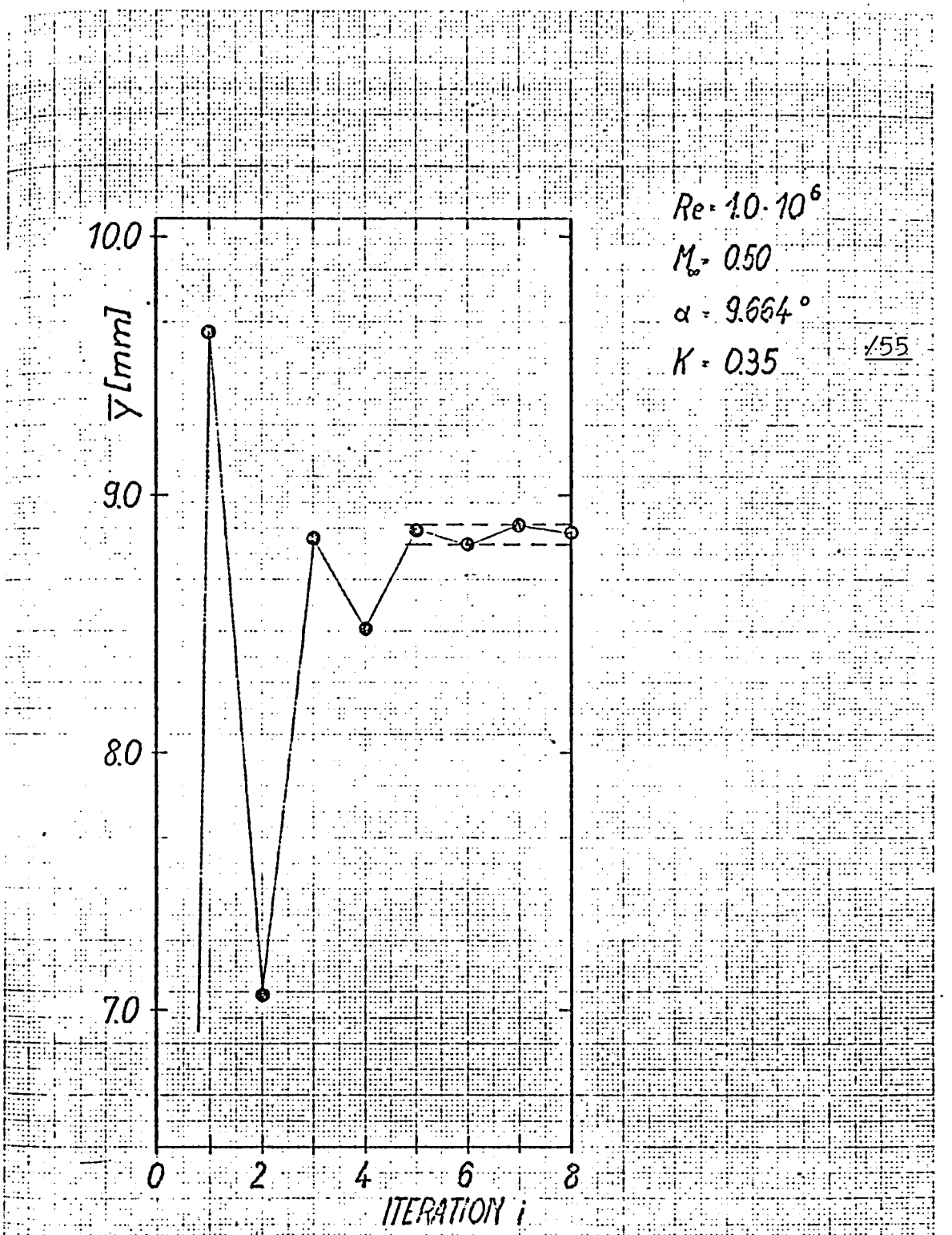

FIGURE 36. CHANGE IN THE AVERAGE WALL DEFLECTION

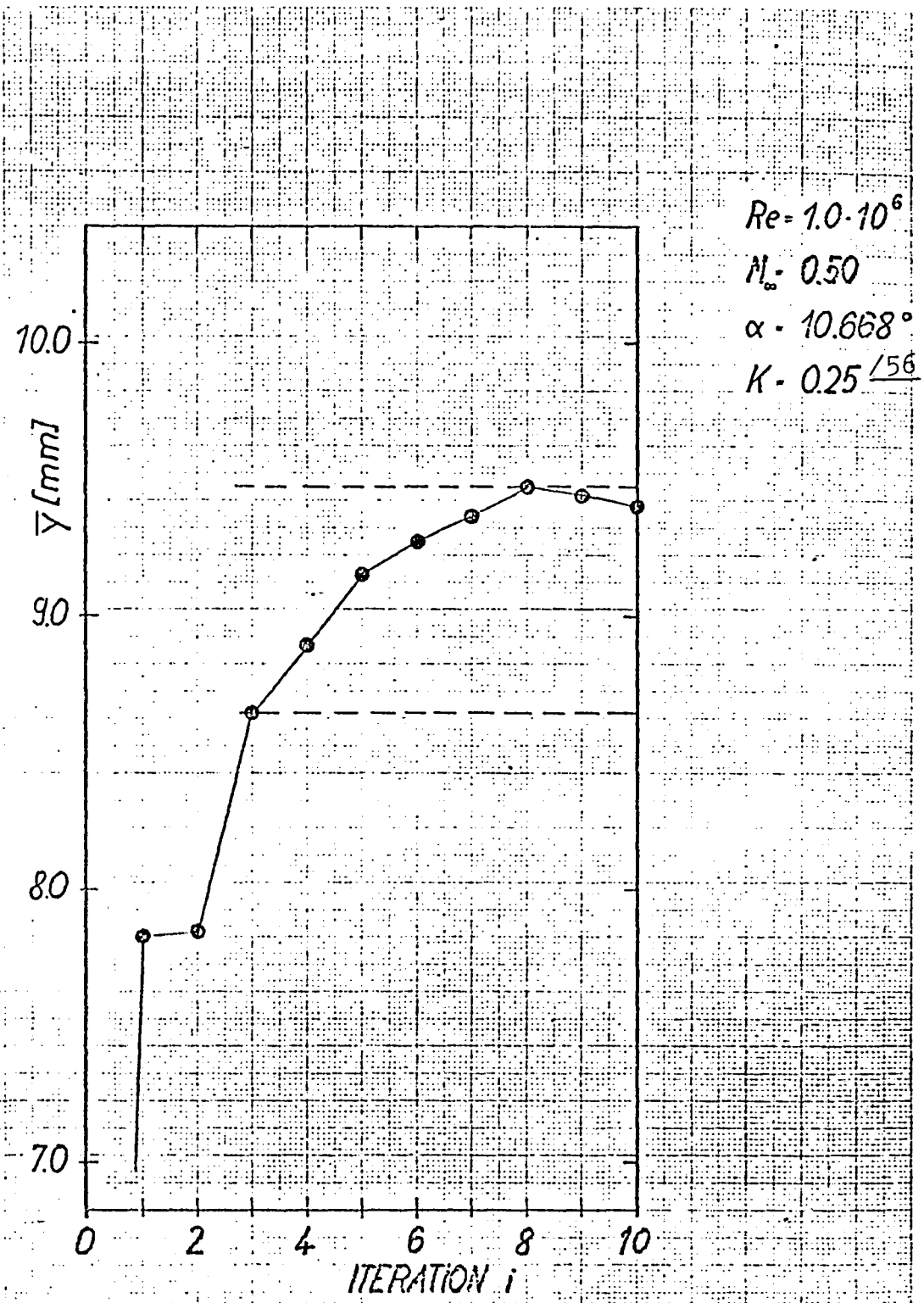

FIGURE 37. CHANGE IN THE AVERAGE WALL DEFLECTION

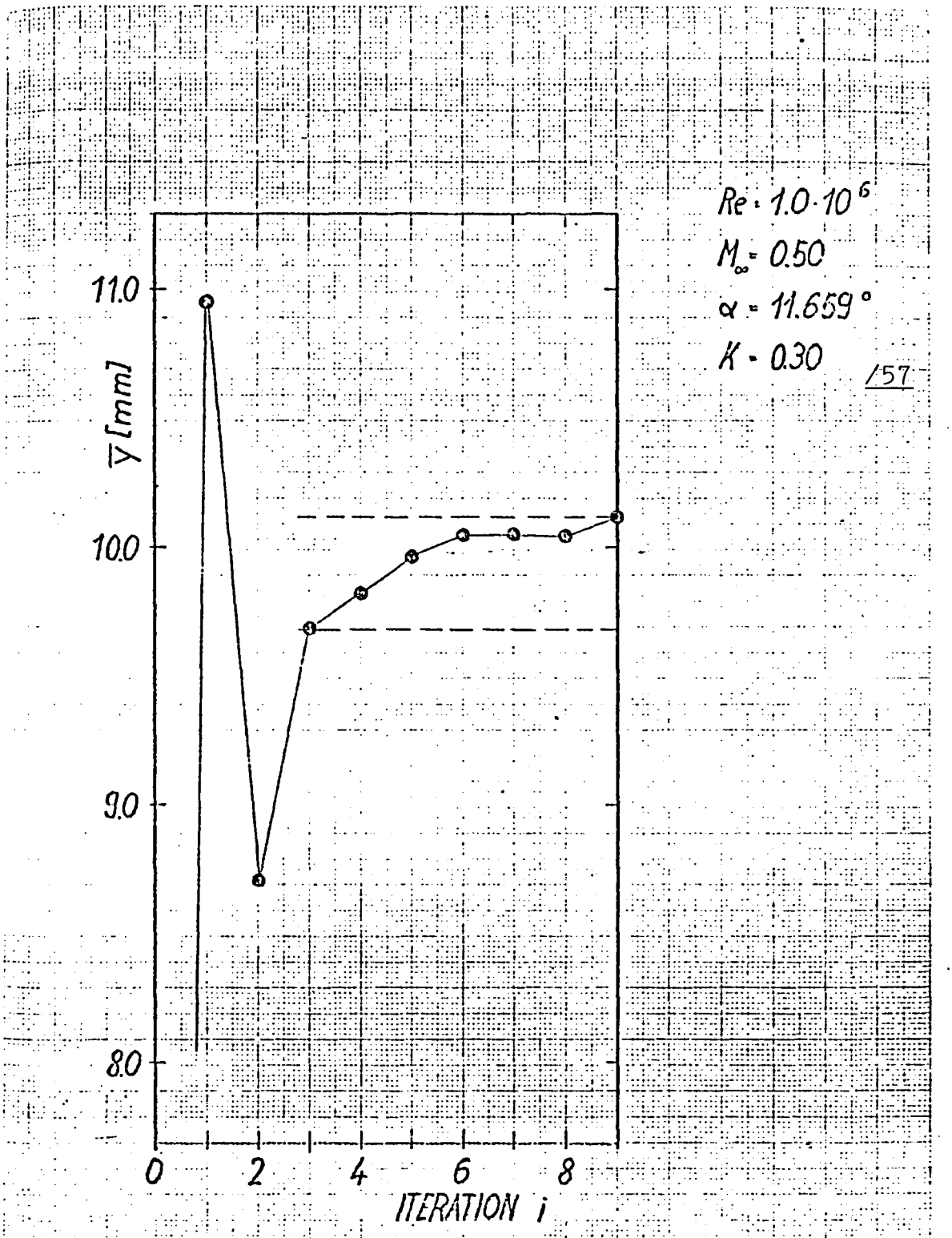

FIGURE 38. CHANGE IN THE AVERAGE WALL DEFLECTION

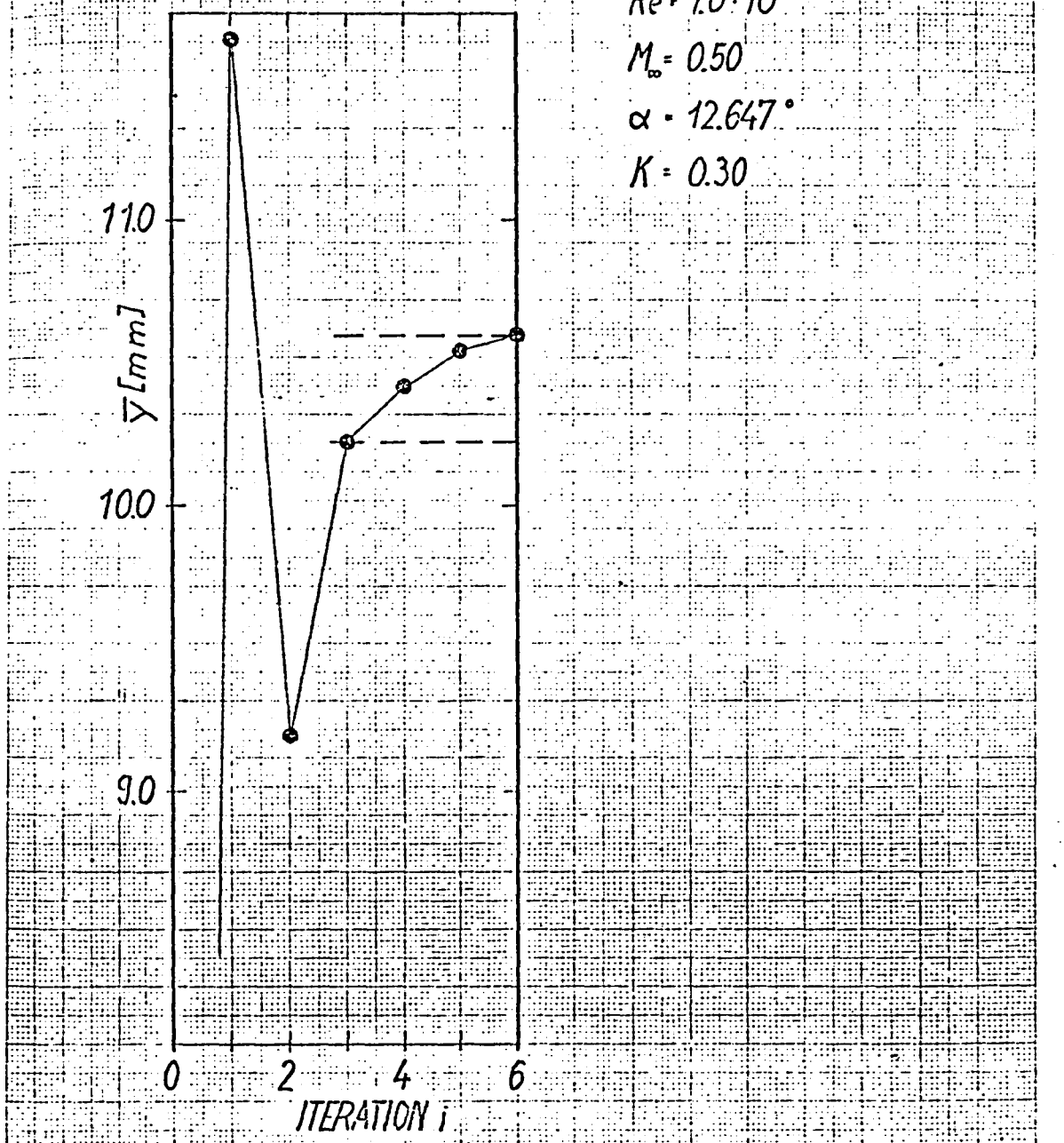

FIGURE 39. CHANGE IN THE AVERAGE WALL DEFLECTION

/59

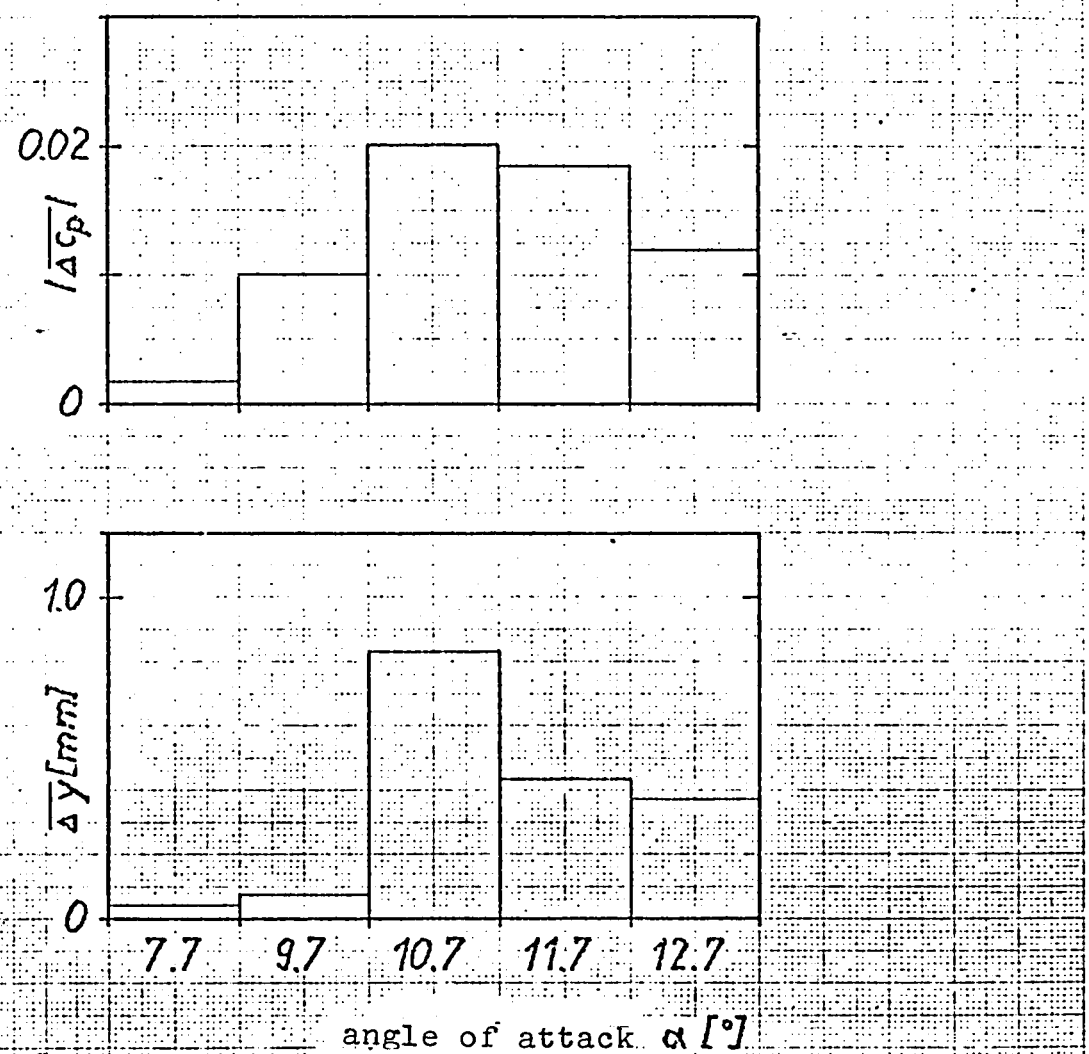

FIGURE 40. RESIDUAL FLUCTUATIONS OF PRESSURE AND CORRESPONDING WALL DISPLACEMENTS

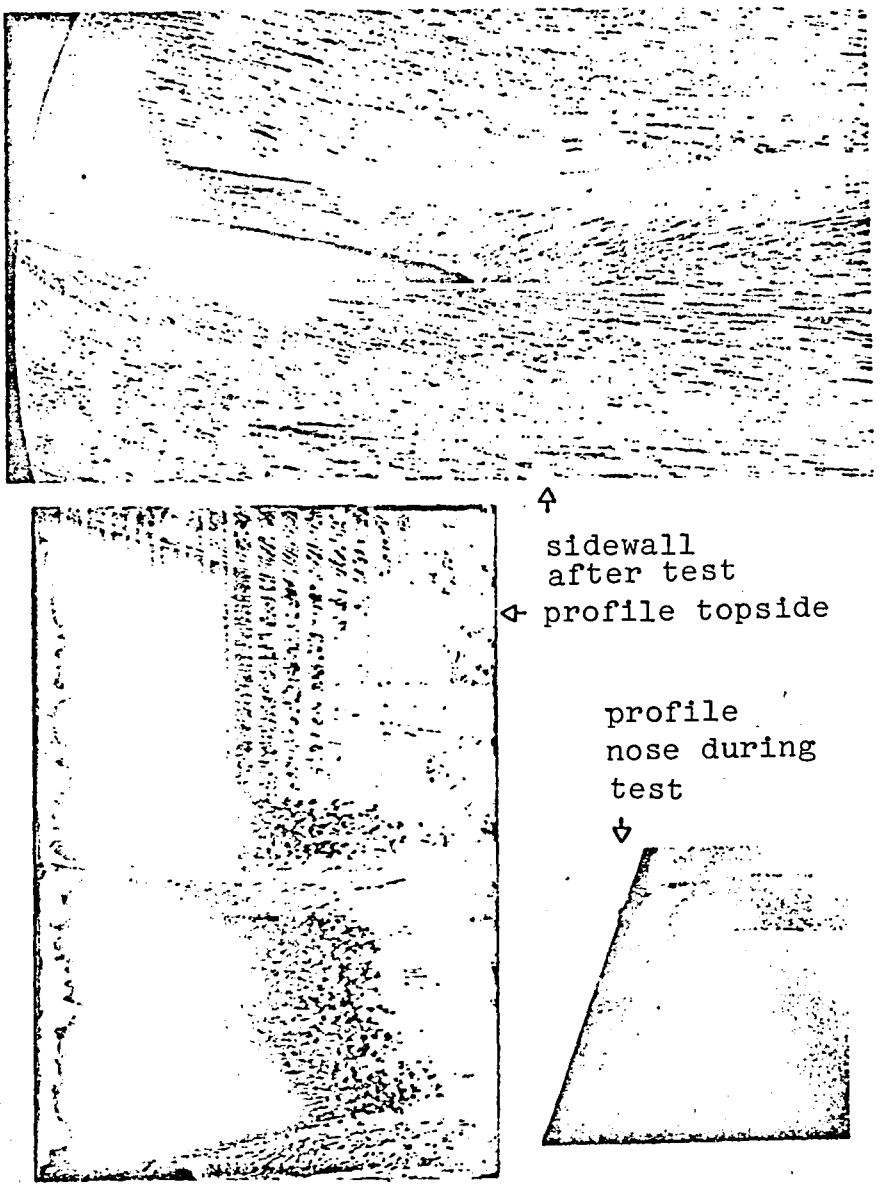

OIL FILM PHOTOGRAPHS
WITHOUT ROUGHNESS
ADAPTIVE WALL

NACA 0012
$Re = 1.0 \cdot 10^6$
$M_\infty = 0.50$ $\alpha = 7.686°$

FIGURE 41

/61

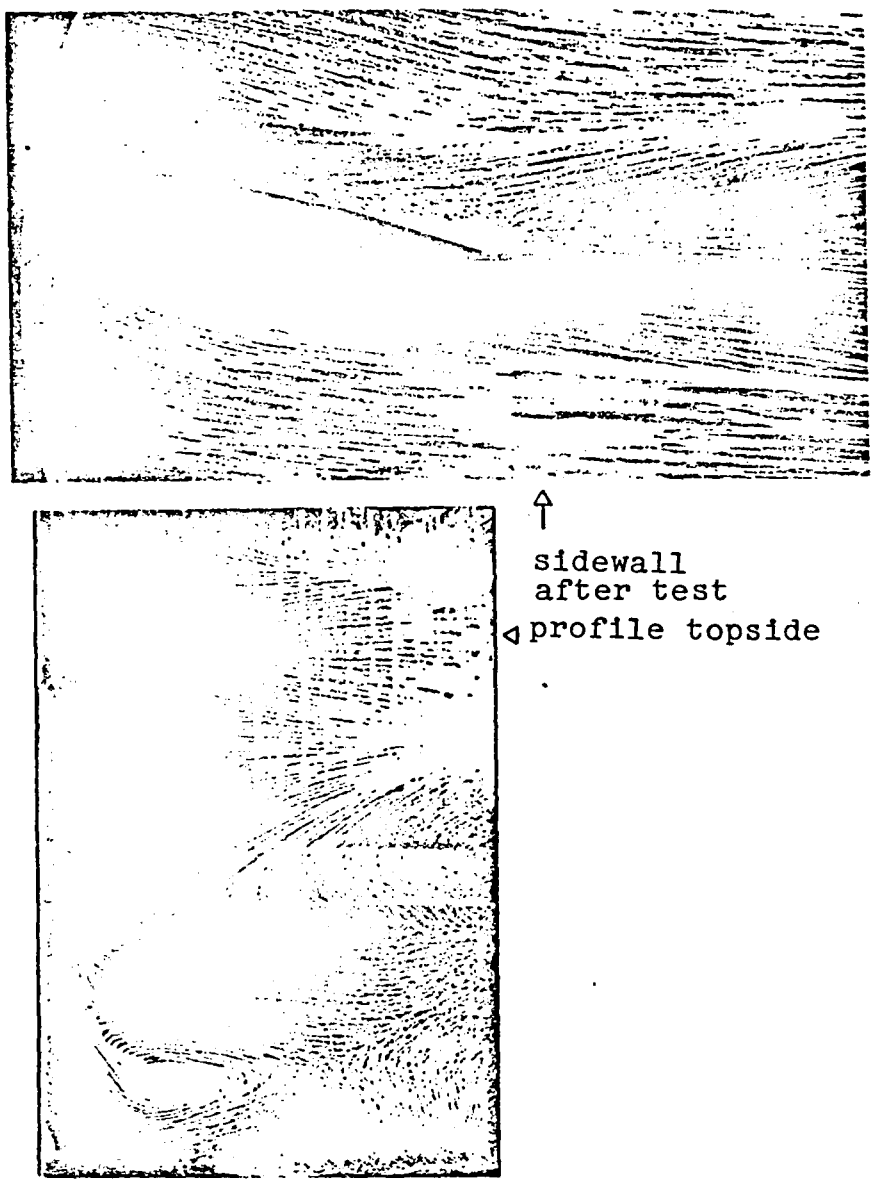

OIL FILM PHOTOGRAPH
WITHOUT ROUGHNESS
ADAPTIVE WALL

NACA 0012
$Re = 1.0 \cdot 10^6$
$M_\infty = 0.50$ $\alpha = 9.664°$

FIGURE 42

/62

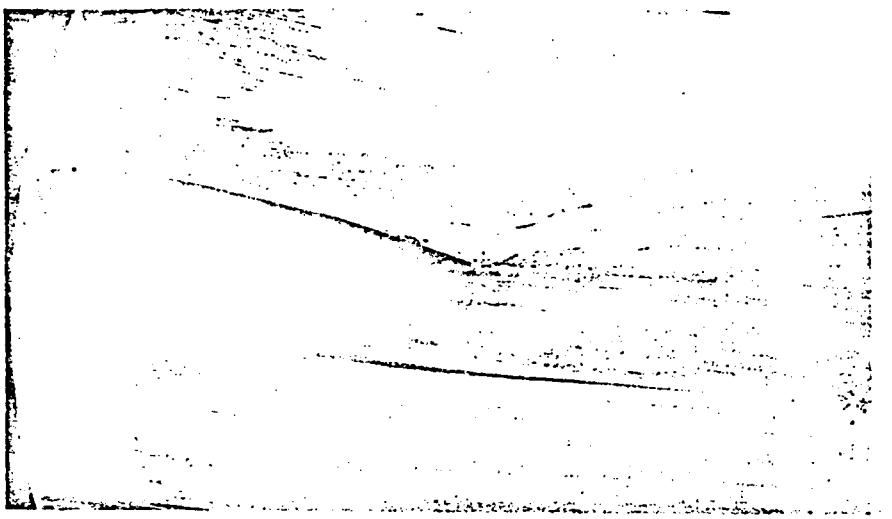

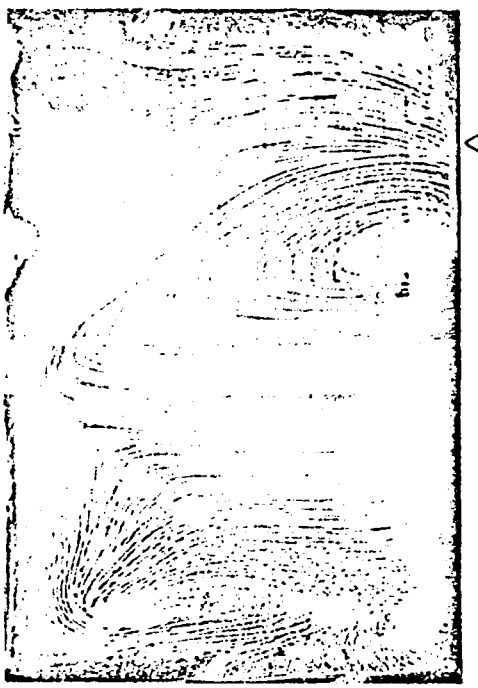

sidewall
after test

profile topside

OIL FILM PHOTOGRAPH
WITHOUT ROUGHNESS
ADAPTIVE WALL

NACA 0012
$Re = 1.0 \cdot 10^6$
$M_\infty = 0.50$ $\alpha = 10.668°$

FIGURE 43

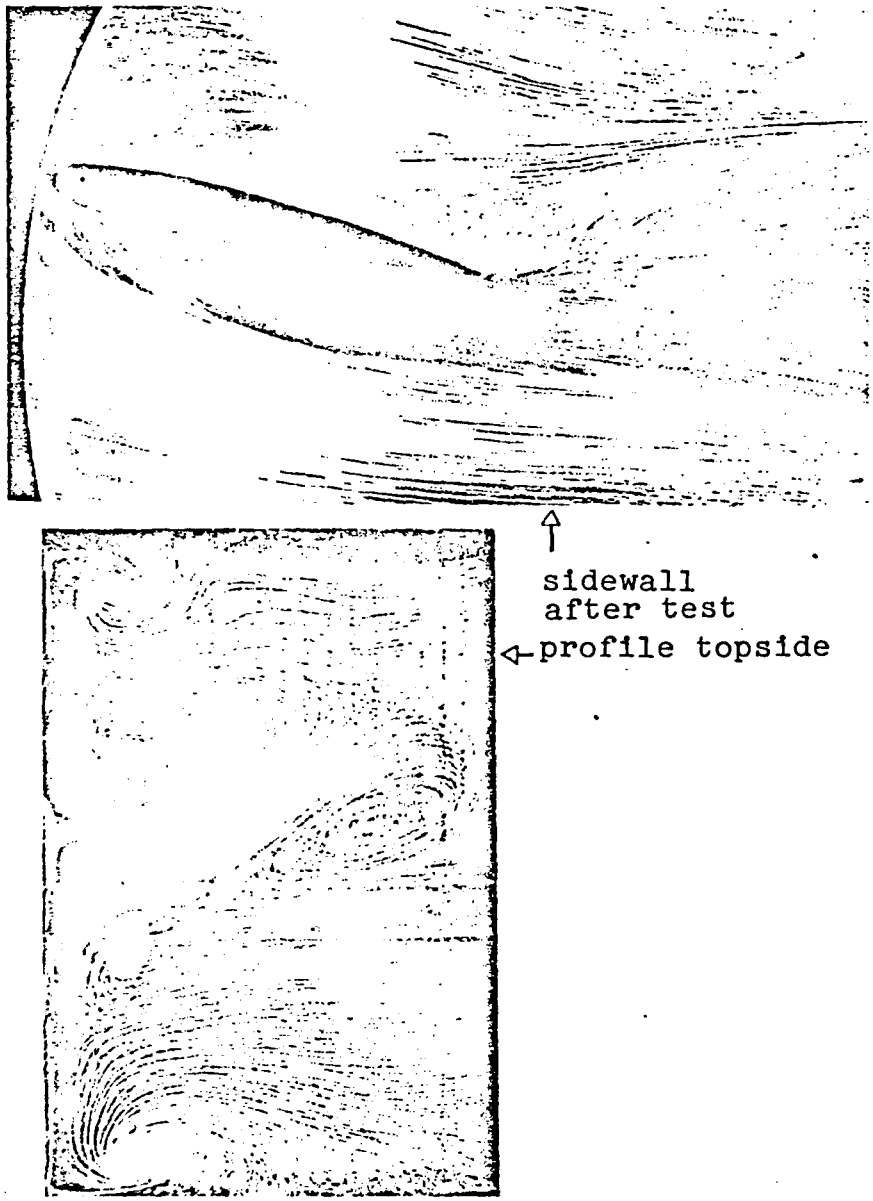

/63

OIL FILM PHOTOGRAPH
WITHOUT ROUGHNESS
ADAPTIVE WALL

NACA 0012
$Re = 1.0 \cdot 10^6$
$M_\infty = 0.50$ $\alpha = 11.659°$

FIGURE 44

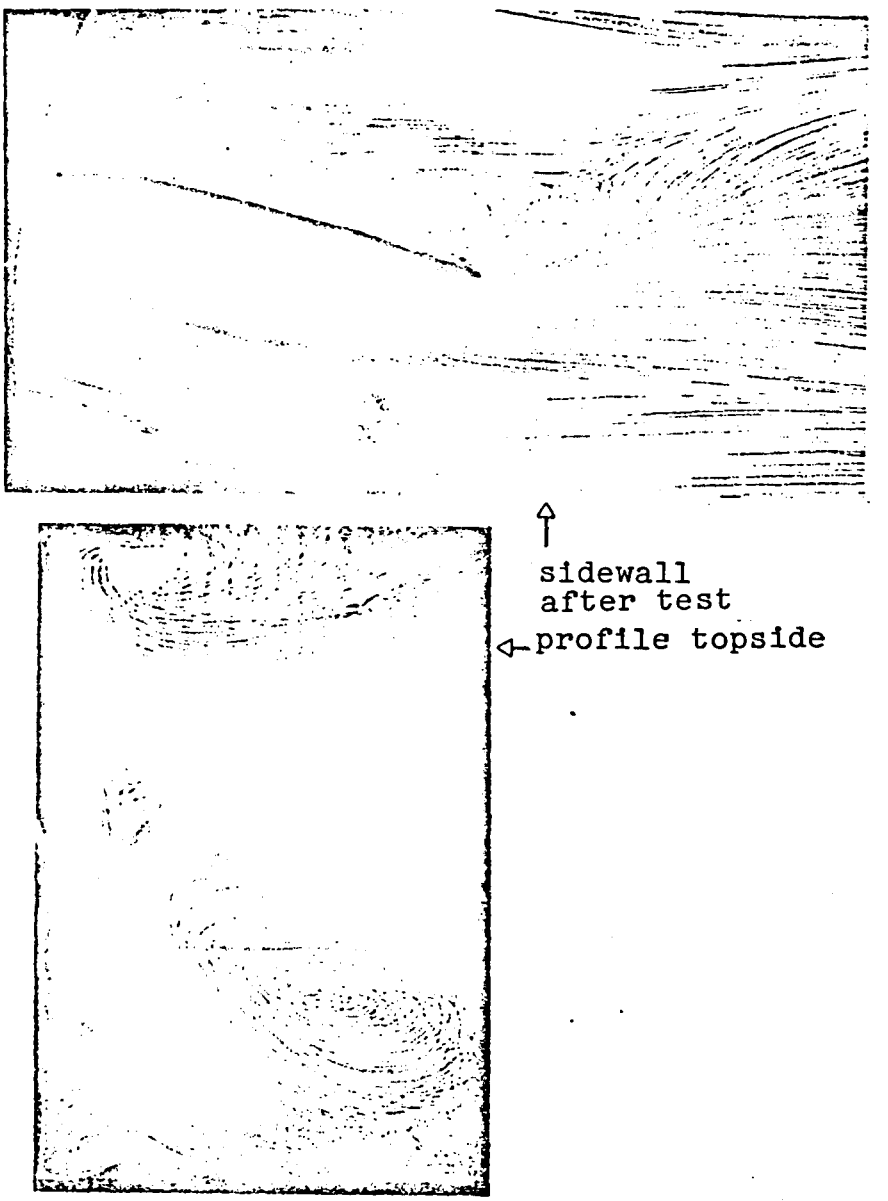

/64

OIL FILM PHOTOGRAPH
WITHOUT ROUGHNESS

ADAPTIVE WALL

NACA 0012
$Re = 10 \cdot 10^6$
$M_\infty = 0.50$ $\alpha = 12.647°$

FIGURE 45

APPENDIX

Data set from the ILR high speed wind tunnel

1.	Profile		
	1.1	Profile name	NACA 0012
	1.2	Profile type	symmetric (see Figure 2a)
		1.2.1 Profile geometry	$y/l = \pm 0{,}60\,(0{,}2969\,\sqrt{x/l} - 0{,}126\,x/l - 0{,}3516\,x^2/l + 0{,}2843\,x^3/l - 0{,}1015\,x^4/l)$
		nose radius	$r/l = 1{,}58\ \%$
		maximum thickness	$t/l = 12\ \%$
		trailing edge thickness	0.252% profile chord
		1.2.2 Design condition	mathematical definition according to already known effective profiles
	1.3	Additional remarks	none
	1.4	References on profile	[1]
2.	Model geometry		
	2.1	Profile chord	100 mm
	2.2	Span	340 mm
	2.3	Present model coordinates and accuracy	see Figures 2b and 2c
	2.4	Maximum thickness	no data
	2.5	Trailing edge thickness	no data
	2.6	Additional remarks	none
	2.7	References on model	none
3.	Wind tunnel		
	3.1	Name	ILR high speed wind tunnel
	3.2	Wind tunnel type	hot water jet ejector
		3.2.1 Stagnation pressure	1 bar
		3.2.2 Stagnation temperature	external temperature
		3.2.3 Humidity/dew point	
	3.3	Test section	rectangular
		3.3.1 Dimensions	150 x 150 mm^2
		3.3.2 Type of walls	flexible walls top and bottom, fixed sidewalls

3.4	Flow field (empty test section)		/A2
	3.4.1	static reference pressure	recorded on the lower wall, 2.45 profile chords upstream from model
	3.4.2	Angle perturbation of flow	no data
	3.4.3	Mach no. distribution	no data
	3.4.4	Pressure gradient	no data
	3.4.5	Turbulence/noise level	no data
	3.4.6	Sidewall boundary layer	no data
3.5	Additional remarks		none
3.6	References on wind tunnel		none

4. Measurements

4.1	Type of measurements		-profile pressure distribution -top and bottom wall pressure distribution
4.2	Tunnel/model dimensions		
	4.2.1	Height/profile chord	1.5
	4.2.2	Width/profile chord	1.5
4.3	Flow conditions in the present paper		
	4.3.1	Angle of attack	0° to 12.647°
	4.3.2	Mach number	0.50
	4.3.3	Reynolds number	$1.0 \cdot 10^6$
	4.3.4	Transition	free
		-position of free transition	no data
		-transition fixing	none
	4.3.5	Temperature equilibrium	none
4.4	Additional remarks		none
4.5	References on measurements		none

5. Instrumentation

5.1 Surface pressure measurement

5.1.1	Pressure taps	
	-size	ϕ = 0.3 mm, distance 1-5 mm
	-distribution over spans	see Figure 3
	-distribution over profile chord	see Figure A7 /A3
5.1.2	Type of measurement data transmitter	0-15 psia transducer ±15 psid pressure transducer
5.1.3	other	see Figure A6 on tap coordinates on top and bottom side
5.2	Wake measurements	none
5.2.1	Type and size of instruments	-
5.2.2	Positioning	-
5.2.3	Type of measurement transmitter	-
5.3	Boundary layer measurements	none
5.3.1	Type and size of instrumentation	-
5.3.2	Location	-
5.3.3	Type of measurement data transmitter	-
5.4	Surface friction measurements	none
5.4.1	Type and size of instrumentation	-
5.4.2	Location	-
5.4.3	Type of measurement data transmitter	-
5.5	Flow visualization	yes
5.5.1	Flow field	-
5.5.2	Surface flow at	α = 7.686° to 12.647°
5.6	Others	none
5.7	Additional remarks	none
5.8	References on instrumentation	none

6. Data

6.1	Accuracy (wall interferences excluded)	
6.1.1	Angle of attack adjustment	±0.12°
6.1.2	Incident Mach number:	
	-adjustment	±0.002
	-change during tests	no indication
6.1.3	Pressure coefficient	$\overline{\lvert\Delta c_p\rvert} = 0{,}0025$ for non-separated flow /A4
		$\overline{\lvert\Delta c_p\rvert} = 0{,}0160$ at $\alpha = 9{,}664°$ and $\overline{\lvert\Delta c_p\rvert} = 0{,}0220$ at $\alpha = 12{,}647°$ for separated flow
6.1.4	Aerodynamic coefficients	-
6.1.5	Boundary layer thickness	no data
6.1.6	Reproducibility	no data
6.1.7	Remarks	none
6.2	Wall interference corrections	general by adaptive wall
6.2.1	Angle of attack	
6.2.2	Blocking	
6.2.3	Streamline shape (lift)	
6.2.4	Others	
6.2.5	Remarks	
6.2.6	References on wall corrections	
6.3	Presentation of data	
6.3.1	Aerodynamic location	-
6.3.2	Surface pressure	see Figures 5 to 18 $M = 0{,}50$; $\alpha = 0°$/ $3{,}829°$/ $7{,}686°$/ $9{,}664°$/ $10{,}668°$/ $11{,}659°$/ $12{,}647°$
6.3.3	Boundary layer thickness	-
6.3.4	Wall interference correction included ?	yes
6.3.5	Corrections for model deviation	no
6.3.6	Empty test section calibration considered	no

6.3.7	Other corrections contained	no
6.3.8	Additional remarks	none
6.4	Work test performed in various installations?	no

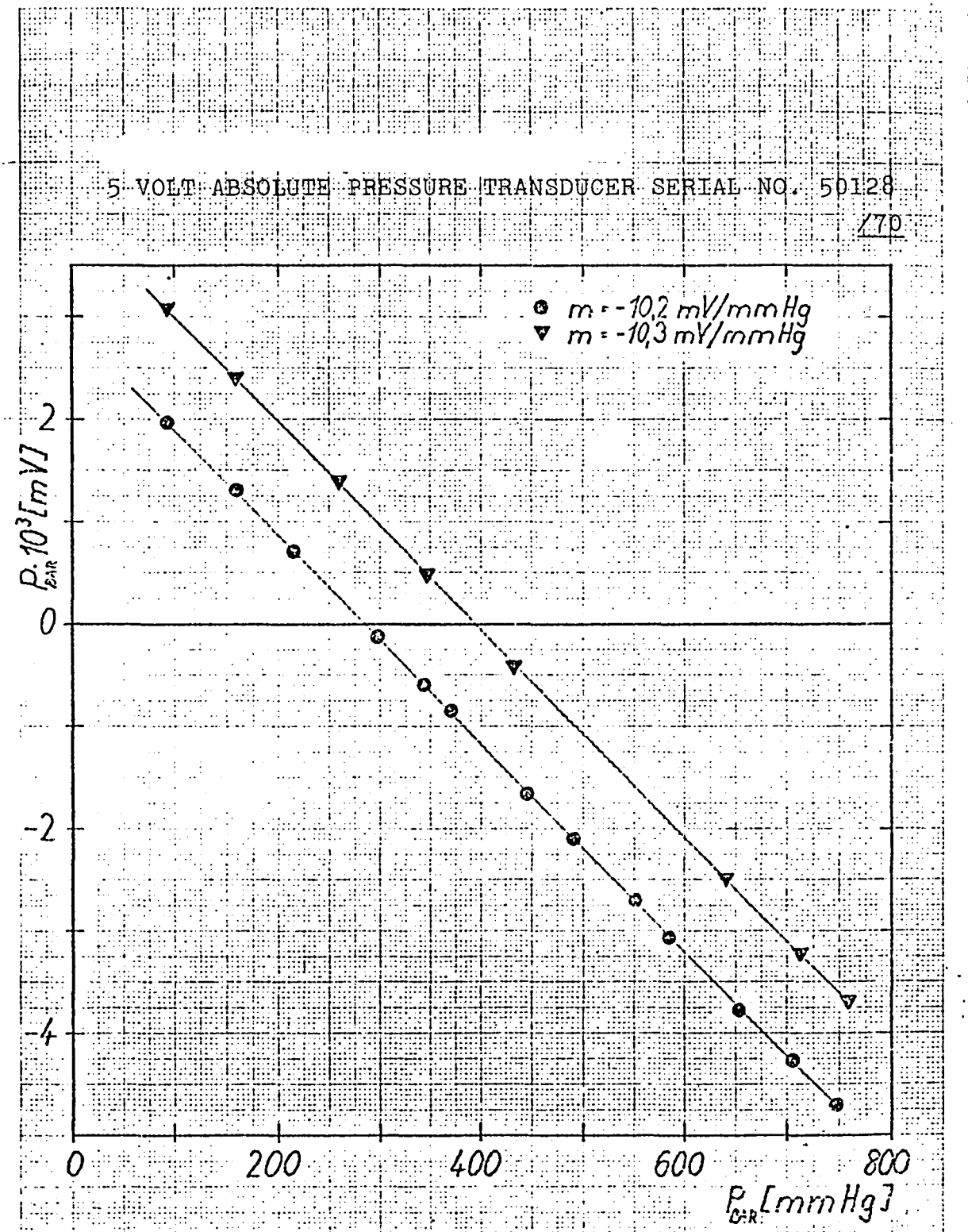

FIGURE A-1. PRESSURE TRANSDUCER CALIBRATION

5 VOLT ABSOLUTE PRESSURE TRANSDUCER SERIAL No. 50128

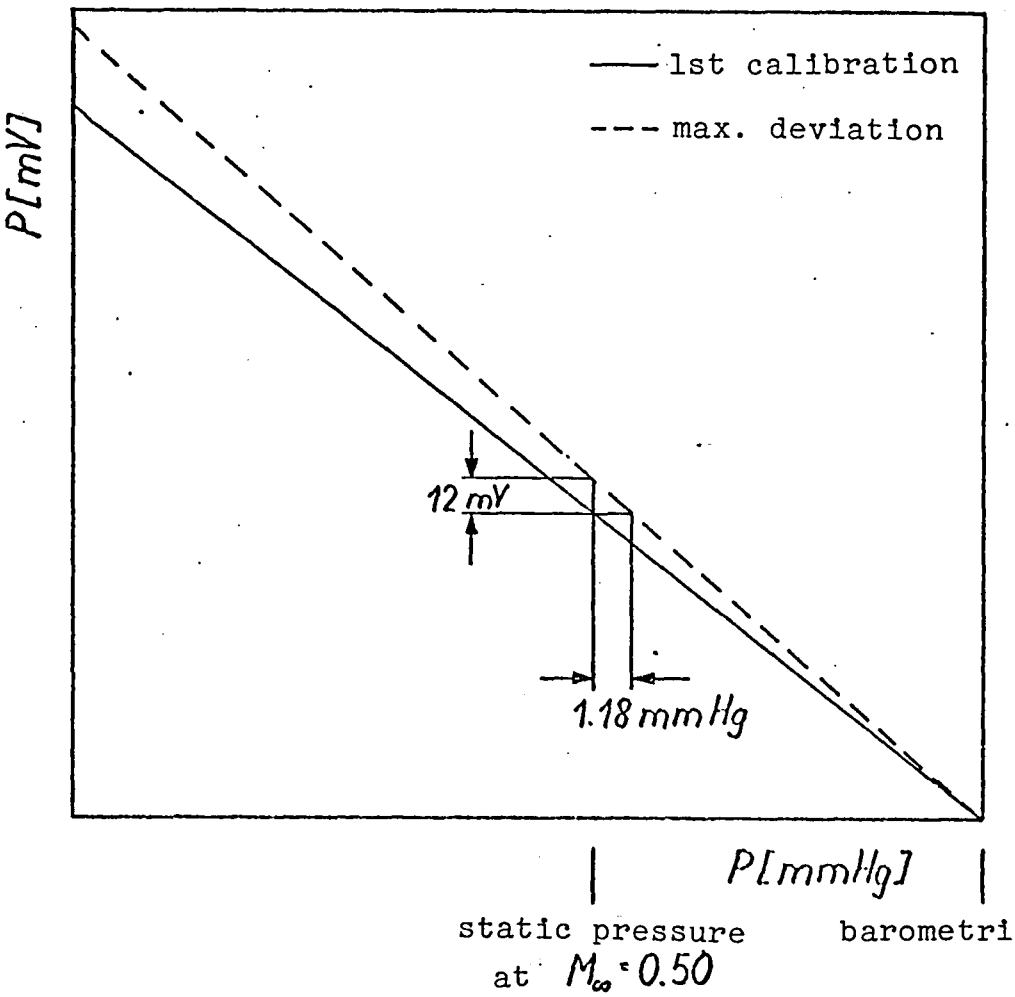

DEVIATION : 0.1 mV / mm Hg

Δp : 120 mm Hg

$\Rightarrow$ FALSE MEASUREMENT : 12 mV AND 1.18 mm Hg RESPECTIVELY

p_∞ = 640 mm Hg $\pm$ 0.59 mm Hg

ERROR : $\pm$ 0.09 %

FIGURE A-2: PRESSURE TRANSDUCER CALIBRATION

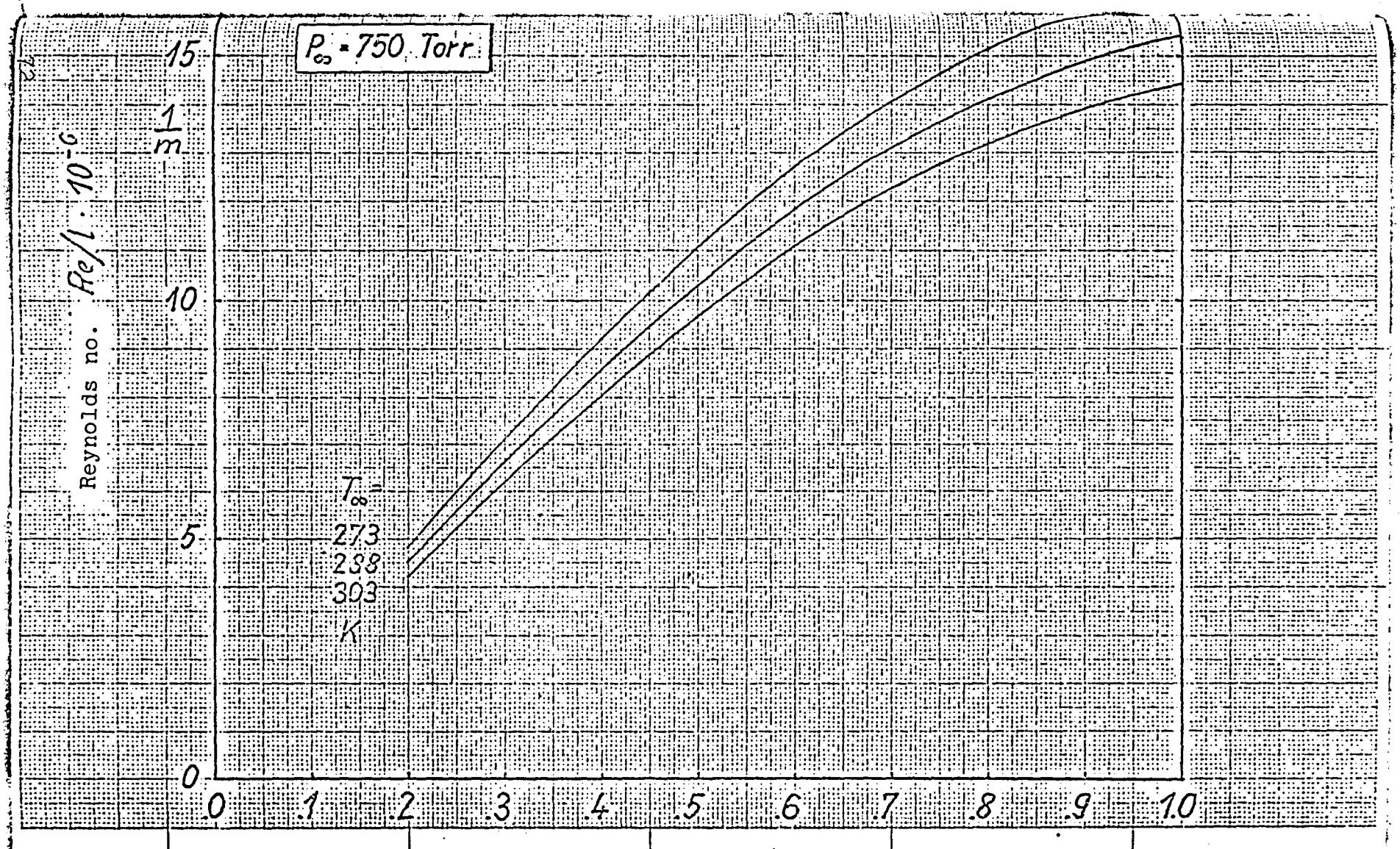

FIUGRE A-3

172

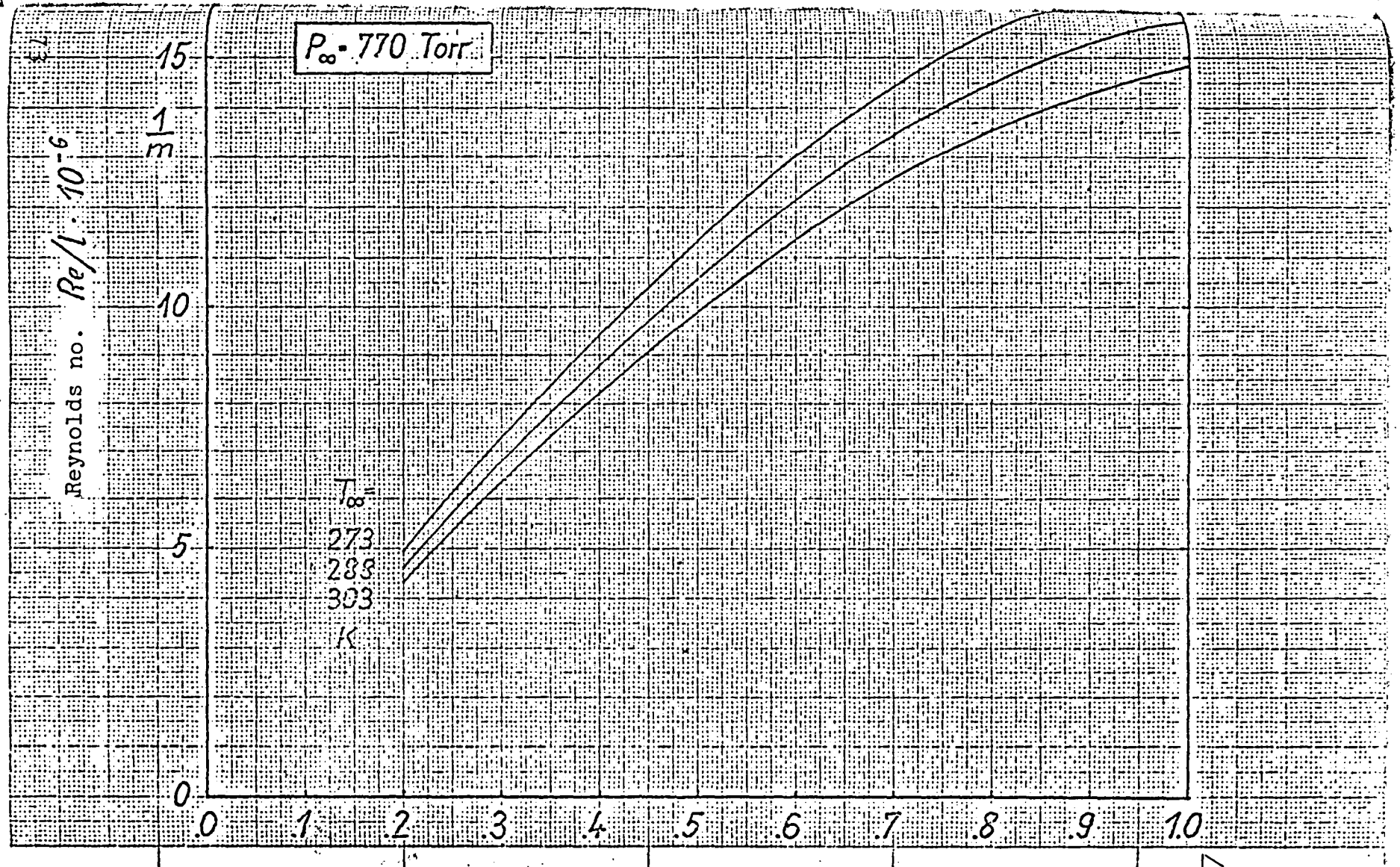
P_∞ = 770 Torr
Reynolds no. $Re/l : 10^{-6}$ $\frac{1}{m}$
15
10
5
0
T_∞ =
273
288
303
K
.0
.1
.2
.3
.4
.5
.6
.7
.8
.9
1.0
Mach no. M_∞

FIGURE A-4

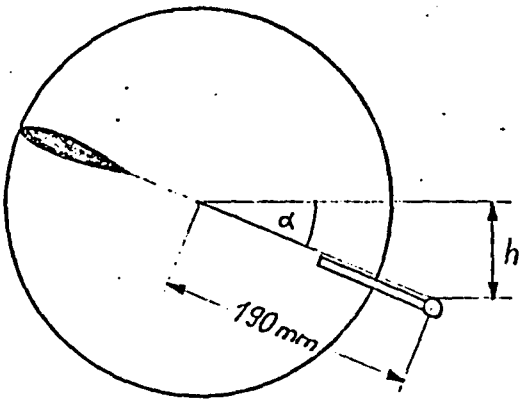

/74

angle of attack α	separator h [mm] right	left
0^{o}	1,20	1,10
$3,829^{o}$	+ 12,69	+ 12,70
$7,686^{o}$	+ 25,41	+ 25,50
$9,664^{o}$	+ 31,90	+ 32,00
$10,668^{o}$	+ 35,17	+ 35,26
$11,659^{o}$	+ 38,40	+ 38,50
$12,647^{o}$	+ 41,60	+ 41,70

Indication: The side disk with the engraved "V" is on the left side in the flow direction. For the angle of attack adjustment, the separator on the right side is decisive.

FIGURE A-5. ANGLE OF ATTACK ADJUSTMENT OF PROFILE.

upper and lower wall

/75

x/l
-2.00
-1.65
-1.40
-1.15
-0.90
-0.60
-0.35
-0.15
0.05
0.20
0.35
0.55
0.75
0.95
1.20
1.40
1.65
1.85
2.05
2.25
2.50
2.75
3.00

FIGURE A-6. POSITION OF WALL PRESSURE TAP.

upper side profile	bottom side profile
x/l	x/l
0.00	0.005
0.01	0.020
0.03	0.040
0.05	0.075
0.10	0.125
0.15	0.175
0.20	0.225
0.25	0.275
0.30	0.325
0.35	0.375
0.40	0.425
0.45	0.475
0.50	0.525
0.55	0.575
0.60	0.625
0.65	0.675
0.70	0.725
0.75	0.775
0.80	0.825
0.85	0.875
0.90	0.925
0.95	0.925

FIGURE A-7. POSITION OF WALL PRESSURE TAP.

End of Document